DOCTORAL THESIS UNDER JOINT SUPERVISION

PREPARATION OF TUBULAR ALUMINA-BASED MEMBRANES INCORPORATED WITH COAL FLY ASH AND APPLICATION AS SUPPORT TO ZSM-5 MEMBRANES

MELISSA RODRIGUES DE LA ROCHA

The PhD thesis defense took place on April 14th, 2021 in Porto Alegre, Brazil

JURY COMPOSITION

REVIEWERS

Dr. Benoit LOUIS, CNRS Research Director, Université de Strasbourg, France

Dr. Marco DI LUCCIO, Professor, Universidade Federal de Santa Catarina – UFSC, Brazil

SUPERVISORS

Dr. Nilson R. MARCÍLIO, Professor, Universidade Federal do Rio Grande do Sul – UFRGS, Brazil

Dr. Andrei KHODAKOV, CNRS Research Director, Université de Lille, France

INVITED MEMBERS

Dr. Isabel TESSARO, Professor, Universidade Federal do Rio Grande do Sul – UFRGS, Brazil

Dr. Liliane D. POLLO, Professor, Universidade Federal do Rio Grande do Sul– UFRGS, Brazil

JURY PRESIDENT

Dr. Benoit LOUIS

APRIL 2021

This PhD thesis was performed in the Chemical Engineering Department of the Federal University of Rio Grande do Sul - UFRGS (Porto Alegre, Brazil) and at the Unit of Catalysis and Chemistry of Solids, UCCS, of the University of Lille (Lille, France). The work was supported by the National Council for Scientific and Technological Development (CNPq, BR), National Council for the Improvement of Higher Education (CAPES, BR), Research Support Foundation of the State of Rio Grande do Sul (FAPERGS), and CEMOP team of the UCCS (UMR 8181 CNRS) laboratory (FR).

THÈSE DE DOCTORAT EN COTUTELLE

PRÉPARATION DE MEMBRANES TUBULAIRES À BASE D'ALUMINE INCORPORÉES AVEC DES CENDRES VOLANTES DE CHARBON ET APPLICATION COMME SUPPORT AUX MEMBRANES ZSM-5

MELISSA RODRIGUES DE LA ROCHA

La soutenance de thèse a eu lieu le 14 avril 2021 à Porto Alegre, au Brésil

COMPOSITION DU JURY

RAPPOTEURS

Dr. Benoit LOUIS, Directeur de Recherche au CNRS, Université de Strasbourg, France

Dr. Marco DI LUCCIO, Professeur, Universidade Federal de Santa Catarina – UFSC, Brésil

DIRECTEURS DE THÈSE

Dr. Nilson R. MARCÍLIO, Professeur, Universidade Federal do Rio Grande do Sul – UFRGS, Brésil

Dr. Andrei KHODAKOV, Directeur de Recherche au CNRS, Université de Lille, France

MEMBRES INVITÉS

Dr. Isabel TESSARO, Professeure, Universidade Federal do Rio Grande do Sul – UFRGS, Brésil

Dr. Liliane D. POLLO, Professeure, Universidade Federal do Rio Grande do Sul– UFRGS, Brésil

PRESIDENT DU JURY

Dr. Benoit LOUIS

AVRIL 2021

Cette thèse de doctorat en cotutelle a été réalisée au Département de Génie Chimique de l'Université Fédérale de Rio Grande do Sul - UFRGS (Porto Alegre, Brésil) et à l'Unité de Catalyse et Chimie des Solides, UCCS, de l'Université de Lille (Lille, France). Le travail a été financé par le Conseil National pour le Développement Scientifique et Technologique (CNPq, BR), le Conseil National pour l'Amélioration de l'Enseignement Supérieur (CAPES, BR), la Fondation d'Appui à la Recherche de l'État du Rio Grande do Sul (FAPERGS) et l'équipe CEMOP du laboratoire UCCS. (UMR 8181 CNRS).

AKNOWLEDGMENTS

I would like to gratefully thank my supervisors, Dr. Isabel Cristina Tessaro, Dr. Nilson Romeu Marcílio and Dr Andrei Khodakov, and my contributors, Dr. Liliane Damaris Pollo, Dr. Mirella Virginie, for the guidance in the development of this research.

I would like to express my gratitude to some people and laboratories that carried out the analysis of this work, such as Dr. Alexandre Fadel and Dr. Philippe Recourt for the scanning electron microscopy and the dispersive energy spectroscopy analysis, Eng. Jean-Charles Morin for the Fourier-transform infrared spectroscopy analyzes, the Ceramic Materials Laboratory (LACER) from UFRGS for carrying out the granulometric analyzes, the Biomaterials Laboratory (LABIOMAT) from UFRGS for the mechanical strength analyzes, the Design and Material Selection Laboratory from UFRGS and to the Center for Microscopy and Microanalysis (CMM) for performing morphological analyzes, the latter also for making the diamond saw available for sample preparation, the Analytical Center of the Chemical Engineering Department at UFRGS for carrying out the X-ray diffraction and X-ray fluorescence analyses.

I would like to thank my colleagues at UCCS, LASEM, LATEM and LPR, specially to colleagues and friends MSc. Ana Katiuce Fellenberg, Dr. Claudia Luchese, Dr. Deizi Peron, MSc. Helena Schneider and Dr. Renata Bertotto for their great contributions to this work.

To the Graduate Program in Chemical Engineering from UFRGS.

To CNPq, FAPERGS, CAPES, CAPES/Cofecub and the CEMOP team for their financial support.

To the members of the jury for accepting to contribute and to be part of this work.

Finally, I would like to thank also to Renato Bruno, and my family for their unconditional support.

Thank you all.

ABSTRACT

Synthetic membranes are increasingly used in different applications for the concentration, fractionation, and efficient purification of components present in solutions and mixtures of liquids or gases. Ceramic membranes have a large potential over the polymeric ones for applications at high temperature, pressure, and in aggressive environments. However, the preparation of ceramic membranes is expensive. The coal fly ash (CFA) is a burning coal by-product with structural qualities, mainly composed of silica and alumina oxides, being an appropriate and inexpensive raw material for ceramic membrane addition. Thus, the main objective of this work is to prepare and characterize tubular alumina-based membranes incorporated with CFA, without additive and binder-free, using the centrifugal casting method. In addition, this work aims to use these ceramic membranes as support for the ZSM-5 zeolites prepared without using organic structure-directing agents for application in catalytic processes.

The centrifugal casting method with high-speed mold rotation has produced asymmetric membranes with different morphologies at the inner and outer surfaces of the tubes. High CFA fraction in the membranes resulted in higher porosity levels and water permeability, accompanied by a decrease in mechanical strength and in linear shrinkage. Moreover, the observed permeate flux was in the range between 116 and 370 L m^{-2} h^{-1} bar^{-1}, and the retention for the cornstarch solution was above 99 % for all the membranes. To test the zeolitic deposition on these tubes, the synthesis of the ZSM-5 zeolite was performed with a theoretical Si/Al ratio of 50. The ZSM-5 zeolite membranes could be successfully synthesized on the tubes using the seeding method followed by the direct hydrothermal synthesis. The prepared materials were characterized by X-ray diffraction, Fourier transform infrared spectroscopy and scanning electron microscopy and tested for separation of organic compounds and xylene isomerization

reaction. The ceramic membranes CFA-based showed potential application for wastewater treatment and can be used as support to selective layer coatings as the ZSM-5 zeolite.

Keywords: centrifugal casting; ceramic membrane; CFA; ZSM-5

RÉSUMÉ

Les membranes synthétiques sont de plus en plus utilisées dans différentes applications pour la concentration, le fractionnement et la purification efficaces des composants présents dans les solutions, ainsi que dans les mélanges de liquides ou de gaz. Les membranes céramiques ont un grand potentiel par rapport aux membranes polymères pour des applications à haute température, à haute pression et dans des environnements agressifs. Cependant, la préparation des membranes céramiques est coûteuse. La cendre volante de charbon (CFA, de l'anglais *coal fly ash*) est un sous-produit de la combustion du charbon dont les qualités structurelles, principalement composées d'oxydes de silice et d'alumine, sont une matière première appropriée et peu coûteuse qui peut être ajoutée à des membranes céramiques. Ainsi, l'objectif principal de ce travail est de préparer et de caractériser des membranes tubulaires à base d'alumine incorporées avec la CFA, sans additif et sans liant, en utilisant la méthode de coulée centrifuge. En outre, ce travail vise à utiliser ces membranes céramiques comme support pour les zéolithes ZSM-5 préparées sans utiliser d'agents organiques directeurs de structure pour les procédés catalytiques.

La méthode de coulée par centrifugation avec rotation du moule à grande vitesse a produit des membranes asymétriques de morphologies différentes sur les surfaces intérieures et extérieures des tubes. La fraction élevée de CFA dans les membranes a entraîné des niveaux de porosité et une perméabilité à l'eau plus élevée, accompagnés d'une diminution de la résistance mécanique et du retrait linéaire. De plus, le flux de perméat observé était compris entre 116 et 370 L m^{-2} h^{-1} bar^{-1}, et la rétention pour la solution d'amidon de maïs était supérieure à 99 % pour toutes les membranes. Pour tester le dépôt zéolitique sur ces tubes, la synthèse de la zéolite ZSM-5 a été réalisée avec un rapport théorique Si/Al de 50. Les membranes de la zéolite ZSM-5 ont pu être synthétisées avec succès sur les tubes en utilisant la méthode d'ensemencement

suivie de la synthèse hydrothermale directe. Les matériaux préparés ont été caractérisés par la diffraction des rayons-X, la spectroscopie infrarouge à transformée de Fourier et la microscopie électronique à balayage et ils ont été testés pour la séparation des composés organiques et la réaction d'isomérisation du xylène. Les membranes céramiques à base de CFA ont montré une application potentielle pour le traitement des eaux usées et peuvent être utilisées comme support pour le dépôt des couches de catalyseur comme la zéolite ZSM-5.

Mots clés: coulée centrifuge; membrane céramique; CFA; ZSM-5

RESUMO

As membranas sintéticas são cada vez mais utilizadas em diferentes aplicações para concentração, fracionamento e purificação eficiente de componentes presentes em soluções e misturas de líquidos ou gases. As membranas cerâmicas têm grande potencial sobre as poliméricas para aplicações em alta temperatura, pressão e em ambientes agressivos. No entanto, a preparação de membranas cerâmicas é cara. A cinza volante de carvão (CFA, do inglês *coal fly ash*) é um subproduto da queima do carvão com qualidades estruturais, composta principalmente por óxidos de sílica e alumina, sendo uma matéria-prima adequada e de baixo custo para adição a membranas cerâmicas. Assim, o objetivo principal deste trabalho é preparar e caracterizar membranas tubulares à base de alumina incorporadas com CFA, sem aditivos ou ligantes, utilizando o método de *centrifugal casting*. Além disso, este trabalho visa utilizar essas membranas cerâmicas como suporte para zeólitas ZSM-5 preparadas sem o uso de agentes orgânicos direcionadores de estrutura para aplicação em processos catalíticos.

O método de *centrifugal casting* com rotação do molde em alta velocidade produziu membranas assimétricas com morfologias diferentes nas superfícies interna e externa dos tubos. A alta fração de CFA nas membranas resultou em maiores níveis de porosidade e permeabilidade à água, acompanhados por uma diminuição na resistência mecânica e na retração linear. Além disso, o fluxo de permeado observado situou-se na faixa entre 116 e 370 L m^{-2} h^{-1} bar^{-1}, e a retenção obtida para a solução de amido de milho apresentou valores acima de 99 % para todas as membranas. Com a finalidade de testar a deposição zeolítica nesses tubos, a síntese da zeólita ZSM-5 foi realizada com relação Si/Al teórica de 50. As membranas de zeólita ZSM-5 puderam ser sintetizadas com sucesso nos tubos usando o método de semeadura seguido pelo direto síntese hidrotérmica. Os materiais preparados foram caracterizados por difração de raios-X, espectroscopia no infravermelho com transformada de Fourier e

microscopia eletrônica de varredura e testados para separação de compostos orgânicos e reação de isomerização do xileno. As membranas cerâmicas à base de CFA apresentam potencial de aplicação para tratamento de efluentes e podem ser utilizadas como suporte para deposição de camadas seletivas como a zeólita ZSM-5.

Palavras-chave: *centrifugal casting*; membrana cerâmica; cinzas de carvão; ZSM-5

SUMMARY

LIST OF FIGURES

LIST OF TABLES

LIST OF SYMBOLS

A	Membrane permeation area	[m^2]
b	Centrifugal acceleration	[$m\ s^{-2}$]
c	Component concentration	[$g\ L^{-1}$]
C_b	Bulk concentration	[$g\ L^{-1}$]
C_f	Feed concentration	[$g\ L^{-1}$]
C_p	Permeate concentration	[$g\ L^{-1}$]
d	Particle diameter	[m]
d_0	Sample outer diameter	[m]
d_i	Sample inner diameter	[m]
D	Diffusion coefficient of a component	[$m^2\ s^{-1}$]
F	Flexural load	[N]
J	Permeate flux	[$g\ m^{-2}\ s^{-1}$]
k	Difference between L_0 and L_1	[m]
K_s	Sorption coefficient of a component	[$mol\ m^{-2}\ Pa^{-1}$]
K	Hydraulic permeance	[$L\ m^{-2}\ h^{-1}\ bar^{-1}$]
K'	Permeability of the medium	[$L\ m^{-2}\ h^{-1}\ bar^{-1}$]
L_f	Final specimen length	[m]
L_i	Initial specimen length	[m]

L_I	Inner support distance	[m]
L_0	Outer support distance	[m]
L_p	Permeability coefficient	[L m^{-1} h^{-1} bar]
p_p	Partial pressure of a component in the permeate	[Pa]
p_f	Partial pressure of a component in the feed	[Pa]
P	Transmembrane pressure	[bar]
r	Radius	[m]
R_{obs}	Observed retention	[%]
S_T	Total specimen shrinkage	[%]
t	Time	[h]
T_0	Turbidity in the final feed solution	[NTU]
T_f	Turbidity in the permeate stream	[NTU]
V	Volume	[L]
V_P	Terminal particle velocity	[m s^{-1}]
W_{dry}	Sample weight dry	[g]
W_{imm}	Sample weight immersed	[g]
W_{wet}	Sample weight wet	[g]
x	Membrane thickness	[m]

LIST OF GREEK LETTERS

ε	Membrane porosity	
μ	Dynamic viscosity	[g m^{-1} s^{-1}]
ρ_l	Liquid density	[g m^{-3}]
ρ_p	Particle density	[g m^{-3}]
σ	Strength	[M Pa]
τ	Tortuosity	
ω	Angular velocity	[rad s^{-1}]
Φ_L	Thiele modulus	

LIST OF ABREVIATIONS

AP	Apparent Porosity
ATR	Attenuated Total Reflectance
ASTM	American Society for Testing and Materials
BAS	Brønsted Acid Sites
BBU	Basic Building Unit
CFA	Coal Fly Ash
CVD	Chemical Vapor Deposition

DTA	Differential Thermal Analysis
FTIR	Fourier Transform Infrared
GS	Gas Separation
HS	Hydrothermal Synthesis
ISO	International Organization for Standardization
IUPAC	International Union of Pure and Applied Chemistry
IZA	International Zeolite Association
LAS	Lewis Acid Sites
LPH	Liters per hour
MFI	Mordenite Framework Inverted
MOR	Mordenite Framework
MR	Membrane Reactor
MWCO	Molecular Weight Cut-Off
MX	*Meta*-xylene
OSDA	Organic structure-directing agent
OX	*Ortho*-xylene
PDS	Product Data Sheet
PMMA	Poly(methyl acrylate)
PV	Pervaporation
PVD	Physical Vapor Deposition

PX	*Para*-xylene
Py	Pyridine
SBU	Secondary Building Unit
SEM	Scanning Electron Microscope
TGA	Thermogravimetric Analysis
TPD	Temperature-Programmed Desorption
VP	Vapor Permeation
WHSV	Weight Hourly Space Velocity
XRD	X-Ray Diffraction
XRF	X-Ray Fluorescence
ZSM-5	Zeolite Socony Mobil-5

CHAPTER 1

INTRODUCTION

There is currently a growing interest in the development of ceramic membranes for the separation and purification of solutes from aqueous solutions or a mixture of gases, as well as for the use of these membranes as supports for metallic, zeolite or polymeric coatings and for other applications. Ceramic membranes have a large potential over polymeric membranes for applications at high temperature, pressure and in aggressive environments. One of their most promising applications is membrane reactor where chemical conversion and product purification by separation take place in the same device. By selectively separating one or more reaction products through the membrane wall, it is possible to achieve significant enhancement over the equilibrium conversion of the reactor feed stream.

In general, the ceramic membrane costs are higher when compared to polymeric membranes due to both costs of the ceramic materials and complexity of their preparation. Research with ceramic membranes was initially directed at the manufacture of alumina membranes, being widely applied today. Currently, several other materials like zirconia, titania, and silica are being considered for the preparation of ceramic membranes, most of them, however, are rather expensive. On the other hand, the high cost of preparation is because ceramic membranes are produced by ‘colloidal’ or ‘suspension processing’, which implies that an essential step in the process is the dispersion of particles in a suitable carrier liquid and the subsequent consolidation of the powder into a ‘green body’. Therefore, much attention is paid to the ‘powder technology’ of ceramic materials, in which powder preparation, consolidation, drying, and sintering are essential steps.

Membranes can be prepared using different techniques and using a wide variety of materials. Membranes of inorganic materials are commonly prepared by pressing, extrusion, slip casting, and tape casting. The centrifugal casting is another technique used for tubular membranes preparation. The method at high rotational velocity can generate a settling gradient between the inner and the outer tubular surface. The result is a membrane with a high internal surface smoothness and a porous external surface, turning the membrane especially adequate for support applications.

Numerous efforts have been made to design compact, low-cost membranes from abundant and cheap raw materials. In order to reduce the costs of the ceramic membranes, it was sought to manufacture them with cheaper supplies, as well as to incorporate these materials into more expensive materials. Among these materials can be mentioned the coal fly ash (CFA), a by-product of burning coal considered a waste with disposal problems. The CFA composition is dependent from the source coal, however mainly silica, alumina and iron oxides constitute it. Other elements, with insignificant proportions are Mg, Cr, Mn, Ni, Zn, Rb, Sr, and Zr. In this way, membranes prepared with CFA can be an affordable option for applications in the separation of solutions from both bench scale and large scale.

Ceramic membranes can also be used as a support for different materials, which have insufficient mechanical strength for self-supporting membranes, such as carbon and zeolites. Most of the studies on the syntheses of zeolitic and carbon membranes have been performed on porous ceramic supports, such as clay, alumina, and zirconia. These ceramic composite membranes can perform specific and important separations of gas, vapor, or liquid mixtures. The ceramic support must provide a good adhesion surface to the coating and the required robustness with minimal mass transfer resistance. In the catalysis area, zeolitic films deposited on ceramic membranes can perform the separation and isomerization reaction of large

hydrocarbon molecules, which have a close melting point (precluding separation by distillation).

Thus, it was recognized the need for more studies related to the preparation of ceramic membranes using alternative and cheaper materials to reduce the costs of ceramic membranes. The centrifugal casting technique was chosen to explore the advantages of this technique for preparing asymmetric ceramic membranes. Also, zeolitic composite membranes have been developed for catalytic applications.

General Objective

This PhD thesis aims to prepare and to characterize tubular alumina-based membranes incorporated with coal fly ash (CFA), without additive and binder-free, using the centrifugal casting method. Thereafter, use the ceramic membranes as support to ZSM-5 zeolites prepared by *in-situ* crystallization applying the seeding method without organic structure-directing agents (OSDAs) was evaluated for potential application in catalytic processes, involving acid catalyst and effects of shape-selectivity.

Specific Objectives

- Characterization of the raw materials – CFA from Candiota coalmine and α-alumina CT 3000 SG, Almatis (particle size distribution, elemental composition, apparent density and thermal degradation).

- Preparation of the tubular alumina-based membranes incorporating different amounts of coal fly ash by centrifugal casting.

- Evaluation of the membrane preparation conditions (alumina and CFA concentrations) on the structural characteristics (morphology, porosity, linear shrinkage, mechanical resistance) of the membranes.

- Evaluation of the membrane preparation conditions on the performance related to the hydraulic permeability and selectivity to cornstarch.

- Preparation of the ZSM-5 composite membranes by secondary growth method using as supports the tubular alumina/CFA-based membranes.

- Characterization of the zeolitic ZSM-5 layer (crystalline phases, morphology and thickness).

- Application of the zeolitic composite membranes in separation and in catalytic processes.

CHAPTER 2

LITERATURE REVIEW

The scheme presented in Figure 1 defines the main sections addressed in the literature review.

Figure 1 – Flowchart with the main sections covered in the literature review.

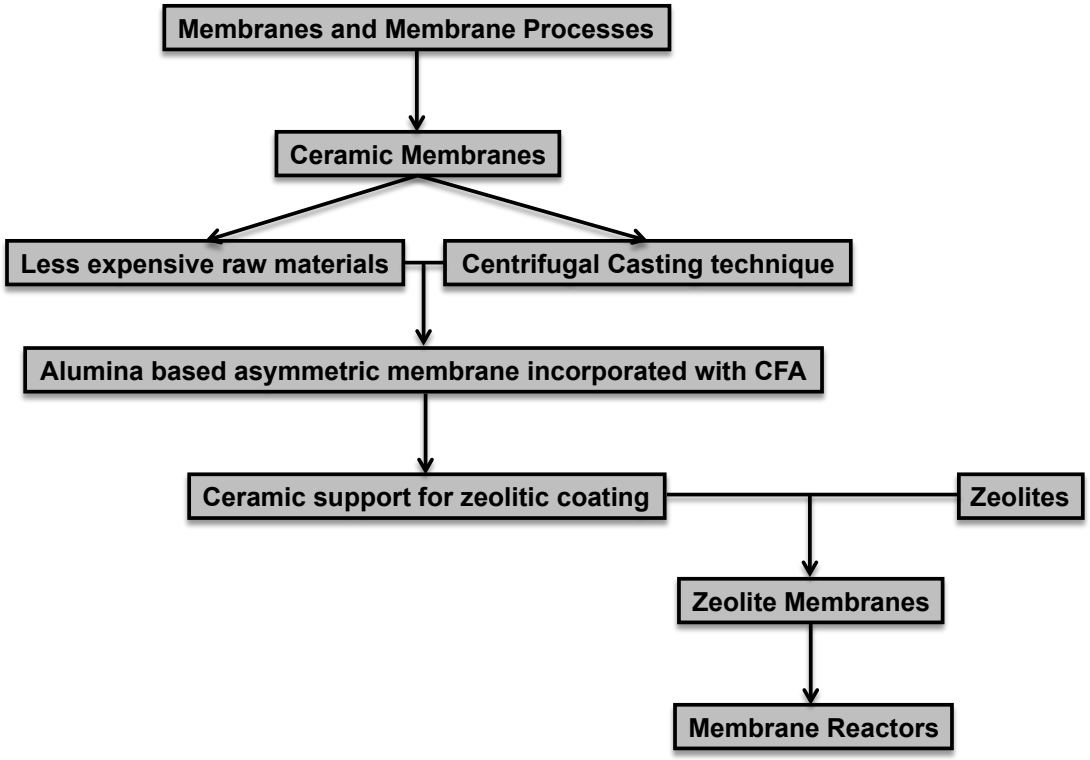

2.1 Membranes and membrane processes

Membranes are barriers that restrict partially or totally the transport of one or more species of interest. Their development started in the 1940s, as stated by Bhave and Ramesh (1991), with the nuclear industry and the membranes for uranium isotopes enrichment by

gaseous diffusion, a difficult operation to be reached through other processes. After that, the membranes started to be used in liquid processes in ultrafiltration and microfiltration industries and, more recently, are being used in a big range of industrial applications (BAKER, 2004).

Widely applied, the membrane processes can be seen in chemical, food and pharmaceutical industries and sectors like water treatment, medicine, and biotechnology. The use of membrane technology for separation processes in the industry is a clean and energetically efficient alternative to conventional methods as distillation, physical and chemical adsorption, and crystallization (BISSETT, 2005).

Membranes are compact systems, where separation occurs without phase change, making the separation energetic and economically interesting. Membrane processes can be applied in mild temperature and pressure conditions; however, membranes are also indicated to separate or purify compounds unable to experience variations on these parameters, preventing losses during critical process conditions.

The membrane separation, purification and concentration can occur in the solid, liquid or gaseous phases (HAN; SHEN; WICKRAMASINGHE, 2005; ZANG et *al*., 2009; YAO *et al*., 2011; HE *et al*., 2016), through the affinity of a given component for the membrane or by size difference between the solutes. In such manner, solutes presenting more affinity with the membrane material or smaller sizes than the membrane pores will pass (permeate stream), while the other solutes will be retained (feed/concentrate stream) as depicted in Figure 2.

Figure 2 – Schematic representation of membrane process.

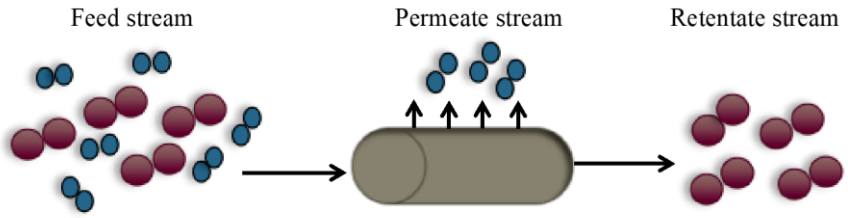

The transport across the membrane occurs due to a driving force expressed as the chemical potential difference and electrical potential difference. The gradient of chemical potential depends on pressure, temperature, and chemical composition. In the processes at constant temperature, the driving force can be expressed in terms of the pressure or concentration gradient.

2.1.1. Membranes morphology

According to the morphology, the membranes can be classified into porous or dense, symmetric or asymmetric.

Symmetric (or isotropic) membranes possess homogeneous structure along the cross-section that can be porous or dense. The asymmetric (or anisotropic), on the other hand, present gradual changes along the cross-section, being porous, dense, or composite, as exemplified in Figure 3.

Figure 3 – Schematic representation of the classification of membranes concerning morphology.

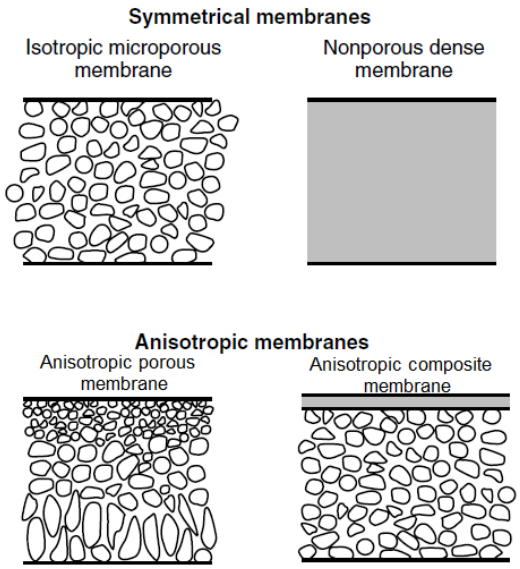

Adapted from Baker (2004).

Porous membranes contain pore diameters in the order of 0.01 to 10 μm, and the separation in this type of membrane occurs due to considerably differences in molecular size (BAKER, 2004). The restriction to the components larger than the maximum pore size results in fractionation.

The dense membranes are constituted by a dense layer also called nanoporous layer since only nanometric pores are present. The dense symmetric membranes generally present very low fluxes that limit their application. To overcome this limitation, were developed the asymmetric membranes consisting of a very dense top layer supported by a porous sublayer. If the top layer and sublayer are from different materials, the membrane is known as composite; each layer can be optimized independently. The support is an asymmetric membrane (porous asymmetric membrane), on which a selective dense layer is deposited. This deposition can be performed by different methods as dip-coating, interfacial, in-situ, or plasma polymerization (MULDER, 1996).

The porous asymmetric membranes can be constituted by a single material or by different materials and can present more than two porosity levels along the cross-section. The support in the asymmetric composite membranes gives mechanical resistance to the dense layer, responsible for the selectivity. Figure 4 shows the micrograph of the cross-section of a composite membrane, in which different materials, silica and γ-alumina, constitute the thin, dense skin and the porous support, respectively.

Figure 4 – SEM micrograph of the cross-section of a composite membrane with a silica top layer and a γ-alumina sublayer (150000x and 12.0 kV).

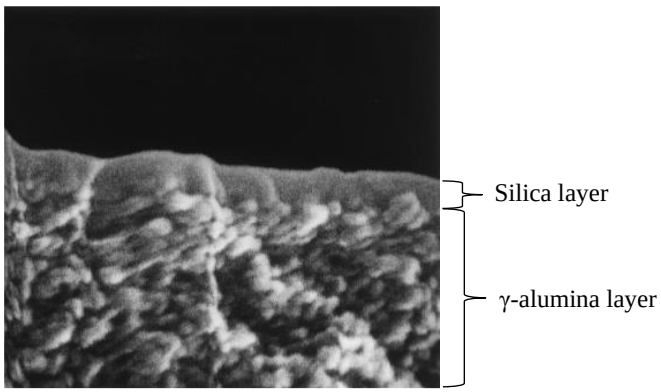

Adapted from De Vos and Verweij (1998).

2.1.2. Membrane processes

Membrane technologies differ according to the membrane structure and driving force and are applied to the separation of solutions, liquid or gas mixtures. As quoted by Baker (2004), the main membrane processes industrially developed are microfiltration, ultrafiltration, reverse osmosis, and electrodialysis. Developing technologies in the membrane separation include gas separation and pervaporation.

- Microfiltration (MF) – the microporous membrane is used to filter particulates from liquids, retaining particles bigger than 100 nm. It possesses as driving force the pressure

gradient and presents low hydrodynamic resistance, i.e., small pressures are sufficient to obtain high fluxes (MULDER, 1996). Filters small particles and bacteria.

- Ultrafiltration (UF) – the membrane is used to separate macromolecules from aqueous solutions with the sizes between 2-100 nm. The driving force is the pressure gradient (ΔP ranging from 1.0 – 5.0 bar). The main applications of UF comprise protein fractionation and concentration, pigment and recovery, and oil recovery.

- Nanofiltration (NF) – the membrane is used to separate molecules with a molar mass in the range between 500 and 2,000 Da. The driving force is the pressure gradient (ΔP ranging from 5.0 – 20 bar). Mainly used for enzyme purification.

- Reverse Osmosis (RO) – dense membrane with pores between 3 and 5 Å. The driving force is the pressure gradient (ΔP from 10 – 100 bar), with high hydrodynamic resistance. The separation occurs by solution-diffusion mechanism, and the main application is seawater desalination.

- Electrodialysis – electrically charged membranes are used to separate ions from aqueous solutions. The driving force for ionic transport is the electrical potential difference. The main application is brackish groundwater desalination.

- Gas separation – the dense membrane is used to separate gas mixtures at elevated pressures. The solution and diffusion of one component occur selectively on the membrane surface. The permeate side is enriched in this species with more affinity by the membrane. One of the main applications is hydrogen separation from mixtures of hydrogen-nitrogen.

- Pervaporation – the membrane is dense with an asymmetric structure, the separation occurs with phase change, and the driving force is the vapor pressure gradient. A liquid mixture is permeated through solution-diffusion mechanism, and vapor is collected in

the permeate side. Therefore, pervaporation offers the possibility of separating closely boiling mixtures or azeotropes that are difficult or non-possible to separate by distillation (BAKER, 2004). The main application is the organic solvents dehydration.

2.1.3. Materials for manufacturing membranes

Membranes can be produced from inorganic materials – carbonic, metallic, ceramic, or mineral – and organic materials, polymers, such as polyamide, polyetherimide, and polyvinyl alcohol. Usually, membranes of an organic nature have a lower production cost than inorganic ones.

Most membranes used commercially nowadays are organic due to both the production cost and the variety of materials available. In recent years, however, the application of other types of membranes has increased, mainly in processes requiring thermal stability and high resistance to solvents or an aggressive cleaning protocol (BAKER, 2004).

The use of polymers for membranes manufacturing is based on specific characteristics from structural factors of these polymers, such as the molecular weight, chain flexibility and chain interactions. These factors can determine the thermal, chemical and mechanical attributes and also the permeability of the polymeric material (MULDER, 1996). The commercially applied polymers are the polyethylene and the polysulfone, both hydrophobic, low-surface-energy materials, poly(vinylidine fluoride), polyamides, and the cellulose acetate, a hydrophilic material that often carries charged surface groups.

The criteria for selecting a membrane depend on the application: the characteristics of the feed solution and the component to be separated, as well as parameters such as permeability, selectivity, mechanical and chemical resistance, and desired thermal stability. Table 1 shows a

general comparison between ceramic and polymeric membranes. Inorganic membranes are the focus of this work and will therefore be presented in greater detail, and more specifically ceramic and zeolite membranes.

Table 1 – General comparison between organic and inorganic membranes.

Ceramic Membranes	Polymeric Membranes
Do not swell	Do swell
Chemically resistant to solvents	Not chemically stable
Resistant to low pH	Degradable at low pH
Thermally stable	Not thermally stable.
	Degradable at high temperatures
High cost of production	Lower cost of production
More brittle	Less brittle

Adapted from Daramola, Aransiola and Ojumu (2012).

Inorganic membranes

Among the inorganic membranes, carbon, metallic, ceramic and zeolitic membranes stand out. A brief explanation of each type will be presented with emphasis to the ceramic and zeolite membranes.

- Carbon membranes are porous inorganic membranes usually obtained from the thermal decomposition (pyrolysis) of polymeric membranes used as precursors, standing out as a promising alternative for gas separation, mainly due to their high separation capability, through the molecular sieving mechanism, compared to polymeric membranes (HAMM et al., 2017).

- Metallic membranes are considered dense membranes, according to IUPAC (1997), having pores smaller than 0.5 nm; therefore, the separation is due to the affinity

of one of the components for the metallic film. Some commonly used metals are platinum, copper, gold, palladium, and silver, each with a specific indication of use. These membranes can be applied in the methane reform and highly pure hydrogen production once palladium, and nickel, for example, have a high affinity with the H_2 gas.

- Mineral membranes are composed by zeolite or other minerals such as peroviskite. Zeolites are hydrated aluminosilicates that have regular microporous structures (3 to 10 Å) and excellent ion exchange capacity, as well as thermal, mechanical and chemical stability (AUERBACH; CARRADO; DUTTA, 2003). Zeolite membranes can be applied in gas separation, catalysis, corrosion protection and solvent dehydration.

- Ceramic Membranes are produced mainly from Al_2O_3, TiO_2, ZrO_2, SiO_2 or a combination of these materials. These membranes are usually composed of several layers of one or more different ceramic materials. The sintering treatment makes the manufacture of the ceramic membrane extremely expensive. Mostly commercialized in disk, plate or tubular configurations (LI, 2007). Can be applied in the separation of solutions under extreme conditions of temperature and pH, and when there are organic solvents in the system.

2.2 Ceramic membranes

Ceramic membranes consist of a metal with a non-metal combination in the oxide, nitride, or carbide form. Alumina (Al_2O_3) membranes are the most applied, but the zirconium (Zr_2O) and silicon (SiO_2) ceramic membranes or a combination of these oxides are also vastly known and studied. These membranes show advantages, as long lifetime, pressure resistance, stability at high temperatures, and the capacity of being chemically inert, like this being widely used in the food, pharmaceutical, and biotechnology industries. Besides, ceramic membranes

have also been used for gas separations and membrane reactors (GALLUCCI; BASILE, 2011). The main limitations in using ceramic membranes are related to the high costs of production (equipment and raw materials) and the reduced packing density in the production of modules compared to polymeric membranes.

Ceramic membranes composed of several layers of one or more different ceramic materials with different degrees of porosity/pore size can be classified as supported (same material) or composite (different materials). These layers are divided into a support layer, one or more intermediate layers, and a selective layer. This asymmetric (anisotropic) structure can also be called gradual or hierarchical. The support layer provides mechanical resistance, while the intermediate layers and the selective layer are responsible for the separation (DA SILVA BIRON; DOS SANTOS; ZENI, 2017; PABBY; RIZVI; SASTRE, 2015). The use of asymmetric ceramic membranes aims to minimize the resistance of the permeate flux. The pressure drop on a porous layer is greater the smaller the pore diameters, as there is a greater restriction on fluid passage.

Some organic components can be used with the purpose of pore formation in the ceramic membrane structure. The organic agent with known particle size is added to the ceramic membrane slurry according to the desired porosity. During the sintering process at high temperatures, thermal decomposition occurs, leaving empty spaces in the membrane structure. Works using the cornstarch as a pore-forming agent were written by Wang *et al.* (2006), Baumann *et al.* (2011), and Dong *et al.* (2011), among others.

2.2.1 Structural and separation membrane parameters

Structural parameters

Ceramic membranes are porous by nature, so the structure of these membranes is directly related to the pores present. Physical parameters such as pore size and distribution, shape, tortuosity, interconnectivity, and density affect the permeate flux and selectivity. The membrane pores will dictate the size of molecules that must pass through it and the transport mechanism.

The pore sizes of the membranes are classified by the International Union of Pure and Applied Chemistry (IUPAC) into macropores (diameter > 50 nm), mesopores (between 50 and 2 nm), and micropores (< 2 nm). Micropores are further subdivided into supermicropores (0.6 nm < d < 2.0 nm) and ultramicropores (d < 0.6 nm) (LOWELL *et al.*, 2004). According to Bhave and Ramesh (1991), the average pore diameter in a membrane is difficult to measure directly. It must often be inferred from the size of the molecules that permeate the membrane or by other indirect techniques. Pores can be thought of as many tubes with tortuous paths. Thus, the mean pore radius of the membrane can be described by the Hagen-Poiseuille (Equation 1)

$$J = \frac{\varepsilon \pi r_p}{8 \mu \delta \tau} \Delta P \qquad \textbf{(Equation 1)}$$

where J is the permeate flux ($m^3 m^{-2} s^{-1}$), ΔP is the pressure drop across the membrane (Pa) and r_p is the average pore radius in meters. μ is the liquid viscosity (Pa s) and τ is the tortuosity. The ε is the surface porosity.

The membrane porosity (ε) is the relation between the membrane empty volumes and the total membrane volume. According to Guechi *et al.* (2015), typical microporous membranes present average porosities in the range of 0.3 – 0.7. Porosity can also be given by the ratio of total pore area ($A_p = n\,\pi\,r_p^2$) to the total membrane area, A_t, (LI, 2007).

$$\varepsilon = A_p/A_t \qquad \textbf{(Equation 2)}$$

Porous media are complex systems, with pore sizes varying over a wide range. Thus, the paths for fluid flow are not straight, but tortuous and winding (GHANBARIAN *et al.*, 2013). The membrane tortuosity (τ) reflects the relation between the average length of the pore and the membrane thickness; it could be related to the asymmetry of the membranes.

Material nature, particle size, shape, arrangement, preparation method and sintering temperature can affect the porosity, therefore, they must be considered when preparing a porous membrane.

Separation parameters

The permeate flux, the hydraulic permeability and the retention/selectivity are the main performance parameters in pressure-driven membrane processes.

For porous membranes, if the driving force is the hydraulic pressure difference, the Darcy's Law is applied as expressed by the Equation 3.

$$J = L_p \,.\frac{\Delta P}{\Delta x} \qquad \textbf{(Equation 3)}$$

where J is the permeate flux (L m^{-2} h^{-1}), L_p is the permeability coefficient (L m^{-1} h^{-1} bar^{-1}), Δx is the membrane thickness (m) and ΔP is the transmembrane pressure (bar). If water is the fluid, the L_p coefficient is called hydraulic permeability, a parameter used to quantify the permeation performance of the membrane.

During the process, the membrane can be compacted, and its thickness becomes unknown. Thus, the Hydraulic Permeance, K, (L m^{-2} h^{-1} bar^{-1}) is considered as the ratio between Lp and Δx (Equation 4).

$$K = \frac{L_p}{\Delta x} \quad \textbf{(Equation 4)}$$

Thus, the permeate flux (J) can be expressed by Equation 5, and the hydraulic permeance can be obtained through the slope of a curve obtained by the permeate flux as a function of the operating pressure:

$$J = K\,\Delta P \quad \textbf{(Equation 5)}$$

The permeate flux and the intrinsic retention of the membrane can be affected due to the accumulation of components on the surface. The accumulation leads to the concentration polarization, in which a layer is concentrated at the membrane interface and offers additional resistance to mass transfer. After reaching stable conditions, the decline in flux is no longer observed, becoming constant over time. An additional pressure increase will not result in an increase in flux (Figure 5), because the resistance of the limit layer has increased so that the limit flux, J_∞, is reached (MULDER, 1996).

The critical flux (J_c) is defined as the flux at which the transmembrane pressure starts to distance from the pure water line, which is represented by the straight line.

Figure 5 – Schema showing the relation between flux and transmembrane pressure.

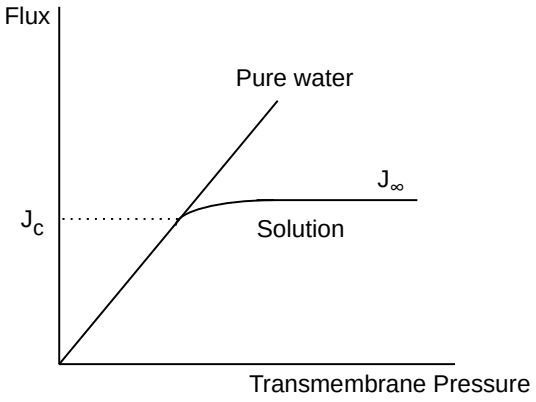

Obtained from Mulder (1996).

The separation mechanism for separating solutes from aqueous solutions using porous membranes is related to the difference between the size of the substance and the size of the pore. The observed retention, R_{obs} (Equation 6), is an important parameter for the characterization of membranes and it is directly related to its selectivity. The R_{obs} represent the fraction of a certain component present in the feed solution retained or rejected by the membrane. The intrinsic or true retention considers the concentration of the component close to the membrane surface (C_b), which, in most cases, is difficult to determine.

$$R_{obs} = 1 - \frac{C_p}{C_f} \qquad \textbf{(Equation 6)}$$

where C_p is the component concentration in the permeate stream and C_f is the component concentration in the feed stream.

The separation of gas mixtures can occur due to differences in molar masses, size or shape, or differences in the affinity between the gas molecules and the membrane surface. Thus, several theoretical models can be used to analyze gas transport data in porous ceramic membranes, the most common being convective flow, Knudsen diffusion, superficial diffusion, and molecular sieve.

The permeate flux through the membrane can be derived from Fick's Law, considering the driving force as the gradient of chemical potential expressed in terms of the partial pressure difference of the components between the feed and permeate sides (Equation 7).

$$J_i = P_i \frac{(p_2 - p_1)}{l} \qquad \textbf{(Equation 7)}$$

where J_i ($cm^3\ cm^{-2}\ s^{-1}$) is the permeate flow of component i, P_i is the permeability in Barrer (1 Barrer = 10^{-10} $cm^3_{(CNTP)}$ cm cm^{-2} s^{-1} $cmHg^{-1}$). The pressures of component i in the permeate and in the feed are p_1 and p_2, respectively.

In asymmetric structures, the thickness of the selective layer is difficult to measure; therefore, the permeability per unit of thickness, or permeability (P_i/L), is more used to characterize the flux through the membrane, using in this case, the GPU unit. (1 GPU = 10^{-6} $cm^3_{(CNTP)}$ cm^{-2} s^{-1} $cmHg^{-1}$).

The permeability (P_i) can also be written in terms of kinetic (D_i) and thermodynamic (S_i) parameters, according to the Equation 8.

$$P_i = D_i \,.\, S_i \qquad \textbf{(Equation 8)}$$

To assess the selectivity of the membrane, the permeability of a pair of gases is generally compared using the ideal selectivity ($\alpha_{i/j}$), which is the ratio between the permeability of the two pure gases i and j, according to Equation 9.

$$\alpha_{i/j} = \frac{P_i}{P_j} \quad \textbf{(Equation 9)}$$

2.2.2 Raw materials for membrane manufacturing

Ceramic materials commonly used for membrane production are alumina (Al_2O_3), silica (SiO_2), zirconia (ZrO_2), Kaolinite [$Al_2Si_2O_5(OH)_4$] and mullite ($Al_6Si_2O_{13}$) (RAHAMAN, 2003). In addition, several materials are studied in order to participate in ceramic membranes synthesis with the finality to decrease the costs associated with manufacturing. Recent research works are focused on the use of cheaper raw materials such as apatite, dolomite, kaolin (GUECHI *et al.*, 2015), clay, silicon carbide (ZHOU *et al.*, 2011), sawdust (BOSE; DAS, 2013), and coal fly ash (FANG *et al.*, 2011; LIU *et al.*, 2016), among others. The coal fly ash (CFA) is a residue from coalmines, and its composition is predominantly silica. This residue was used in this work to reduce the costs of ceramic membranes manufacturing. The materials used for the manufacture of ceramic membranes that are important for this work will be presented in greater detail as follow.

2.2.2.1 Alumina

Nowadays is one of the main applied raw materials for ceramic membranes and supports preparation. The alumina or aluminum oxide (Al_2O_3) is abundant, presents good chemical and thermal stability, and relatively good strength.

The allotropic forms of alumina (α, γ, δ, η, θ, and χ) are generated when the bauxite, the main source of aluminum in nature, is heated. When sintered above 1000 °C, allotropic forms become α-Al_2O_3, the last on the sintering scale and the most thermodynamically stable alumina allotrope, which exhibits melting point of about 2047 °C. If impurities and alloying elements are present, they will melt at significantly lower temperatures (GITIS; ROTHENBERG, 2016).

Al_2O_3 ceramic membranes are normally manufactured by sintering powders of α-Al_2O_3 and γ-Al_2O_3 at high temperatures (> 1300 °C) and have sizes in the order of tens to hundreds of nanometers, making them suitable as support layers for composite membranes (GITIS; ROTHENBERG, 2016).

The most used techniques for producing Al_2O_3 membranes are powder pressing, paste processing, and colloidal processing (MONASH; PUGAZHENTHI; SARAVANAN, 2013).

2.2.2.2 Silica

Another common raw material applied for ceramic membranes manufacturing is SiO_2, silicon dioxide or silica that offers interesting characteristics for the membranes, regarding the separation of gases and liquids (DA SILVA BIRON; DOS SANTOS; ZENI, 2017; GITIS; ROTHENBERG, 2016). The flexibility of Si-O-Si bonds and the “almost” free rotation around the axis give SiO_2 amorphous unique properties, applied for the preparation of thin coatings with layers up to 30 nm and used in molecular sieve processes. According to Benes, Nijmeijer and Verweij (2000), microporous silica membranes have a high potential for gas separation and pervaporation at high temperatures in chemically aggressive environments. Amorphous silica presenting nanometric pores is a suitable material for highly selective membranes. Chemical

vapor deposition (CVD) and sol-gel are common methods for such supported membranes preparation (KIM *et al.*, 2001).

According to Cheraitia *et al.* (2010), microporous silica membranes can be easily prepared by the sol-gel method. However, in conditions of steam in high temperatures, occurs Si–OH removal and Si–O–Si bonds formation, decreasing silica films microporosity. During hydrothermal exposure, Si–O–Si bonds can be hydrolyzed, creating vicinal hydroxyl pairs, which are subject to recondensation. This depolymerization–reconstruction process allows the silica network to relax in a more stable denser structure. This fact can compromise permeability, the selectivity and eventually can lead to the formation of micro-defects, causing silica layer fragility (BOFFA *et al.*, 2013). Fotou, Lin and Pratsinis (1995) studied the hydrothermal stability of microporous silica membranes prepared by the sol-gel process at 600 and 800 °C. The membranes remained microporous after calcination and hydrothermal treatment at 600 °C for 30 h, but there was a 77 % decline in the volume of the micropore, while after the same processes at 800 °C there was complete densification of the membranes.

2.2.2.3 Coal fly ash

CFA is a heterogeneous material, by-product of burning coal, which presents structural qualities and has composition dependent from the coal source, constituted mainly by silica and alumina oxides. In 2011, world coal production reached 7.2 billion tons, with just over 15 % of that total being commercialized (HEIDRICH; FEUERBORN; WEIR, 2013). According to data obtained from Mallmann (2018), more than 3.7 million tons of coal fly ash is produced in Brazil per year. Only a small amount of the total CFA produced is used in cement industry, for paving and brick's manufacture. These data confirm CFA disposal problems and highlights the need

to find other uses for this waste, making it a valuable raw material to participate in the manufacture of ceramic membranes.

Some works already explore the potential of using CFA in the production of ceramic membranes. Jedidi *et al.* (2009) proposed a CFA-based microfiltration membrane for wastewater treatment in the textile industry. For the membrane preparation, first was obtained a macroporous support, then the support was coated by an active microfiltration layer using the slip casting technique. Both the support layer and the microfiltration layer were prepared from the same material, containing 4 wt.% of CFA, 30 wt.% of polyvinyl alcohol (PVA) as binder, and 66 wt.% of deionized water. The water membrane permeability found was 475 L h^{-1} m^{-2}.

Fang *et al.* (2011) synthesized a tubular macroporous support for microfiltration, mixing the CFA with water and methylcellulose to prepare the dough for extrusion. The extrusion method was followed by the slip-casting process to obtain an intermediate and a top layer of CFA aqueous solution with a dispersant and a binder. The results showed a crack-free CFA membrane could be prepared and that the slip concentration, contact time, and speed are the key factors affecting the membrane characteristics. The average water permeability was 1.56 x 10^4 L m^{-2} h^{-1} bar^{-1}, a high value compared to the same type of membranes reported in the literature.

Singh and Bulasara (2015) prepared disk-type membranes using CFA as the major constituent. The sintering temperature effect on membrane properties was investigated. The membranes were defect-free and presented a uniform pore size distribution and an average pore diameter of 1.2 µm when sintered at 900 °C. The pure water permeability of the membranes varied from 1.2 to 5.5 L m^{-2} h^{-1} bar^{-1}. Also, at 900 °C was found the maximum oil rejection of 99.2 % in the oil-in-water emulsion separation, indicating that the membranes with CFA can be applied for microfiltration.

Available literature about using CFA for manufacturing membranes shows the following shortages. Very little information is available about the synthesis of membranes containing larger amounts of CFA (> 10 wt.%). There is a research gap in forming ceramic asymmetric membranes using CFA in just one step, as performed in this work by centrifugal casting technique. In most publications, the authors use expensive organic compounds to bring stability and mechanical strength to the membranes. The use of additives and binders increases raw materials and production costs since a slow thermal treatment is necessary for the safe removal of these organic compounds. Besides, after removal, the organic compounds are released into the environment, becoming an environmental issue.

2.2.3 Techniques for ceramic membranes preparation

Membranes can be synthesized in flat or tubular configurations. Tubular membranes, in comparison to flat membranes, according to Biesheuvel *et al.* (2001), offer a larger surface area since this conformation generally results in a higher packing density, and consequently, higher flow rates. Also, flow profiles are better defined, with less risk of dead zones, and a better match to existing reactor concepts in tubular membrane geometries.

The main processes to prepare ceramic membranes consist of submitting a dry powder to the pressing methods (LORENTE-AYZA *et al.*, 2015) or preparing a dough for being shaped by the extrusion technique (ZHOU *et al*., 2011). In other techniques, a particle suspension, or slurry, is prepared for applying in the slip-casting (FANG *et al*., 2011), tape-casting (DAS; MAITI, 1999), or centrifugal casting methods (KIM *et al*., 2002).

- Pressing – is based on the conformation of a powder, which is inside a rigid or flexible mold, applying pressure. In the uniaxial pressing (Figure 6(a)), the powder or a granular material undergoes simultaneous uniaxial compaction and shaping in a rigid die. The isostatic

pressing (Figure 6(b)) involves the application of a uniform hydrostatic pressure to the powder in a flexible rubber container (RAHAMAN, 2003). The sintering is necessary after the pressing for both operating modes to provide mechanical resistance to the membranes (CALLISTER; RETHWISCH, 2007). The membranes obtained from this technique have a symmetrical structure. Thus, to increase the selectivity and retention of these membranes, oxide layers with different granulometry can be pressed, or the application of coatings using, for example, the sol-gel technique.

Figure 6 – Schema of (a) uniaxial pressing and (b) isostatic pressing processes.

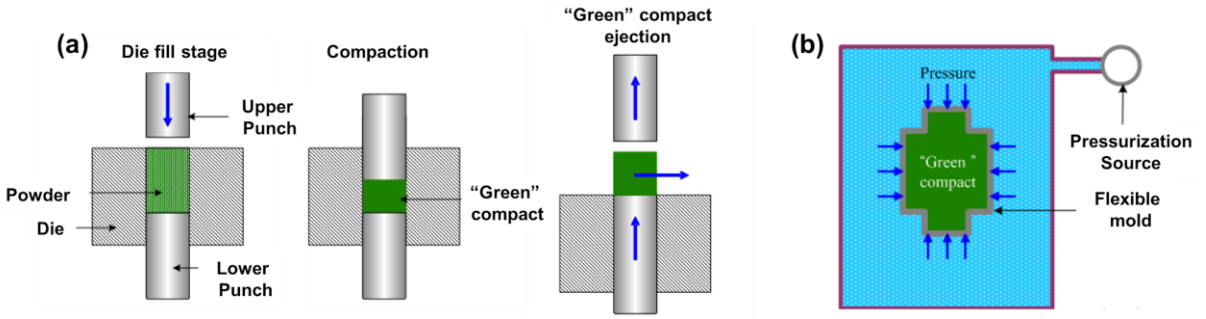

Adapted from www.substech.com.

- Extrusion – the most conventional method of preparing ceramic tubes, the extrusion is a mechanical process where a homogeneous paste is forced through the opening of a die with the aid of an endless screw or drill, acquiring the shape predetermined by the die shape (Figure 7). In the extrusion technique, the choice of the matrix allows the membranes to be produced according to the desired specifications. It is possible to change some parameters, such as the number of channels and inner and outer diameters of the tubes. The membranes prepared using this technique have a homogeneous structure along the cross-section; to increase selectivity and retention, there is the need to apply coatings of other materials (LIANG et al., 2021).

Figure 7 – Schema of the extrusion process.

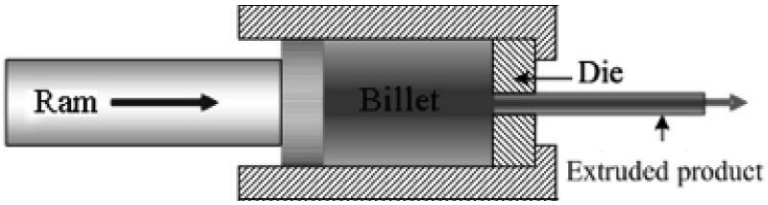

Adapted from https://techminy.com.

- Slip Casting – the slurry, a suspension of particles as clay and/or other nonplastic materials in water, is poured into a porous mold. The water is absorbed by the porous mold and when the liquid is totally removed from the slip, the solid powder material is left in the shape of the mold. As the cast piece dries and shrinks, it will release from the mold. In this way, slip casting is useful for making irregular and complex shapes (Figure 8). It is a low-cost, simple technique, able to produce membranes in any shape, depending on the mold. The drying and heat treatment are more time-consuming. The main difficulty is to obtain stable slurries, which must have a high specific gravity and be fluid and pourable. Such characteristics will depend on the solid-to-water ratio and other agents added (CALLISTER; RETHWISCH, 2007).

Figure 8 – Principle of slip casting process.

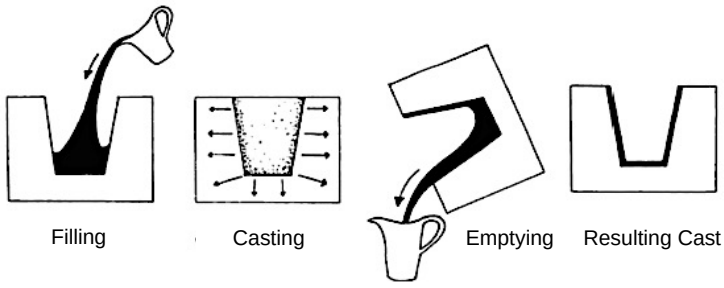

Obtained from Hubadillah *et al.* (2018).

- Tape Casting – produces thin sheets from ceramic slurry cast in a thin layer onto a flat surface, combined with a doctor blade for controlling the membrane's thickness (Figure 9). In the drying process, the warm air source also removes volatile components by evaporation. The slurry consists of a suspension of ceramic particles in an organic liquid with binders and plasticizers incorporated to impart strength and flexibility to the sheets (CALLISTER; RETHWISCH, 2007). After, the obtained green bodies are dried and sintered. It is a low-cost, easy fabrication process, and only flat sheet membranes can be obtained.

Figure 9 – Schema of the tape casting process.

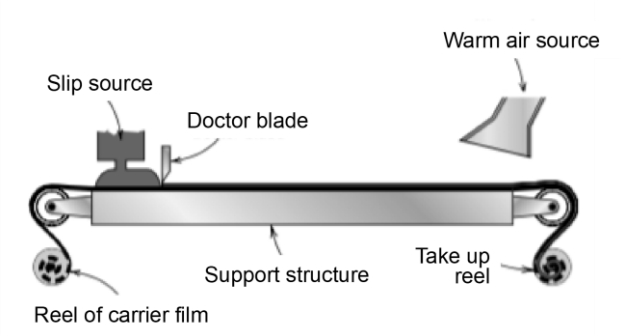

Adapted from Callister, Rethwisch (2007).

2.3 Centrifugal casting

The centrifugal casting is used for tubular membrane preparation. In this process, a cylindrical mold is filled with a suspension of particles with a higher density than the matrix liquid and rotated around its center axis. Subsequently, particles start to move towards the cylinder wall due to the centrifugal force and form a cast with increasing thickness. The solid particles are settled in the tube inner surface, creating a settling gradient along with the tube thickness due to the different particle sizes (KIM *et al.*, 2002; NARENDRANATH;

KUMAR, 2013). After cast release and proper post treatment, a firm and homogeneous tubular structure can be obtained (Figure 10).

Figure 10 – Centrifugal casting process schema.

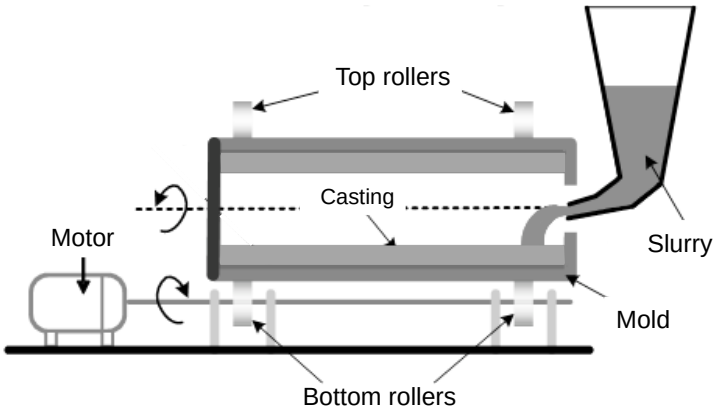

Adapted from www.substech.com.

Structures made by centrifugal casting have distinct properties compared to more traditional techniques as extrusion and isostatic pressing. This technique is suitable for manufacturing high-quality tubes with homogeneous particle packaging and a smooth and dense inner surface, ideal for the deposition of a thin and defect-free top layer. From the variation of the initial characteristics of the colloidal suspension and the process parameters, it is possible to obtain membranes with distinct structures, symmetrical or asymmetrical (BIESHEUVEL *et al*., 2001; BISSETT; ZAH; KRIEG, 2008; MERTINS; KRUIDHOF; BOUWMEESTER, 2005).

According to Biesheuvel *et al*. (2001), supports made from this technique can combine the settling of small particles on the inner surface with large particles over the external part, resulting in high permeance of the support when compared to supports consisting of the same inner surface particles.

Sacks, Lee, and Rojas (1988) stated that when suspensions are prepared with a unique powder type, the settling classification occurs due to particle size distribution; first, the larger particles move to the mold wall, followed by the smaller particles. Meanwhile, in suspensions with assorted powder types, in general, the ordination occurs due to particle sizes and/or densities differences; particles with higher density and/or larger size tend to concentrate in the outer sample surface, and smaller or lower density particles accumulate in the inner tube side.

Chen *et al.* (2005) synthesized porous alumina tubes with homogenous microstructures in centrifugal casting equipment. The commercial alumina was mixed with polymethylmethacrylate (PMMA) with two different particle sizes as a pore-forming agent. The proportion between PMMA fine and coarse particles was used to control the pore morphology. Porosity values increased linearly with increasing PMMA amount.

Huisman, Graule and Gauckler (1995) proposed the synthesis of high reliability alumina membranes with centrifugal casting to compare with isostatically pressed alumina membranes. The authors studied the solids loading, suspension conditions, sedimentation velocity, centrifugal acceleration, sintering behavior and microstructures. Homogeneous microstructures were achieved by centrifugal casting of α-alumina. The wet processing, associated to the centrifugal method, provided better particle packing and a lower flaw incidence when compared to the dry process.

2.3.1 Formation of colloidal dispersion

The successful fabrication of ceramic membranes is a task that demands expertise on choosing appropriate raw materials and methods. Is necessary for that, understand the constituents and their rheological characteristics, once it has directly influence in the final

membrane (KUMAR; GHOSHAL; PUGAZHENTI, 2015). The addition of a second phase to dispersed slurry introduces numerous possibilities for changing the rheological behavior and other phenomena, which may include coagulation, differential sedimentation, enhanced dissolution reactions, and specific adsorption (FISHER *et al*. 2001).

The use of colloidal techniques for the consolidation of powders from a suspension increased after the realization of the importance of the green body microstructure on the subsequent firing stage (RAHAMAN, 2003). The formation of the colloidal dispersion in the centrifugal casting technique is of great importance for the consolidated membrane. The study of the characteristics of the powders in the colloidal dispersion, such as the particle size distribution, together with the firing process can guide to the definition of the final body microstructure. The use of powders with large particle size results in membranes with high porosity and permeability, and low linear shrinkage and mechanical resistance, when compared to those produced with small particles, for the same process conditions, i.e., centrifugal velocity, drying and sintering temperatures (BISSETT; ZAH; KRIEG, 2008; KIM *et al*., 2002; STEENKAMP *et al.*, 2001).

Small particles suspended in a liquid move randomly, which is called Brownian movement, generating particle-particle collisions. The stability of colloidal suspensions is directly dependent on how the particles interact during these collisions. Often are formed clusters, caused by Van der Walls forces, sequestering part of the liquid available what decreases the distance between the particles, increasing collisions and thus increasing the suspension's viscosity. In presence of these cluster or agglomerates, the sedimentation process is favored, hindering homogeneity and stability. In this case, agglomerates can generate pores in the structure, impairing the mechanical properties of the sintered bodies. Dispersed suspensions are less viscous and therefore allow the use of higher concentrations of solids

during processing. These suspensions allow the formation of compact green bodies with high density and a homogeneous microstructure, due to the good packaging of the particles. In addition, it results in low shrinkages in the formed bodies during drying and sintering (OLIVEIRA *et al*. 2000; REED, 1995).

In the centrifugal casting technique, the use of different particle sizes promotes a settling gradient along the thickness of the tube. The microstructure of the non-uniform tube presents also a gradient of porosity, which can lead to the breakage of the tubes during drying and/or sintering steps. This limitation can be overcome by using suspensions with high solid contents (> 40 wt.%). However, a high quantity of solids increases the viscosity and requires high centrifugal accelerations to obtain a uniform microstructure, hindering practical application (KIM *et al*., 2002). The use of certain additives is often applied to control the characteristics of the feed material, to obtain the desired shape and to control the uniformity of packaging of the green body. The additives are of organic or inorganic composition. Organic additives are more useful in the formation of advanced ceramics, as they can be removed almost completely by thermal methods (pyrolysis). While inorganic additives are used when they do not harm the final product (RAHAMAN, 2003). The additives may be divided into four main categories:

- Solvents – applied to provide fluidity to the powder during ceramic formation and disperse and/or dissolve additives.

- Dispersants (or deflocculants) – applied to increase the repulsion between the particles, avoiding flocculation, to stabilize the slurry.

- Binders – applied in order to providing strength to the green body by forming bridges between the particles.

- Plasticizers – applied to soften the binder in the dry state, increasing the

flexibility of the green body.

2.3.2 Drying, thermolysis and sintering

After the green body formation, drying, thermolysis and sintering are the three stages of heating that give the membrane its final properties (Figure 11).

Figure 11 – Scheme of the three thermal stages used in the preparation of ceramic membranes.

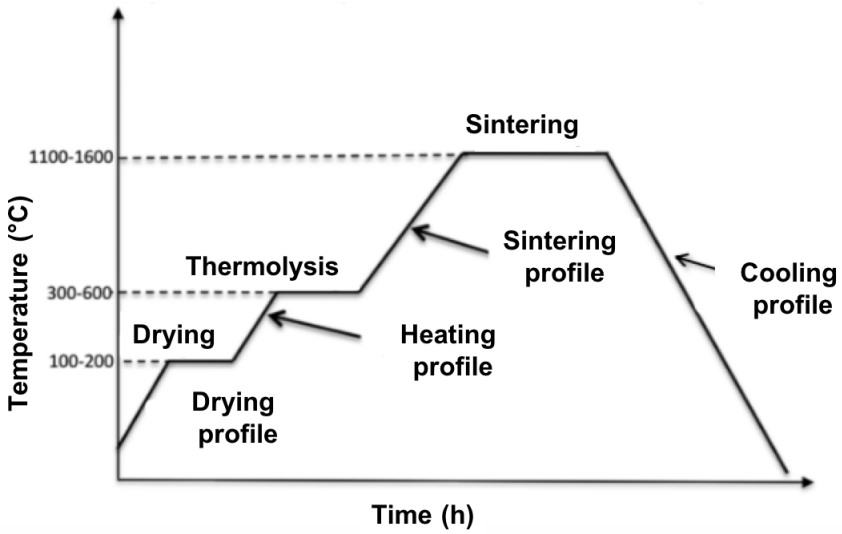

Adapted from Gitis and Rothenberg, 2016.

Drying

Drying is the initial thermal stage and occurs at room or elevated temperatures. In this step, occurs the vaporization of water chemically combined from the surface of the particles or formed within inorganic phases. The adsorbed moisture can persist in the membrane material up to a temperature above 200 °C. Therefore, care must be taken to avoid cracks in the material due to the stresses of the vapor pressure released or the differential thermal expansion of the phases. At this moment the solvent evaporates while the grains are moving closer to each other

until they come into direct contact. The ceramic body shrinks to what will become the final membrane structure. The resulting green body has the desired shape, but it is still weak (GITIS; ROTHENBERG, 2016; LI, 2007).

Thermolysis

Thermolysis is a process in which the organic components such as binders and dispersants suffer degradation at high temperatures. Incomplete binder removal and uncontrolled thermolysis may introduce membrane defects. These defects may decrease the performance of the membrane. With the proper choice of binders for the membrane and controlled heating in an appropriate atmosphere, the membrane structure should survive thermolysis without deformation, distortion, formation of cracks or expanded pores (GITIS; ROTHENBERG, 2016; LI, 2007).

Sintering

Sintering is normally thought to occur in three stages: initial, intermediate, and final stage. The movements of particles have different features at each stage and are attributed to full density with initial neck contact, grain coarsening and pores closing (GITIS; ROTHENBERG, 2016; LI, 2007).

The high temperature applied leads to the solid softening and, consequently, to the material densification and retraction favoring. According to Xue and Chen (1991), the use of fine starting powders, elimination of agglomerates and use of additives can improve the materials sintering, reducing temperature necessary to densification and structure porosity. As

sintering densification occurs, and grains disappear, new contacts between grains are formed and local growth or shrinkage starts.

Sintering occurs over a range of temperatures but is accelerated as the particles approach their melting range. It takes place faster as the particle size decreases, since diffusion distances are shorter and curvature stresses are larger (GERMAN; SURI; PARK, 2009). The processes involved in the sintering stage are presented in Figure 12. All these mechanisms would lead to growth of necks between particles. The neck growth produces bonding between the particles, so the strength of the consolidated powders increases during sintering (LI, 2007).

Figure 12 – Schema demonstrating spherical grains and the mass transport processes involved during sintering process.

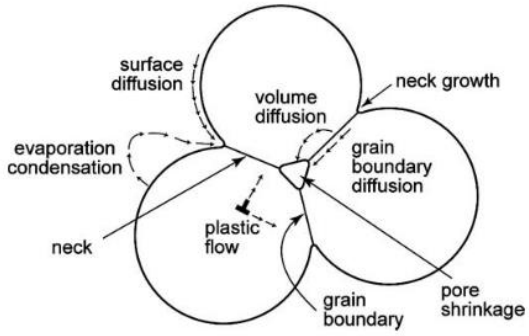

Obtained from German (2010).

The grain growth, according to German (2010) can occur in two ways. On the one hand, when the grain is surrounded by similar grain sizes, there is the occurrence of what is called “neck growth” (boundary between two grains), and material coalescence followed by shrinkage. On the other hand, if the grain is surrounded by larger grains, it will be consumed to accommodate the larger grains growth.

2.4 Composite membranes

Desirable properties for membrane separations typically include a combination of high fluxes and selectivity, mechanical, chemical, and thermal stability under the applied operating conditions, long and reliable lifetime, and accessible production costs. Besides, the transport resistance in most ceramic membranes is very high due to their symmetric structure. The permeation flux depends on the thickness of the membrane, usually being inversely related to the membrane thickness. Therefore, it is necessary to develop a technique for fabricating thin membranes to maximize the permeation flux. Many attempts are being made to reduce the thickness of the membranes; most of these efforts have been based on the concept of composite membranes where a dense thin film is coated on a porous substrate by various methods such as spin-coating or dip-coating, chemical vapor deposition and some other methods. The film thickness must be well controlled. In general, it is quite difficult for one single material to satisfy all these requirements (DAVID; KOPAC, 2011). When the top layer material is different from substrate material, the top layer is usually unstable especially at elevated temperature.

The quality of the support surface is of crucial importance to the membrane integrity since this part directly interacts with the top-layer membrane. Supports made from ceramic materials provide the mechanical strength on which a metallic, carbon or zeolitic films can, successfully, be deposited.

The **metallic** membranes are generally used for hydrogen separation and purification due to the affinity of some metals as Vanadium, Niobium, Tantalum, Palladium, Nickel and others to the hydrogen. The H_2 transport in metallic membranes occurs through the solution-diffusion mechanism with hydrogen adsorption, dissociated into H atoms, in the metallic film. Diffusion in the layer, recombination of hydrogen atoms and, finally, H_2 molecule desorption. The metal deposition methods available in literature are the Chemical Vapor Deposition (CVD),

Physical Vapor Deposition (PVD), Sputtering, Electrochemical methods using electric current and Electroless Plating (ABEGUNDE *et al*., 2019).

The **carbon** membranes can be obtained by thermal decomposition (pyrolysis) of polymeric precursors in an inert atmosphere or vacuum. Poly(furfuryl alcohol), phenolic resins, polyacrylonitrile, coal tar, poly(ether imide), polyimides are the precursors for such membranes. Due to the fragile characteristic of the thin carbon selective layer, the carbon membranes must be manufactured along with the porous support, usually ceramic or metallic, for commercial purposes. Thus, a membrane is formed with improved mechanical resistance and thermal stability, supporting high temperatures and pressures, ideal characteristics for gas separation in several applications (HAMM, 2018).

During the last few years, ceramic and zeolite-based membranes have begun to be used for a few commercial separations. These membranes are composite structures formed by coating a thin selective zeolite layer onto a porous ceramic support, presenting exceptional selectivity for several important separations (BAKER, 2004). Zeolite's top-layers have a specific pore size and chemical properties to ensure the required separation of specific mixtures.

2.5 Zeolites

Zeolites are hydrated microporous crystalline aluminosilicates composed of alkaline or alkaline earth metals, mainly sodium, potassium, magnesium, and calcium. Are structured in three-dimensional crystalline networks, composed of a tetrahedra type TO_4 (T = Si, Al) connecting the neighboring tetrahedrons through oxygen atoms. Figure 13 shows a basic zeolite arrangement with the siliceous and aluminum framework. A tetrahedra composed only by Si–O is neutral, once the 4+ charge at the silicon is balanced by four oxygen atoms, with charge 2-, belonging to two tetrahedra (STÖCKER, 2005). When occurs the Al substitution, the 3+

charge on the Al makes the tetrahedra structure negatively charged. The charge requires a balance with a proton or a cationic metal to turn the structure back into neutral (AUERBACH; CARRADO; DUTTA, 2003). The cations, represented by H^+ in Figure 13, are called extra-framework or compensation cations and are exchangeable, giving the zeolites an important ion exchange capacity.

The tetrahedra are the Basic Building Units (BBU) of zeolites. When connected in rings, the BBUs will originate the Secondary Building Units (SBUs). The way these BBUs and SBUs are organized and linked to each other establishes chains, which may build innumerous three-dimensional structures (BROACH, 2010). According to Auerbach, Carrado, and Dutta (2003), as a result, channels are created in the intercrystalline spaces, which constitute the zeolite pores.

Figure 13 – Basic zeolite structure

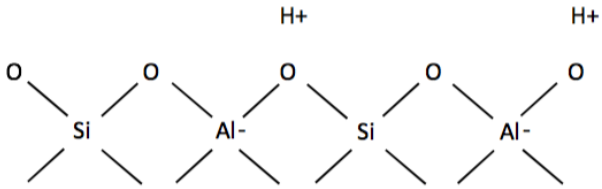

Adapted from Stöcker (2005)

The zeolites can be found in the nature or can be synthesized. The Al in the structure varies over a wide range, and in this way, it is possible to have the relation Si/Al varying from 1 to infinity. As the Si/Al ratio of the structure increases, both the hydrothermal stability and the hydrophobicity increase. Some examples of zeolites and their Si/Al ratios can be cited (AUERBACH; CARRADO; DUTTA, 2003).

- A and X zeolites: Si/Al ratio ≤ 2 (low).
- Y zeolite: $2 <$ Si/Al ratio ≥ 5 (intermediary).

- ZSM-5 zeolite: Si/Al ratio > 5 (high).

According to Stöcker (2005) and Tavolaro and Drioli (1999), the zeolites are widely used due to their catalytic properties. Also, the zeolites present other interesting properties such as a high degree of hydration, thermal stability, cation exchange, and reversible dehydration, a microporous character with uniform pore dimension and the high adsorption of gases and vapors, which gives to the zeolites the ability to act as molecular sieves. The selectivity of zeolites is the basis for their use in molecular adsorption. This ability to adsorb certain molecules while excluding others has opened up a wide range of uses in separation and purification processes.

Table 2 - Main zeolites studied in the literature. Adapted from Julbe (2007).

Zeolite	Pore size (Å)	Application
Sodalite (SOD)	2.8	GS, PV
Sapo 34 (CHA)	3.8	GS, PV
Na-A (LTA)	4.2	GS, PV, MR
ZSM-35 (FER)	5.4	PV, GS
ZSM-11 (MEL)	5.4	PV
Silicalite-1 (MFI)	5.6	GS, PV, MR, VP
ZSM-5 (MFI)	5.6	GS, PV, MR, VP
Linde-T (ERI-OFF)	5.1 – 6.8	PV, MR
Mordenite (MOR)	7.0	PV, GS
Na-X and Na-Y (FAU)	7.4	GS, PV, MR, VP
Beta (BEA)	7.6	GS, PV, MR

GS = Gas Separation, PV = Pervaporation, MR = Membrane Reactor, VP = Vapor Permeation

The Si/Al ratio can determine the character hydrophobic or hydrophilic of the zeolite. Low silica content zeolites are hydrophilic, while high silica content zeolites are hydrophobic. The transition occurs around a Si/Al ratio equal to 10 (AUERBACH; CARRADO; DUTTA,

2003). Zeolites with a higher silica/alumina ratio are used for catalytic applications in cracking and isomerization; they can remove and recover organics from water streams and carry out separations and catalysis in the presence of water. As the Alumina content is increased, the acid resistance and thermal stability of the zeolite reduce. Low and intermediate Si/Al zeolites are used to remove water from organics and carry out separations and catalysis on dry streams (FLANIGEN; BROACH; WILSON, 2010).

The main studied zeolites are displayed in Table 2 with the maximum pore size and main applications. A three letters framework type code from The International Zeolite Association (IZA) is also exhibited.

The MFI framework (ZSM-5 and Silicalite-1) presents a three-dimensional pore system consisting of sinusoidal 10-ring channels (5.1 x 5.5 Å) and intersecting straight 10-ring channels (5.3 x 5.6 Å). The ZSM-5 is one of the most studied MFI zeolites. Argauer and Landolt patented the crystallization and preparation of the ZSM-5 in 1972. This framework can be prepared, according to Auerbach, Carrado, and Dutta (2003), with Si/Al ratios from about 8 to infinity. This MFI zeolite has a high thermal and acid stability and consists of a system of intersecting straight channels, as shown in Figure 14.

Figure 14 – ZSM-5 channels structure with the pore sizes in directions a-b and the typical prismatic crystal or coffin-shaped.

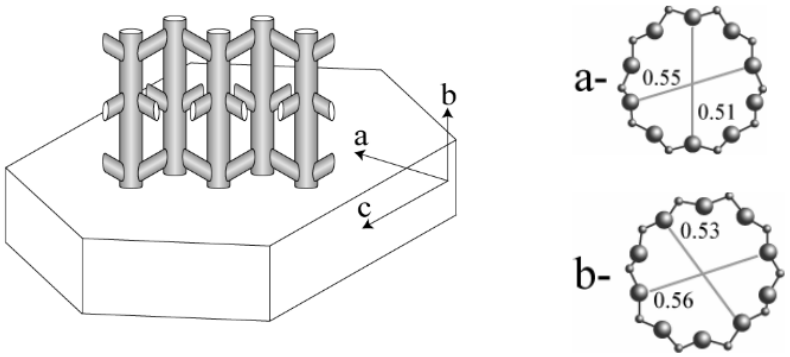

Image from Andersson (2007).

The ZSM-5 presents void volume around 0.17 mL g^{-1} and pores of 0.51 to 0.56 nm, offering the range to the motion important of industrially interesting aromatic compounds as benzene and para-xylene (VAN DER GAAG, 1987). The ZSM-5 pure silica form is silicalite-1.

2.6 Zeolite membranes

Over the last decade, much attention has been focused on the development of continuous zeolite-based separation processes. For such purposes, the natural configuration of the zeolite material is in the form of a thin film or membrane supported on or deposited in a porous substrate. A well-fabricated zeolite membrane would be expected to behave as a continuous separation device, with reasonably high selectivity and flux (AUERBACH; CARRADO; DUTTA, 2003).

MFI-type zeolites are the most studied for the preparation of zeolite membranes. MFI-type zeolites are easy to prepare, leading to a greater understanding of synthesis and the production of promising membranes (KOSINOV *et al*., 2016). Also, zeolites of the MFI type

have pores of a convenient size, and it is possible to modify their chemical composition, which makes them interesting industrially (JULBE, 2007).

The zeolite can be self-supported or prepared on a porous support. Various types of supports as α-Al_2O_3, γ-Al_2O_3, TiO_2, SiC, ZrO_2, or mullites, as quoted by Julbe (2007), have been used for the synthesis of supported zeolite membranes. The support shape, chemical composition, porous structure (pore size, pore size distribution, porosity), microstructure, macrostructure, and pre-treatment influence considerably in the membrane characteristics. Also, many factors may influence the zeolite coatings, including gel composition, time, support, crystal orientation, temperature, synthesis procedure and Si/Al ratio. These factors can be manipulated to produce the desired characteristics for a selected reaction and/or separation (BASILE, 2013).

Defects on the zeolite membranes are defined as intercrystalline spaces that are larger than zeolite pores. Such intercrystalline pores decrease the selectivity and can be minimized by optimizing membrane preparation or by selectively blocking. Permeation of molecules that are too large to adsorb in MFI pores can be used to estimate defect sizes (YU; NOBLE; FALCONER, 2011).

2.6.1 Methods for zeolite membrane preparation

The synthesis solution is the reaction medium for the formation of zeolite. Briefly, according to Cundy and Cox (2005), the zeolite synthesis can be explained as: firstly, the amorphous reactants containing silica and alumina are mixed with a cation source, usually in a basic medium. These oxide elements containing Si – O and Al – O bonds will build the zeolitic structure. The aqueous reaction mixture is heated, at temperatures higher than 100°C in a sealed

autoclave. For some time after raising the synthesis temperature, the reactants remain amorphous. Gradually, after the ‘‘induction period’’, the amorphous material is entirely replaced by crystalline zeolites containing Si-O-Al linkages (Figure 15). The zeolite is recovered by filtration, washing and drying.

Figure 15 – Simplified schema of hydrothermal zeolite process.

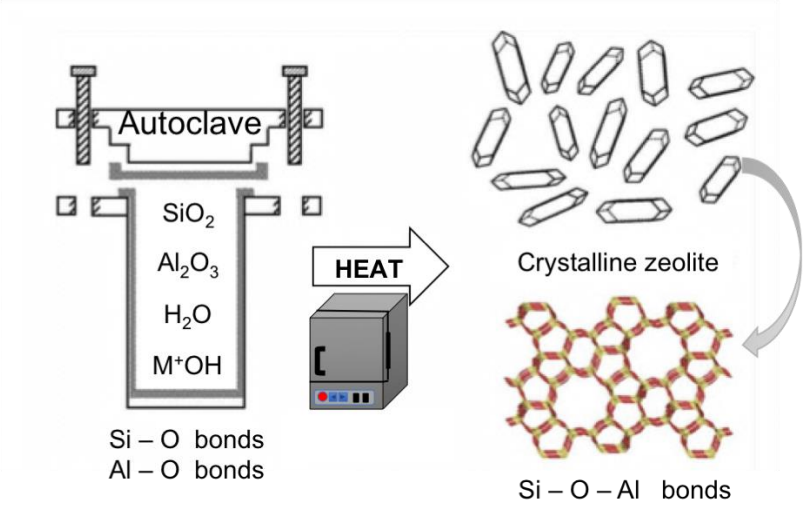

Adapted from Cundy and Cox (2005).

Several sources of silicon (tetraethylorthosilicate (TEOS), colloidal silica (LUDOX®, Levasil®), fumed silica (AEROSIL®, Reolosil®) and sodium silicate) and aluminum (aluminum sulfate, aluminum hydroxide, sodium aluminate or aluminum foil) can be used (GAVALAS, 2006). The use of colloidal silica and sodium silicate leads to a greater selectivity of MFI zeolite when compared to the use of precipitated silica and sodium silicate (OTAKE, 1994). These authors suggest that this is due to the rapid rate of dissolution of these materials. As an aluminum source, sodium aluminate is given because it is in an anionic form.

Along with these, mineralizing agents and a source of cations are added in, generally, high pH medium containing water as a solvent (PAILLAUD; PATARIN, 2016). The mineralizing agent most used is the anion OH^- (sodium and potassium hydroxides, for

example). The functions of the mineralizing agent are to convert the reactants (sources of silicon and aluminum) into mobile forms, to provide chemical reactivity so that these mobile forms react to form the zeolitic structure, and, finally, to disconnect from this new structure so that it exists as a stable solid phase. In other words, the mineralizing agent promotes the dissolution of silicon and aluminum, accelerates the crystallinity growth and shortens the induction period (VISWANATHNATHAN; SIVASANKER; RAMASWAMY, 2002). In a way, it can be said that the mineralizing agent acts as a catalyst for the synthesis of zeolite (CUNDY; COX, 2005). Also, the amount of water influences the geometry of the crystal and, therefore, the type of zeolite formed. It is believed that water interacts strongly with the cations present in the solution. The zeolitic structure formed around this hydrated cation will have the size of its opening controlled by the size of the hydrated cation (SZOSTAK, 1989).

The induction period is the time between the start of the reaction and the point at which the crystalline product is first observed. The reaction mixture contains small crystals of zeolite, already formed and in the growth phase. After induction period, changes in the amorphous phase involve an increase in structural ordering but without the establishment of the final zeolite lattice. For this, the nucleation, i.e., the time to form a stable nucleus has to occur. The discreet step of nucleation provides a discontinuity in which is provided the establishment of a periodic crystal lattice, capable of propagation. The crystal growth stage occurs through a construction process from small, mobile species ordered by the participating cations (CUNDY; COX, 2005).

The formation of a zeolite membrane requires the development of a homogenous and defect-free layer of zeolite crystals, ensuring exclusive transport within the zeolite pores. Factors such as crystallization rate, type of zeolite, size, distribution, and morphology of the crystals are susceptible to parameters such as the synthesis temperature, aging, seeding, alkalinity, dilution, silica-alumina ratio, presence of inorganic cations, the concentration of the

organic template, and also the order of reagent mixture (AUERBACH; CARRADO; DUTTA, 2003; BRECK, 1974).

The methods to obtain a supported zeolite membrane are the in-situ direct crystallization, secondary growth crystallization, and the dry gel method (JULBE, 2007).

2.6.1.1 In-situ hydrothermal crystallization

The hydrothermal synthesis comprises the zeolite nucleation and crystallization taking place with a silica source, an alumina source, a mineralizing agent, and in presence, or not, of a structure-directing agent (OSDA). The process occurs in a closed hydrothermal system (Teflon® and autoclave) in controlled temperature, for hours or days, which creates an autogenic pressure. In the *in-situ* crystallization method, the porous support is immersed into the hydrothermal synthesis solution. The result is a thin and homogeneous zeolite film formed on the surface of the support.

Membranes synthesized by this method reveal the significant dependence on the characteristic of the support surface. According to Mintova *et al.* (1998), the chemical and structural properties of the surface must favor the crystallization of the zeolite. Although this compatibility depends mainly on the surface properties, it is also affected by the composition and crystallization conditions. *In-situ* hydrothermal synthesis usually needs a long crystallization time of few hours to few days. It can lead to the inconvenient crystallization of more than one type of zeolite (WEE; TYE; BHATIA, 2008).

2.6.1.2 Secondary growth crystallization

Secondary growth crystallization involves the growth of a layer of seed crystals previously nucleated and deposited on the support. The seeding process is followed by the *in-*

situ hydrothermal synthesis. Mostly, the supports are seeded by simple contact (dip-coating for a few minutes) with a suspension of zeolite crystals at an appropriate pH and subsequent washing to keep only a surface monolayer. Other methods to seed the support include slip-casting, vacuum using cross-flow filtration, and electrophoretic deposition in an aqueous or non-aqueous medium (JULBE, 2007).

The seeding method uses commercial or homemade zeolite crystals as seeds to create active sites for growing larger crystals, shifting the equilibrium toward crystal formation. This procedure is typically applied for solutions during recrystallization processes, thus eliminating the need for molecular collision/interaction and decreasing significantly the time required for nucleation.

The decoupling of the nucleation step (at high supersaturating) from the crystal growth (at low supersaturating) makes the formation of a zeolite membrane very rapid compared to direct growth without seeding. As the concentration needed for secondary growth is lower than that for nucleation, further homogeneous nucleation is avoided, and crystal growth occurs only on the existing seeds. Therefore, controlled support seeding is of great importance for growing uniform and good quality membranes, preferably with low infiltration into the porous support (JULBE; DROBEK, 2016). Through the control of composition and concentration of the secondary growth solution, the crystallization of undesired zeolite phases can be avoided, and the direction of crystal growth can be controlled (GORGOJO; IGLESIA; CORONAS, 2008).

2.6.1.3 Dry gel method

The dry gel method consists of depositing a dry aluminosilicate gel on the support and subsequent zeolite crystallization under vapors of amine and/or water. The main advantage of this method is the reduction of reactants waste. However, the large volume shrinkage during

the transformation from gel to zeolite often causes defects in the films (JULBE, 2007; GORGOJO; IGLESIA; CORONAS, 2008).

2.6.2 Use of organic structure-directing agents (OSDAs)

The use of OSDAs in synthetic zeolites resulted from the purpose of producing zeolites with lower Al contents. Since zeolites prepared in the presence of inorganic cations have high Al contents due to the need to balance the abundant presence of these inorganic cations. The introduction of organic cations enabled the synthesis of zeolites with high Si/Al ratios (greater than 10), which leads to higher hydrothermal stability and stronger Brønsted acidity. Using OSDAs, the discovery of important zeolites for the chemical industry was possible. Since then, it is known that the addition of OSDA leads to the crystallization of a specific type of structure and that there is a structural relationship between the molecular size and shape of the OSDA and the zeolite structure that crystallizes. (GÓMEZ-HORTIGUELA; CAMBLOR, 2017).

In the process of preparing supported zeolitic membranes in which the formation of the zeolitic layer occurs *in-situ*, the use of OSDA can lead to the formation of defects in the membrane at the time of removal, in addition to these compounds having a high cost and being generally toxic (VIEIRA; RODRIGUES; MARTINS, 2014). According to Gorgojo, Iglesia, and Coronas (2008), a defect-free membrane, after the synthesis of the zeolitic film with OSDA, generally, is nonpermeable due to the obstruction of pores by the template. A heat treatment using temperatures between 350 and 600 °C, reaching 950 °C for small pores, is necessary the elimination of the organic template, which is called the membrane “activation”. The activation step must be accomplished using an appropriate temperature program. Cracks can be generated due to the stress developed by differences in the expansion and contraction of the support and the zeolite framework during the heating and cooling processes.

As observed by Hedlund *et al.* (2009), the MFI crystals first experience a weak contraction at about 175 °C due to dehydration and a strong contraction for the OSDA removal between 275 e 500 °C. Meanwhile, the alumina support expands, and defects and cracks may be created, reducing the separation performance. Although zeolite membranes synthesis can be obtained using a template under controlled synthesis conditions, Dong *et al.* (2000) also depicted the enlargement of the intercrystalline gaps with suitable template removal. These gaps constitute the microporous non-zeolitic pores affecting the permselectivity of single-gas permeation.

In order to avoid the possibility of defects in the structure due to the use of OSDAs and decrease the costs considerably, several studies have developed template-free zeolite membranes. Pan and Lin (2001) used the secondary growth process with a silica sol without an organic template to obtain high-quality MFI zeolite membranes on porous α-alumina supports. Li, Kikuchi, and Matsukata (2003) synthesized thin ZSM-5 zeolite membranes successfully on the surface of porous α-alumina tubes by secondary growth method in the absence of organic templates. In the same way, Kalipçilar and Çulfaz (2006) synthesized a template-free ZSM-5 film on macroporous α-alumina plate supports. It was found an influence of Si/Al ratio on the synthesis gel, crystal morphology, surface coverage, and intergrowth among the crystals. Prismatic ZSM-5 crystals covered the disk surface when the Si/Al ratio was higher than 100, whereas spherical polycrystalline particles of ZSM-5 were obtained with a Si/Al ratio of 80. Mordenite type zeolite was formed due to the incorporation of alumina dissolved from the support when crystallization was extended to 168 h.

2.6.3 Separation in zeolite membranes

The mechanisms of transport of species across zeolite membranes can be sorption-diffusion, Knudsen diffusion, and/or molecular sieving. Mixtures will be separated due to differences in sorption or diffusion rate or differences in size between species (GAVALAS, 2006). Two types of pores are considered: zeolitic pores or intracrystalline micropores and intercrystalline mesopores, which are the defects, cracks, or pinholes in the structure and through which the compounds are also transported.

Sorption is influenced by the interaction of species with the membrane and occurs on the membrane surface. This step is controlled by thermodynamics. Meanwhile, transport by diffusion is controlled by kinetics and is related to how the molecule is transported across the membrane (HABERT; BORGES; NOBREGA, 2006). The adsorption-diffusion mechanism is also applied to the intercrystaline pore, or defects (YU; NOBLE; FALCONER, 2011). If the pores are smaller than the average free path of the gas, the average distance traveled by a molecule between collisions, the diffusing molecules have more collisions with the pore walls than with other molecules. In this case, the mechanism for gas permeation is called Knudsen Diffusion. On the other hand, the separation occurs through the molecular sieve mechanism if the transport is based on the differences in size and shape of the molecules, so molecules of smaller or similar size to the zeolite pore sizes will cross the barrier more easily (MULDER, 1996).

2.7 Zeolite Membranes Applications

The main applications of zeolite membranes are in the pervaporation and gas permeation processes, microdevices, and catalytic membrane reactors. The zeolite properties are undoubtedly attractive for membrane applications. Among these properties can be

highlighted high thermal stability, acidic or basic properties, hydrophilic or hydrophobic character, possible ion exchange, and the regular zeolitic pores with molecular dimensions, which allow applications in the separation of compounds by size and shape selectivity (JULBE, 2007).

To Auerbach, Carrado, and Dutta (2003), the zeolite ability of ion exchanging is one of their most important properties. Once the channels of zeolites are modified by the ion exchange, interesting and valuable ion separations are allowed. One example is the possibility to remove radioactive ions from contaminated waters.

Mordenite, zeolite Y, zeolite A, and ZSM-5 were already depicted as membranes for pervaporation applications due to some particularities, as the pore structure, the adsorption properties, and the mechanical, chemical, and biological stabilities. Pervaporation can be applied for breaking azeotropes and solvents dehydration, among other processes, separating components that are incompatible with distillation conditions (WEE; TYE; BHATIA, 2008). The removal and recovery of volatile organic compounds (VOC), which are among the principal air pollutants, is another important application using hydrophobic molecular sieves, highly siliceous zeolites as Y and silicalite. (FLANIGEN; BROACH; WILSON, 2010).

In the catalytic field, use of membranes in reactors aims to increase the conversion of the reaction by shifting the balance (removing products) or removing inhibitors from the catalyst. Hydrocarbon transformations, as molecules cracking, dehydration and isomerization, are possible due to the strong acidity of certain zeolites prepared via pathways as the exchange of NH_4^+ ion (AUERBACH; CARRADO; DUTTA, 2003). The reactivity and selectivity properties of zeolites as catalysts are determined by active sites provided by an imbalance in charge between Si and Al ions in the framework. Each Al atom contained within the framework structure induces a potential active acid site. Brønsted and Lewis acid models of acidity classify

the active sites on zeolites (SZOSTAK, 1989). The ion exchange step using an ammonium salt and heat treatment to decompose the remaining ammonium ions inside the zeolites generates Brønsted acid sites in the zeolites. In the dehydration of organics, the hydrophilic zeolite membrane adsorbs the water molecule and facilitates the process conditions, making them more feasible. The organic dehydration process originally occurs under extreme temperature conditions, between 600 and 1000 °C (JULBE, 2007).

Although the concentration of acidic sites decreases with an increase in the Si/Al ratio, the acid strength increases with a decrease in the aluminum content. Some methods are applied to determine the acidity of zeolites. One method is temperature-programmed desorption (TPD), which exploits the thermal energy necessary to separate a base, usually NH_3 or pyridine, from strong and weak acidic sites. Information on the quantity and distribution strength of the acidic sites of these materials can be obtained from the TPD/NH_3 profile. However, this method cannot distinguish between Brønsted or Lewis sites. Infrared spectroscopy is used to determine the bonds of hydroxyl groups and thus identify the types of acidic sites. The vibrational frequencies are distinct, with the Lewis-linked site appearing at 1450 and 1600 cm^{-1}, and the Brønsted-linked site appearing at 1520 and 1620 cm^{-1}. Therefore, the presence of the sites on surfaces can be evidenced from the adsorption of molecules, such as pyridine, capable to adsorb to the acidic sites. By combining the two techniques, information about quantity, type, origin and strength distribution of the acidic sites in the ZSM-5 zeolite can be obtained. (AUERBACH; CARRADO; DUTTA, 2003; JIN; LI, 2009).

2.8 Membrane reactors

The concept of process intensification using multifunctional reactors has stimulated research on membrane-based reactive separation processes, in which the separation and

catalytic reactions occur simultaneously in a single unit. When a membrane is used in this type of reaction and separation process, according to IUPAC (1996), the process is called a membrane reactor (MR).

Traditionally in the chemical industry, a chemical process consists of a reaction unit followed by a separation unit. In the reaction unit, the conversion of reactants to desired and undesired products occur, and the removal of the desired product from the reaction mixture occurs in the separation unit. In this conventional system, a large amount of energy is consumed, resulting in huge operating costs (DARAMOLA; ARANSIOLA; OJUMU, 2012). The process intensification is very attractive, as it results in the processes becoming more compact, less capital intensive, and with lower processing costs than traditional processes (Figure 16).

Figure 16 – (a) Traditional process with one reaction and one separation unit and (b) intensification process, with reaction and separation at the same unit.

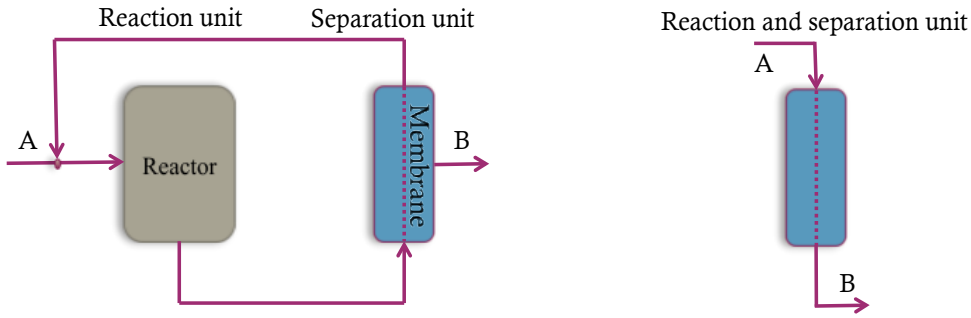

In the work of Bernal *et al.* (2002), a catalytically active H-ZSM-5 membrane was able to integrate reaction and separation efficiently during ethanol esterification with acetic acid. The conversion obtained using the same feed rate and catalyst loading was greater than in the

conventional fixed bed reactors, or reactors where the zeolite membrane was kept separated from the catalyst.

Kong *et al.* (2007) reported the application of a membrane reactor containing a stainless-steel-supported zeolite silicalite-1 membrane for the catalytic dehydrogenation of ethylbenzene to styrene. The obtained conversion was about 7 % higher than in the fixed-bed reactor for temperatures above 600 °C. The conversion improvement was mainly attributed to the instantaneous removal of hydrogen from the reaction zone through the zeolite membrane during the reaction process.

Gallucci, Paturzo, and Basile (2003) published a study about the experimental performance of a zeolite membrane reactor compared to a conventional reaction system. The methanol synthesis from CO_2 and H_2 has been considered versus temperature, at two different H_2/CO_2 feed ratios. The results showed a good performance of the MR. At the same temperature CO_2 conversion was higher than the one related to the traditional reactor. The MR over less drastic conditions, as lower temperatures, and pressures, could reach CO_2 conversions obtained from a conventional system. The results show a notable decrease in energy demand. The methanol selectivity and yield were also higher concerning a traditional reactor.

2.9 Xylene isomers separation and reaction

The xylene is mainly produced from catalytic reforming of naphtha and presents three isomers: *para*, *meta*, and *ortho*-xylene. The isomers are compounds with the same molecular formula but a different molecular arrangement. Xylene isomers distribution is approximately 50 % – 60 % of *meta*-xylene and 20 % – 25 % *ortho*- and *para*-xylenes. The molecular structure, molecular formula, and some general properties of the isomers of xylene are depicted in Table 3.

Para-xylene is responsible for about 80 % of the xylenes market demand, with *ortho*-xylene being oxidized to phthalic anhydride, mainly used to produce phthalate plasticizers. *Meta*-xylene is converted into isophthalic acid, which is used in the production of unsaturated polyester resins. The *para*-xylene is synthesized to terephthalic acid, used in important polymers such as polyethylene terephthalate (PET) and polybutylene terephthalate (PBT) (PEREGO; POLLESEL, 2010).

Table 3 – Xylene isomers molecular structures, formula, and main properties.

Properties	*ortho*-xylene	*meta*-xylene	*para*-xylene
Molecular structure			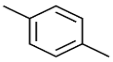
Molecular formula	C_8H_{10}	C_8H_{10}	C_8H_{10}
Density (g mL^{-1})	0.88	0.86	0.86
Phase at 25°C	Liquid	Liquid	Liquid
Boiling point (°C)	144	139	138
Critical diameter (nm)	0.73	0.73	0.66

The xylene isomers' separation is difficult to be reached by fractional distillation due to their close boiling points (Table 3). Numerous researchers studied the use of acid catalysts for xylene isomers separation and isomerization reactions (GOLABEK; TARACH; GÓRA-MAREK, 2018; GU; YAN, 2010; SAKAI; TOMITA; TAKAHASHI, 2001).

Considering MFI zeolite pore sizes around 0.55 nm and the kinetic diameter of *p*-xylene as approximately 0.58 nm, whereas *o*- and *m*-xylene are around 0.68 nm, the xylene isomers separation occurs in the zeolite due to the difference in size and shape between the *para*, *meta*, and *ortho*-xylene molecules. Xylene reaction and separation can be considered a suitable model

reaction for characterizing the acidity and the pore system of catalysts (GUISNET; GNEP; MORIN, 2000), since the kinetics of xylene isomerization are already well established (MIRTH; CEJKA; LERCHER, 1993). Nevertheless, the separation of the xylene isomers through zeolite membranes is mainly an effect of the interaction between the molecules and the surface of the pore. The isomer *p*-xylene is the preferred adsorbed species and should diffuse faster than *o*- or *m*-xylene through the zeolite framework (HAAG *et al*., 2006).

The separation of xylenes over zeolites can be attributed to the differences in the adsorptions and diffusivities of the three-xylene isomers in the zeolite structures (SONG *et al.*, 2015). According to Depla, Mahieu, and Greene 2010, the *para*-xylene separation from a mixture of xylene isomers with a defect-free ZSM-5 zeolite membrane is possible. However, it can be unfeasible due to the presence of defects in the zeolite layer as a consequence, for instance, of the difference in thermal expansion coefficient between the zeolite and the support.

Two kinetic models or paths for the xylene isomerization reaction can be followed (Figure 17). Through path (a), the transformation from *ortho* to *para*-xylene and vice versa is only achieved through *meta*-xylene as an intermediary. It proceeds through consecutive 1,2-methyl shifts. The path (b) shows the possibility of direct transformation of *ortho* to *para*-xylene and vice-versa via 1,3-methyl shifts (COLLINS; MEDINA, 1983; CAPELLAZZO *et al.*, 1991; AL-KHATTAF, TUKUR; AL-AMER, 2005).

Figure 17 – Kinetic paths for xylene isomerization (a) only 1,2-methyl shift (b) 1,2-methyl shift and 1,3-methyl shift.

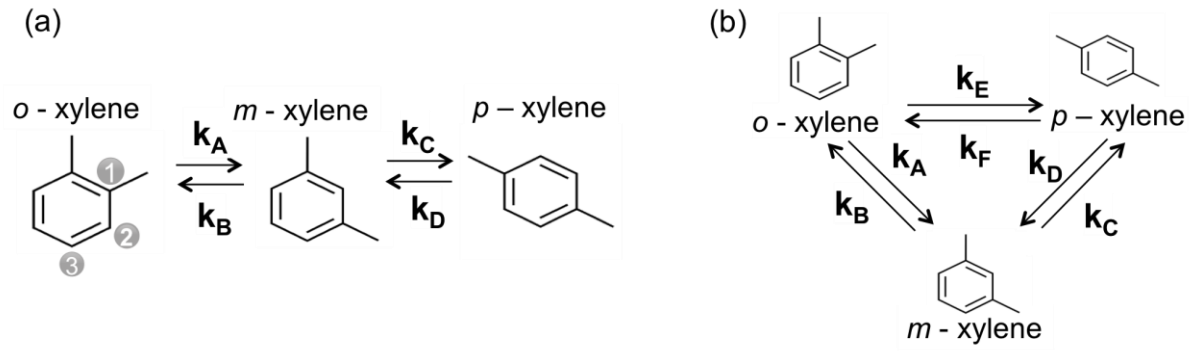

Al-Khattaf, Tukur, and Al-Amer (2005) used the two reaction schemes to model the xylene reactions over ZSM-5 zeolite. The rate constants and activation energies were obtained from simplified kinetic models based on the isomerization of the pure xylene isomers. The results provide ample evidence to suggest that direct isomerization from *o*- to *p*-xylene isomers (1,3-methyl shift) occurred with almost the same rate as the conversion of *m*- to *o*-xylene (1,2-methyl shift) over ZSM-5 zeolite catalyst. The sequence found for the rate constants at 350 °C was $\mathbf{k_D > k_A > k_C > k_B > k_E \approx k_F}$. The reactivity of the xylene isomers was found to decrease in the sequence *p*-xylene > *o*-xylene > *m*-xylene. This reactivity values were attributed to the difference in the diffusion and adsorption capacities of the xylenes, which favors the isomers in the same sequence.

The *para*-selectivity of ZSM-5 is characterized by the *p*-xylene ability to diffuse quickly through the pores, while steric constraints to *o*- and *m*-xylenes are imposed, leading to the transformation into smaller molecules, as *p*-xylene, before crossing the zeolite. The diffusion resistance extent in catalysts can be evaluated via estimation of the Thiele modulus (Φ_L). In the work of Mirth, Cejka and Lercher (1993), the estimation of the diffusion coefficients of pure xylene isomers over ZSM-5 indicated a ratio of 1000: 10: 1 for *p*: *o*: *m*-xylenes.

Xylene isomerization is a thermodynamic equilibrium-controlled reaction, and therefore, total conversion is impossible under conventional conditions. Equilibrium product distributions in the atmospheric pressure for temperatures between 0 and 700 °C are shown in Figure 18 (FRANCK and STADELHOFER, 1988; PEREGO and POLLESEL, 2010).

The mechanism of isomerization of xylenes through the acidic sites of the catalyst occurs by chemisorption, as shown in Figure 19. Due to the high specific internal surface area of microporous crystallites, it can be considered that the most catalytic active sites are distributed within the crystallites. First, the reaction involves combining the xylene molecule and the proton obtained from the acid catalyst. Afterward, carbon isomerization occurs at the active site and finally the xylene desorption.

Figure 18 – *Meta, ortho* and *para*-xylene equilibrium distribution between 0 and 700 °C.

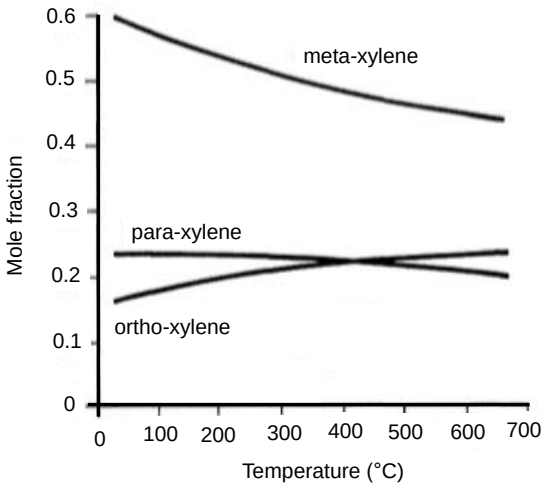

Adapted from Franck and Stadelhofer (1988); Perego and Pollesel (2010).

In ZSM-5, at 200 °C, the reaction kinetic controls the rate of isomerization. Above temperatures of 300 °C, the isomerization rate is controlled by diffusion. The rate of diffusion

of *para*-xylene is higher than that of *ortho*-xylene. The lowest diffusion rate is presented by the *meta*-xylene (PEREGO; POLLESEL, 2010).

Figure 19 – Schema of *meta*-xylene to *para*-xylene isomerization over acid catalyst.

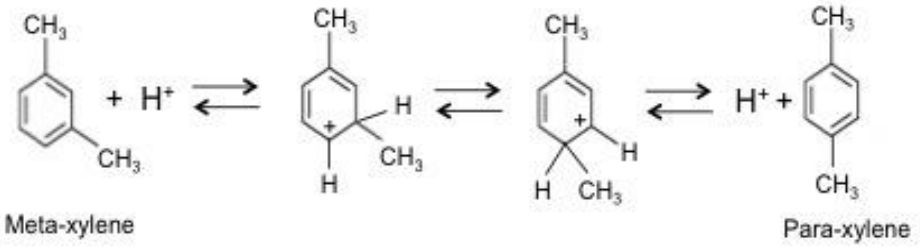

2.10 Conclusion

Ceramic membranes are a promising technology, which has found broad application for the separation of liquid or gaseous mixture. Variation of the membrane chemical composition, membrane synthesis, chemical and temperature pretreatments such as drying, thermolysis and sintering allow efficient control of the mechanical properties, porosity, permeability and stability. Design of composite membranes represents a unique opportunity for combined separation and chemical reaction in a single process in the so-called membrane reactors. Zeolite materials have controlled microporosity. In addition, they may contain functional groups and surface sites active in catalytic reactions.

The use of zeolitic membrane reactors supported on ceramic membranes offers great advantages when compared to conventional reactors. The support provides the necessary mechanical strength, while the thin catalytic layer ensures efficiency and selectivity. The research on the parameters that influence the synthesis of these materials, supports and selective layers, is of great importance. In addition, the reduction or even the substitution of materials aggressive to the environment and of high costs for the production of zeolite and its support must be considered. The use of CFA in obtaining ceramic membranes, without the use of additives and the synthesis of zeolite ZSM-5 without the use of OSDAs aims to present a more economic synthesis route based on environmental purposes.

The goals of this PhD thesis are to prepare and characterize tubular alumina-based membranes incorporated with coal fly ash (CFA), without additive and binder-free, using the centrifugal casting method. The ceramic membranes are then used as support for the ZSM-5 zeolites prepared by *in-situ* crystallization using the seeding method without using organic structure-directing agents (OSDAs) for potential application in the separation combined with catalytic processes involving acid catalyst and effects of shape-selectivity.

CHAPTER 3

EXPERIMENTAL

The experimental part of this manuscript is divided into three main parts: description of the raw materials, characterization methods, details of permeation tests and catalytic experiments.

3.1.Raw materials

The main raw materials, alumina and coal fly ash, used to obtain the ceramic membranes and the characterizations made on these materials will be described below.

3.1.1 Alumina

The commercial alumina CT 3000 SG used in this study was supplied by Almatis GmbH. The typical chemical composition was obtained from the Product Data Sheet (PDS) made available by the supplier and presented Al_2O_3 purity higher than 99 wt.%, as can be seen in Table 4.

Table 4 – Chemical composition of commercial alumina CT 3000 SG (obtained from PDS).

Compound	Proportion (wt.%)
Al_2O_3	99.78
SiO_2	0.03
Fe_2O_3	0.02
CaO	0.02
MgO	0.07
Na_2O	0.08

The characterization of the crystalline phases of the Al_2O_3 CT3000SG sample was performed using the X-ray diffraction technique. The analysis was performed at the Laboratory of Ceramic Materials (LACER) at the Federal University of Rio Grande do Sul (UFRGS). A scanning step of 0.05° in the region of 2θ from 5° to 75° was used. The X'Pert MDP X-ray diffractometer (Phillips, X-ray tube with Cu Kα radiation, CAN) equipped with graphite monochromator and fixed anode operating at 40 kV and 30 mA.

Alumina density was calculated using sample mass and volume by Pycnometry, applying the D854-92e1 Standard Test Method for Specific Gravity of Soils (ASTM D854, 2014). To perform the test, 4 grams of sample were used. The results for particle size were also obtained from the PDS, and the performed method was the Laser Diffraction using CILAS 1180 particle analyzer. Table 5 shows the results, in the range of 0.3 to 0.6 μm for 50 % of alumina CT 3000 SG particles, D(50).

Table 5 – Particle size for alumina CT 3000 SG using Laser Diffraction – CILAS 1180.

	Particle Size (μm)		
	Typical	Minimum	Maximum
D(50) – CILAS	0.5	0.3	0.6
D(90) – CILAS	2.0		3.0

Obtained from the Product Data Sheet (Almatis)

3.1.2 CFA

The coal fly ash (CFA) was supplied by the Candiota Coal Thermoelectric Plant (Candiota, Rio Grande do Sul, Brazil). The CFA was characterized by multiple techniques.

X-ray diffraction (XRD) patterns were measured using D2 Phaser – Bruker diffractometer (30 kV potency and Cu Kα radiation). The 2θ angle was scanned between 5° and 75° with a scan speed of $0.05°s^{-1}$, and the experiments were conducted in the Analytical Central

Laboratory – from the Chemical Engineering Department (DEQUI - Federal University of Rio Grande do Sul/UFRGS - Brazil).

Elemental composition was determined by X-Ray Fluorescence Spectroscopy (XRF) using the RIX 2000 analyzer from Rigaku at the Analytical Central Laboratory from the Chemical Engineering Department (DEQUI - Federal University of Rio Grande do Sul/UFRGS) and allowed the knowledge of CFA chemical composition in terms of components and elements concentration. The content of unburned carbon was evaluated as the loss on ignition (LOI) and performed at the Waste Processing Laboratory following the Standard Test Method for Ash in the Analysis Sample of Coal and Coke from Coal (ASTM D3174). For this test a sample of 2.0 grams of CFA was dried in an oven at 110 °C for 2 h. After being cooled in a desiccator for at least 60 min, the CFA sample was weighed again. The weight loss of the sample is considered as the moisture content. The dried CFA was then placed in a muffle furnace in air atmosphere for 2 h at 850 °C. Finally, the burnt sample was cooled to room temperature in a desiccator and then weighed. The weight loss after the sample burning is the loss on ignition (LOI). Based on the LOI, the XRF values were corrected.

The CFA particle size ranges were obtained by diffraction laser technique with the CILAS 1180 analyzer at the Ceramic Materials Laboratory (Federal University of Rio Grande do Sul/UFRGS). Distilled water was used as the dispersing medium.

The D854-92e1 Standard Test Method for Specific Gravity of Soils (ASTM D854, 2014) was used to determine the apparent density by water Pycnometry. The thermogravimetric analysis of CFA (TGA/DTA) was performed in the Analytical Central Laboratory from the Chemical Engineering Department (DEQUI - Federal University of Rio Grande do Sul/UFRGS), using the SDT Q600 - TA Instruments equipment, with a temperature limit of 1000 °C, a heating rate of 10 °C min^{-1}, and nitrogen atmosphere (100 mL min^{-1}).

3.2.Ceramic membrane characterization techniques

In the following topics, the characterizations performed on the ceramic alumina membranes incorporated with CFA will be described.

3.2.1 Linear shrinkage

The green body, just after preparation in centrifugal casting, presents the same length as the metallic mold. To obtain the membrane length shrinkage, 10 membranes of the same composition were measured at two moments: just after centrifugal casting preparation (L_i) and after sintering at high temperatures (L_f). All the lengths were in centimeter. The total shrinkage percentage (S_T) was calculated by Equation 10, as follows:

$$S_T\ (\%) = \frac{L_i\ -\ L_f}{L_i} \times\ 100 \qquad \textbf{(Equation 10)}$$

3.2.2 Apparent porosity

The Archimedes method was used to estimate the open porosities. This method is based on body water absorption according to the conditions established by standards ISO 10545 and ASTM C373. The method to calculating apparent porosity percentage (AP) is given by Equation 11.

$$AP\ (\%) = \frac{w_{wet}\ -\ w_{dry}}{w_{wet}\ -\ w_{imm}} \times\ 100 \qquad \textbf{(Equation 11)}$$

where w_{dry} is the sample weight after 24 h drying at 105 °C, w_{wet} is the weight sample after boiling for 2 h in distilled water and w_{imm} is the sample weight immersed in distilled water. All the weights were in grams. The schematic process is illustrated in Figure 20.

Figure 20 – Apparent porosity process sequence adopted in this work.

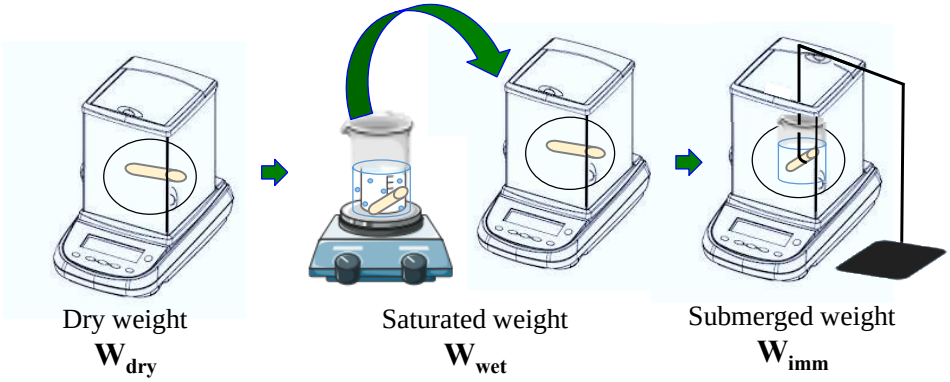

3.2.3 Morphology of the ceramic supports

The tubes' external, internal, and cross-section morphologies were analyzed using Scanning Electron Microscopy (SEM) to find evidence of asymmetry due to CFA addition in the tube's matrix. Sample preparation involved fracturing and settling them in an appropriate support. The samples were fractured with a tool to have the minimum size necessary for the analysis. Afterward, the samples were attached to the stubs with a carbon ribbon. The micrographs were obtained at the Design and Material Selection Laboratory from the Federal University of Rio Grande do Sul/UFRGS –Brazil, in a bench Scanning Electron Microscope - TM3000 Hitachi - with 100x magnification for the inner and outer surfaces and 50x for the cross-section, with beams of 15 keV.

3.2.4 Mechanical strength

Ceramic membranes are known for good performance under critical mechanical conditions. To investigate mechanical strength on the ceramic tubes and investigate how the CFA addition impacts the support structure, the 4 Points Flexural Method was used (Figure 21). This method is based on the ASTM C1684-18 (Standard Test Method for Flexural Strength of Advanced Ceramics at Ambient Temperature) and described in works from Luiten-Olieman *et al*. (2011).

Figure 21 – (a) Equipment used to measure the Four Point flexural load (b) four-point flexural diagram.

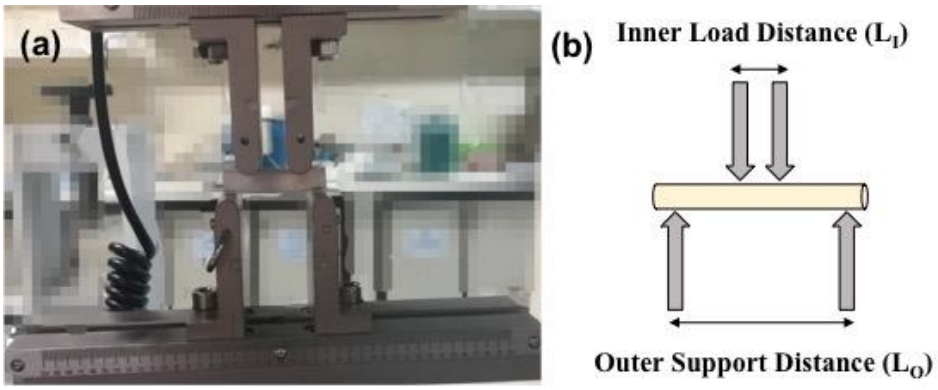

The analysis was performed at the Biomaterials Laboratory (LABIOMAT) at the Federal University of Rio Grande do Sul. The equipment INSTRON 3369 gave the maximum flexural load (F, in Newtons) for five samples of each membrane composition, which were cut into short segments of 0.045 m using a 650 diamond Saw (South Bay Technology Inc., USA). The crosshead speed used was 12 x 10^{-3} m h^{-1}, and the Equations 12 and 13 were applied to calculate the correspondent strength, σ, in MPa (LUITEN-OLIEMAN *et al*., 2011).

$$\sigma = \frac{16\ F\ k\ d_0}{\pi\ (d_0^4 - \ d_1^4)} \quad \textbf{(Equation 12)}$$

$$k\ = \frac{L_0 - \ L_I}{2} \quad \textbf{(Equation 13)}$$

where d_0 and d_1 are, respectively, the sample outer and inner diameters, in millimeters, and L_O and L_I are the distances between the two outer supports and between two inner loads, also in millimeters (Figure 21).

3.2.5 Hydraulic permeance and observed retention

The hydraulic permeance for the ceramic membranes was tested in triplicate. The tests were carried out in a bench-scale permeation unit at the Membrane Separation Laboratory (LASEM) of the Department of Chemical Engineering (DEQUI) at UFRGS. The feed was inserted on the inner side of the membrane, and the permeate current was collected on the outer side.

The permeation system was composed of a homemade stainless-steel tubular module of 13.1 cm long to insert the membrane, a jacketed feed tank of 1.5 L connected to a temperature-controlled water bath (model RM 12 – Lauda, Germany), and a diaphragm pump (Shurflo 8030-813-293 – Peintair, USA) for water/solution circulation. Two manometers (Manotécnica, Brazil) indicate the pressure and two valves (Tecnofluid do Brasil Ltda., Brazil), one for the retentate and one for the by-pass stream complete de system, as shown in Figure 22. The operating mode was total recycle, i.e., concentrate and permeate streams are returned to the feed tank.

Figure 22 – Schematic bench-scale ultra/microfiltration unit with total recycle operating mode.

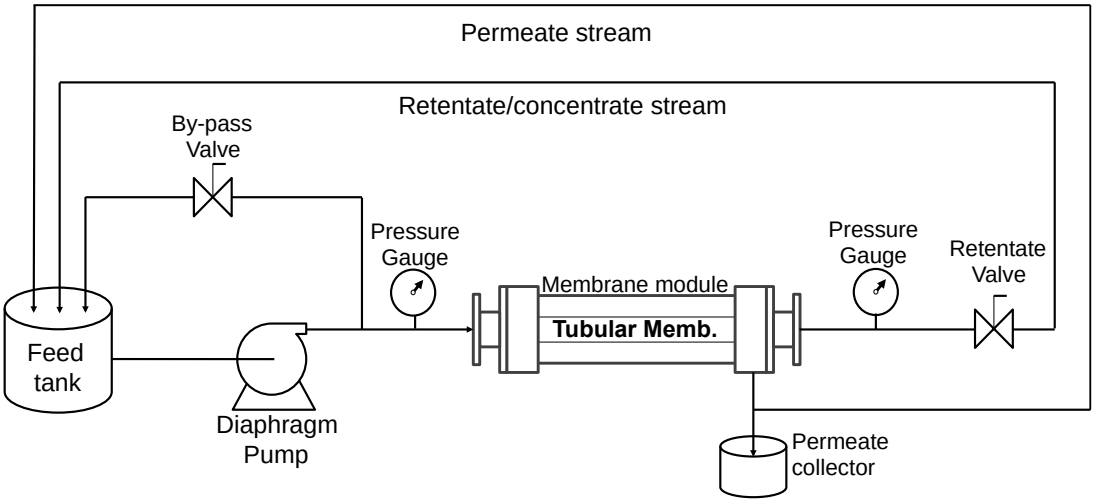

Before insertion in the module, the membranes were cleaned by ultrasound with distilled water for one minute. This technique prevents residues of raw material from adhering to the membrane, decreasing its performance. In the membrane conditioning, the specimens were placed in the module in contact with the current distilled water at constant operating conditions (flow rate, temperature) and room pressure for 10 minutes. This stage can prevent the collapse of pores and facilitate permeation, ensuring the structural integrity of the membrane (DUTOURNIÉ *et al.*, 2017).

The process started with the compaction of the membrane until constant water flux (variation lower than 5 %) using distilled water, under 3 bar transmembrane pressure, feed flow rate of 150 L h^{-1}, and temperature of 24 °C. The permeate flux (J, L $h^{-1}m^{-2}$) was calculated by Equation 15, measuring the time (t, h) to complete a certain volume (V, L), passing through the porous material area (A, m^2). The membrane permeation area was obtained by measuring the length and internal diameters for each permeated membrane.

$$J = \frac{V}{A\,t} \qquad \textbf{(Equation 14)}$$

The results were registered every 5 minutes until the flux variation was lower than 5 %. After the compaction, the water permeate flux (J) was measured for four different transmembrane pressures between 3 and 1.5 bar, at a constant flow rate of 150 L h^{-1}. The hydraulic permeance (K, kg m^{-2} h^{-1} bar^{-1}) was the slope of the curve obtained by plotting the permeate flux as a function of pressure (Equation 5).

The qualitative membrane retention limit was determined using a solution containing 25 x 10^{-5} kg L^{-1} of commercial cornstarch, with particle diameter around 12 µm.

The permeation experiment was carried out at transmembrane pressure of 2 bar, feed flow rate of 150 L h^{-1}, and temperature of 24 °C, for one hour. The observed retention was calculated based on the turbidity in the final feed solution (T_0) and in the permeate stream at the end of the experiment (T_f), as shown in Equation 15. A portable turbidimeter, with Fast Tracker Technology, by a Hanna Instruments HI 98703 EPA Compliant provided the values for turbidity.

$$R_{obs}\,(\%) = \left(1 - \frac{T_f}{T_0}\right) \times 100 \qquad \textbf{(Equation 15)}$$

At the end of the experiments, aliquots of feed and permeate streams were collected. The qualitative iodine test was done by dripping an iodine solution in these aliquots. The obtained color in the solution indicates the presence or absence of starch. Blue coloration indicates the presence of starch in the solution; meanwhile, yellow indicates non-appearance of cornstarch molecule.

3.3.Zeolite membrane characterization

To verify the homogeneity, the type of zeolites and structures obtained in the zeolite film, the length of the zeolite layer, and the presence of superficial defects, the samples were characterized using X-Ray Diffraction, Fourier Transform Infrared Spectroscopy, and Scanning Electron Microscopy (SEM) techniques. Details, including sample preparation and equipment used, are described below.

3.3.1 X-Ray Diffraction (XRD)

X-ray diffraction (XRD) patterns were obtained for the zeolites remaining in the autoclave after every hydrothermal synthesis made. The X-ray diffraction technique was important to confirm the formation of ZSM-5 zeolites with the synthesis method applied and verify the formation of another type of zeolites. The characterization was held at the University of Lille using a diffractometer Bruker D8 Advance using a Cu Kα radiation source. The analysis was performed with the 2θ angle scanned between 5° and 90° with a step of 0.02° and the integration time of 0.5 seconds.

3.3.2 Fourier transform infrared spectroscopy (FTIR)

The FTIR-ATR (attenuated total reflectance) characterization was performed to observe the presence of characteristic vibrations of the tetrahedral TO_4 (T = Si or Al) units and identify the functional groups in the zeolite structure. The analysis was made with the zeolite powder remaining inside the autoclave after hydrothermal syntheses, the same powder used for XRD analyses.

The analyses were made at the University of Lille in a Nicolet iS50 FTIR Spectrometer, and the spectra were obtained in the region 4000 - 400 cm^{-1}.

The pyridine (Py) adsorption experiments followed by Fourier-Transform Infrared Spectroscopy (FTIR) were performed in a Thermo Nicolet 460 Protege instrument equipped with a CsI beam splitter and an MCT detector, averaging 256 scans with a 2 cm^{-1} resolution within the 4000-400 cm^{-1} range. The samples were pressed (1000 kg cm^{-2}) into a self-supported wafer (2.01 cm^2, 10 mg cm^{-2}) and placed in a quartz sample holder in order to align the pellet with respect to the IR beam during measurements and insert it into a furnace for thermal treatments. The sample holder was then placed in a quartz cell equipped with KBr windows, connected to a vacuum line for evacuation ($P_{residual} \simeq 10^{-6}$ Torr) and introduction of probe molecules into the infrared cell. Prior to Py adsorption experiments, samples were reduced at 350 °C under 50 mbar of pure hydrogen and the gas was evacuated under high vacuum ($P_{residual} \simeq 10^{-6}$ Torr) overnight. Py adsorption was carried out at the equilibrium (1.2 mbar) at 100 °C. Pyridine was then evacuated under high vacuum ($P_{residual} \simeq$ 10-6 Torr) at different temperature (150, 250, 350 and 450 °C).

3.3.3 Scanning Electron Microscopy (SEM) and Dispersive Energy Spectroscopy (EDS)

Images of the surface and the cross-section of the membranes were made using scanning electron microscopy (SEM). The dispersive energy spectroscopy (EDS) technique was used to verify the transition between support and zeolitic material and to analyze the Si/Al ratio of the zeolite layer. With the micrographs of the cross-section, the thickness of the zeolitic membrane was calculated.

The first SEM analysis was made as an investigative test to evaluate the zeolite deposition over the internal and external surfaces of the tubular supports. The micrographs were obtained in a microscope ZEISS EVO MA10 (Germany), a conventional scanning microscope with a tungsten filament that operates at voltages between 0.2 kV and 30 kV. The analysis was performed at the Microscopy and Microanalysis Center (CMM) of the Federal University of Rio Grande do Sul. The voltage used was 15kV, and approximations of 1000, 2000, and 5000x were applied. Sample preparation involved fracturing, with a proper tool, accommodation of the samples in appropriate stubs with a carbon ribbon and metallization with a thin gold layer.

The micrographs shown in the continuation of the work were performed on the seeded support, on the cross-section, and on the internal surfaces of samples containing internal zeolite coating with one and two layers, calcined and uncalcined. The microscope was a JEOL JSM-7800F with a Field Emission Gun (FEG) source from the University of Lille – FR. Sample preparation followed the same steps previously detailed; however, the coating, with around 200 angstroms, was done using carbon.

3.4.Zeolitic membrane permeation and catalytic experiments

The performance of zeolite membranes was evaluated by permeation experiments using different organic compounds with different kinetic diameters. Also, the separation and reaction of organic compounds using these membranes were evaluated.

A schema of the experimental setup built is presented in Figure 23. The net feed flow has been set in a programmable syringe pump (Harvard apparatus PHD2000) that propels the mixture by a 20 mL syringe in stainless-steel to the setup line. The driving force of the process was the partial pressure gradient between the components. A N_2 gas and a gas controller provide the carrier gas, which enhances the transport across the membrane. Graphite joints sealed the

stainless-steel module, where the zeolite membrane is inserted. Two cold traps were used for the outlet streams, one to collect the permeated and other to collect the retentate stream with the unpermeated products. Thermocouples were used at the membrane module and at the streams to monitor the temperature of the setup.

Figure 23 – Schematic setup for reaction and separation tests over the tubular zeolite membranes.

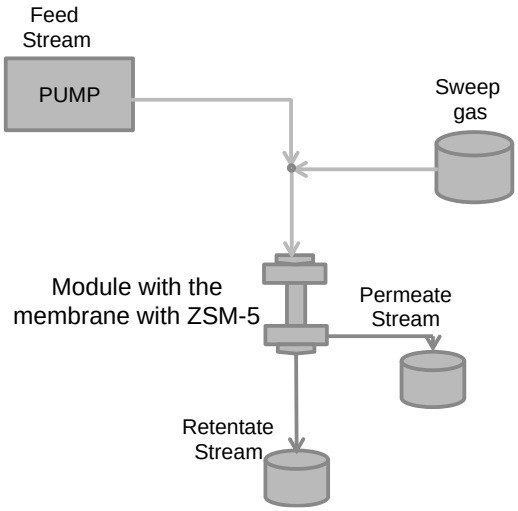

The feed was introduced in the syringe and injected into the setup in the liquid phase. To increase the temperature in the setup and turn the feed into a gas phase, heating lines were addressed to the flexible stainless-steel tubing. In this way, the feed in the gas phase, already mixed with the carrier gas, enters the module accessing the inside of the tubular membrane where the zeolitic deposition was made. For heating the permeation module, a heating tape that reached 450 °C was used.

The output currents were also wrapped in heating tapes, ensuring that the gas phase is maintained and preventing condensation of compounds within the setup. Liquid products were collected in the cold traps. The compositions of the feed and outlet streams were determined by

chromatography in a SCION SQ-GCMS Instrument, using a SC32123, SCION-1MS capillary column. The tests were performed in the setup according to the conditions presented below.

Separation tests

The separation tests were performed using a mixture of *ortho*, *meta*, and *para*-xylene as feed and the composite membranes with one and two layers of zeolite depositions. The tests were carried out in atmospheric pressure and at low temperatures, up to 175 °C, to keep the compounds in the gas phase. The membranes were used without ion exchange; in this way such tests were intended to test only the selectivity of the membrane to xylene compounds. Two values of feed flow rates were used, 450 and 100 μL min^{-1} and the carrier gas, N_2, was maintained in 7 ml min^{-1}. The selectivity (S) was calculated by the Equation 16.

$$S = \frac{\left(C_{\substack{desired \\ compound}} \Big/ C_{\substack{undesired \\ compound}} \right)_{permeate}}{\left(C_{\substack{desired \\ compound}} \Big/ C_{\substack{undesired \\ compound}} \right)_{retentate}} \qquad \textbf{(Equation 16)}$$

Separation and isomerization

The separation and isomerization tests using a mixture of *ortho*, *meta*, and *para*-xylene mixture as feed stream were conducted. Also, molecules with a larger kinetic diameter than xylene isomers were inserted in the feed stream to test the separation of organic compounds: mesitylene with 0,84 nm (NIEN; CHANG; CHANG, 2017) and 1,3,5-Triisopropylbenzene with 0,93 nm (ZAMAN; LOUGHLIN; AL-KHATTAF, 2005). The pressure was settled in 1 bar and temperature was maintained at 320 °C to test the xylene isomerization reaction. The

xylene isomerization tests were performed over the zeolitic membranes considering the weight hourly space velocity (WHSV), which is given by the ratio between the weight of feed flowing through the system, in g h^{-1}, and the weight of catalyst in grams. The catalyst mass was estimated as the weight gain per surface area of membrane in m^2 following values given in Schneider *et al*. 2021.

CHAPTER 4

SYNTHESIS AND PROPERTIES OF ALUMINA-COAL FLY ASH COMPOSITE TUBULAR ASYMMETRIC MEMBRANES

ABSTRACT

Design of new efficient membranes from sustainable sources such as coal fly ash (CFA) has been receiving rapidly growing attention. In the present work, alumina-based tubular asymmetric membranes were incorporated with different amounts of CFA using the centrifugal casting technique. The amount of CFA added to the matrix of the alumina tubes was varied from 10 to 40 wt.% on a dry weight basis. The development of the ceramic membranes containing CFA comprised the following steps: raw materials dispersion, membrane preparation by centrifugal casting using high-speed mold rotation, drying of the green body followed by sintering at 1200 °C. The techniques used for membrane characterization included measuring mechanical strength, apparent porosity, morphology, by scanning electron microscopy, linear shrinkage, hydraulic performance, and cornstarch retention. High CFA fraction in the alumina-based membranes resulted in higher porosity and higher water permeability, accompanied by a decrease in mechanical strength and linear shrinkage. The observed permeate flux was between 116 and 370 L m^{-2} h^{-1} bar^{-1}, and the observed retention was above 99 % for all the membranes tested. The addition of CFA for the preparation of asymmetric tubular membranes based on alumina allows utilization of industrial waste, reduces the cost and is interesting from both an economic and environmental points of view. These membranes have the potential for applications such as wastewater treatment and as a support for selective microporous carbon and zeolite layer coatings.

There is a growing interest in the development of ceramic membranes for the separation and purification of solutes from aqueous solutions or a mixture of gases, as well as for the use of these membranes as supports for metallic, zeolite or polymeric coatings and even for other promising applications, such as catalytic reactors. In general, the costs of the ceramic membranes are higher when compared to the polymeric counterparts. CFA is a by-product of burning coal, which composition is dependent on the coal source. The main components are silica and alumina. Only a small percentage of the total CFA produced is used as building materials for construction and architectural components or in the cement industry, for paving and brick manufacture. These data confirm the CFA disposal problems and highlights the need to find other uses for this waste. Transforming CFA into a raw material for the manufacture of ceramic membranes can be a valuable option.

The objective of this chapter is the preparation of alumina-based tubular asymmetric membranes incorporated with coal fly ash (CFA), additive and binder-free, using the centrifugal casting method. The structural properties and performance of the alumina-CFA composite membranes were characterized using a combination of methods.

4.1.Raw-materials characterizations

The characterization of alumina and CFA, the raw materials used to prepare the ceramic membranes, is shown and discussed below. The characterization of CFA is of great importance since it is a material of great heterogeneity depending on the sources of coal from which it is derived.

4.1.1 X-ray diffraction

Alumina

The X-ray diffractogram of the commercial alumina CT3000SG is shown in the Figure 24. The peaks shown in the 10° to 70° scan region of the diffractogram are characteristic of the alpha (α) crystalline phase of alumina (CONTRERAS *et al*. 2006; MARTÍN-RUIZ *et al*. 2009). According to the analysis, it was possible to verify that the alumina used, manufactured by the company Almatis, is essentially composed by the alpha crystalline phase. The α phase of alumina is considered one of the most stable and with great application possibilities due to its good mechanical, thermal and electrical properties (SALEM; CHINELATTO; CHINELATTO, 2014).

Figure 24 – Alumina CT3000 SG (Almatis) diffractogram.

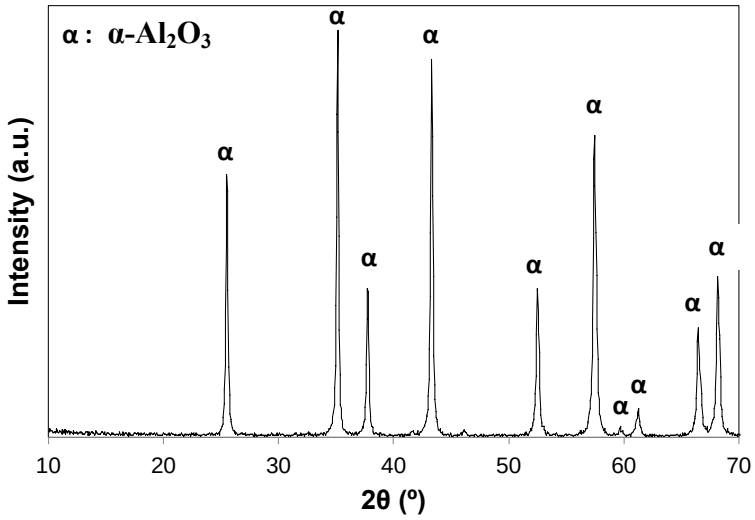

CFA

X-ray diffraction pattern obtained for the CFA sample shows crystallographic phases composed of anhydrite ($CaSO_4$), hematite (Fe_2O_3), mullite ($Al_6Si_2O_{13}$) and, in the majority, of quartz (SiO_2) (Figure 25). Narrow XRD peaks suggest the presence of larger crystallites.

Figure 25 – XRD pattern for CFA evidencing the presence of Quartz (Q), Anhydrite (A), Hematite (H) and Mullite (M).

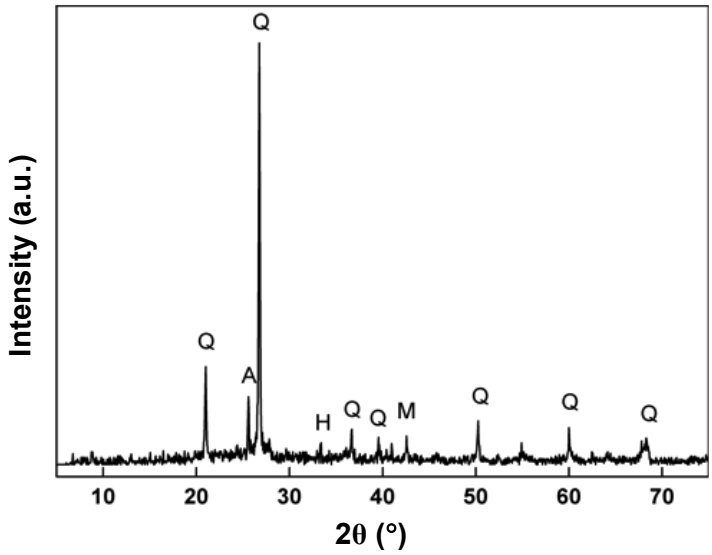

The XRD peak positioned at 26.6° (2 theta) corresponds to quartz, showing a significant presence of this mineral in the CFA matrix. The XRD results are corroborated with the data presented in Santana *et al*. (2011), which also characterized the coal ash from the Candiota coal mine – Brazil, classified as sub-bituminous, with the predominance of quartz, and presence of hematite among other minerals.

4.1.2 CFA chemical composition

The chemical composition of the CFA sample from Candiota coalmine, Brazil, is depicted in **Table 6**. CFA is mainly composed of silica, followed by alumina and iron oxides. According to Heidrich, Feuerborn and Weir (2013), sub-bituminous coals produce ashes with SiO_2 contents in a higher range than bituminous and lignite coals, around 40 to 60 wt.%.

Regarding to the industrial use, fly ash is classified as Class C or Class F. In class C ash, according to Singh *et al.* (2020), the sum of the contents of the oxides of Si, Fe and Al varies

between 50 and 70%. Meanwhile, for the Class F ashes, the same sum reaches values greater than 70%.

Table 6 – Chemical composition of CFA (Candiota coalmine – Brazil) measured by X-ray fluorescence.

Compound	Proportion (wt.%)
SiO_2	62.65
Al_2O_3	16.62
Fe_2O_3	4.92
CaO	2.75
SO_3	3.42
MgO	0.23
Others[a]	3.37
LOI[b]	6.03

[a] K_2O, TiO_2, ZeO_2, Cr_2O_3, MnO, NiO, ZnO and SrO

[b] Loss on ignition

Oxygen, silicon, and aluminum are the dominant elements appearing in the CFA fluorescence analysis, as shown in Figure 26, with lesser proportions of alkalis or alkaline earth and sulfur. The loss on ignition (LOI), shown in **Table 6**, is quantified in 6.0 % and is related to the unburned carbon remaining in the CFA sample. Other elements, with minor proportions, are Mg, Cr, Mn, Ni, Zn, Rb, Sr, and Zr, being responsible for less than 1 % of the CFA sample analyzed.

Figure 26 – Element percentage in the CFA obtained by fluorescence. (Others = Mg, Cr, Mn, Ni, Zn, Rb, Sr, Zr).

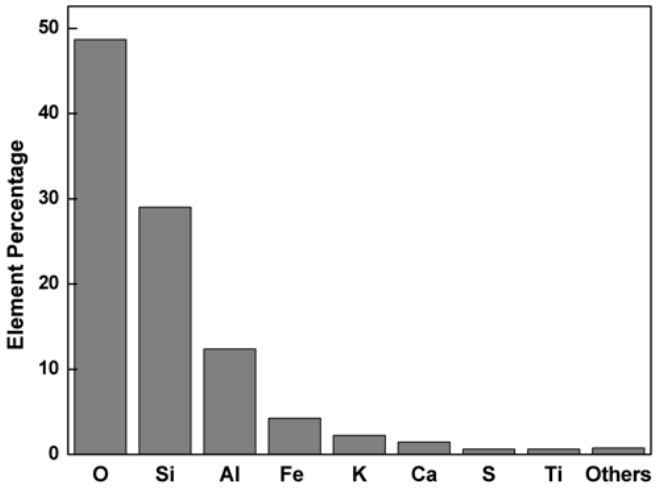

XRF results for the CFA sample agree with the XRD pattern (Figure 25). They are also consistent with the elemental composition of other mineral coal ash, in which the majority compound is the silicon dioxide (JEDIDI *et al*., 2009; ODUNAYO *et al.*, 2016).

The results suggest the presence of a low concentration of impurities in CFA. This allows the potential application of CFA as raw material to be incorporated into alumina-based membranes to reduce their costs and add value to this industrial waste.

4.1.3 Particle size analysis

Alumina

To evaluate the particle size of the commercial alumina CT3000SG, other works by this research group, i.e., Bertotto (2019) applied the sedimentation technique using the dispersion analyzer LUMisizer equipment. The values obtained can be seen in Figure 27 the D50 value was 0.58 μm. This value is within the size range informed by the supplier, which claims to have an average particle size of 0.5 μm.

Figure 27 – Particle size distribution of CT3000SG alumina obtained through the sedimentation technique - LUMisizer.

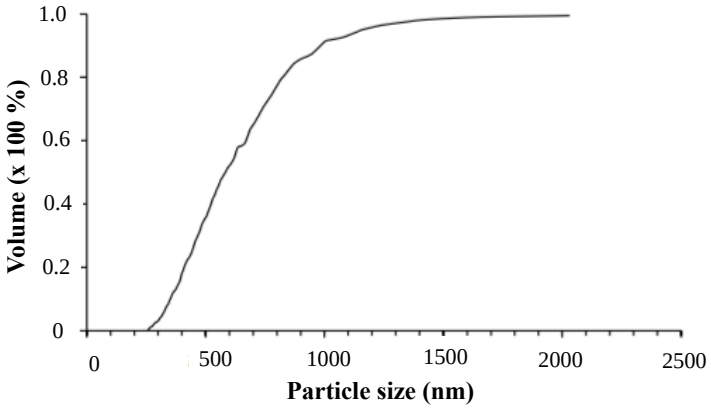

Adapted from Bertotto (2019).

CFA

To obtain smaller grain particles, less heterogeneous particle distribution, and a representative sample, the CFA was sifted in a stainless-steel sieve of mesh 100 (150 μm). In this way, a more homogeneous mixture was used to prepare the ceramic tubes with the alumina particles. The average grain size for the CFA sample obtained by laser diffraction technique was 48.4 μm. The histogram with particle size distribution fractions (vol.%) of the samples can be seen in Figure 28.

The diffraction laser method is based on the analysis of the diffraction pattern produced when particles are exposed to a monochromatic beam of light. The analysis shows 10 % of particles (D10) with a diameter smaller than 9.01 μm, 50 % of particles (D50) presenting medium diameter smaller than 45.4 μm, and the big particles (D90) with a mean size smaller than 90.2 μm.

Figure 28 – Particle size distribution for the CFA sample.

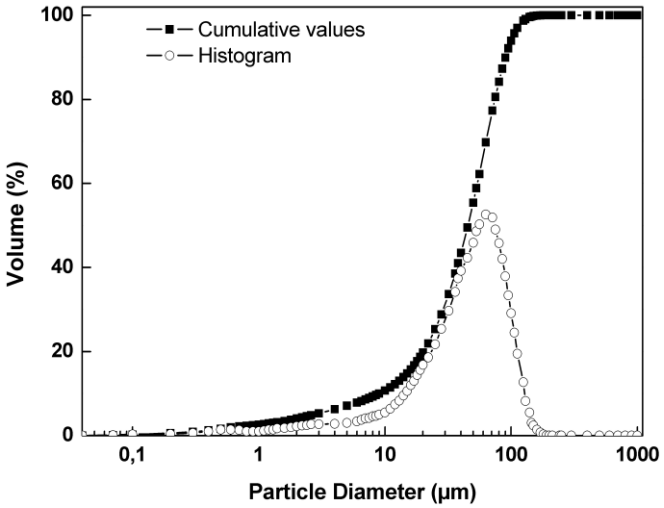

4.1.4 Apparent density analysis

Table 7 shows the average apparent density values obtained for the CFA and alumina samples. The analyses were done in triplicate.

Table 7 – Apparent density results for CFA and alumina samples obtained by pycnometry

Sample	Apparent density (g mL^{-1})
CFA	2.47 ± 0.06
Alumina CT 3000 SG	3.66 ± 0.23

The CFA particles presented a density close to SiO_2, 2.65 g mL^{-1} (PASCUAL, DURÁN, and PASCUAL, 2002) since silica us the main component of CFA. Alumina pycnometry test resulted in a higher value when compared to the CFA sample, close to the density values obtained in the literature for α-Al_2O_3 of 3.95 g mL^{-1} (JIMENEZ *et al*., 2019).

4.1.5 CFA Thermogravimetric and Differential Thermal Analysis

The TGA/DTA analysis provided information about the percentage of mass loss in inert atmosphere, which was estimated to be around 2 % (Figure 29). FAN and BROWN presented a typical TGA weight loss curve for fly ash. As found in this work, about 0.5 % of weight loss occurred until 500 °C, which may be the result from moisture reabsorbed in the sample or deviation from the instrument. After 500 °C, the 2 % weight loss in the sample represents the release of volatile matter.

Figure 29 – TGA/DTA analysis for the CFA sample.

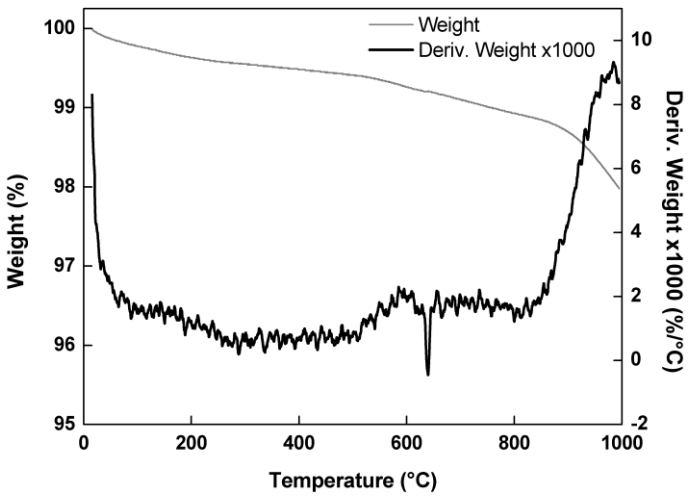

The CFA final mass was quantified in almost 98 % from the initial when the temperature has reached 1000 °C. As described in Masiá *et al.* (2007), the DTA curve for CFA shows a weight loss peak starting around 850 °C and ending at temperatures higher than the equipment limit, 1000 °C.

4.2.Ceramic Membranes Preparation

To prepare the suspension, a formulation containing 45 wt.% solids and 55 wt.% water was used. In this work, the solid was constituted by both alumina and CFA. The CFA content in the dry mass varied from 10 wt.% to 60 wt.%. However, the tubes containing more than 40 wt.% CFA in dry mass were very fragile and brittle after drying or demolding.

The technique applied for the ceramic tubes production was the horizontal Centrifugal Casting. No dispersant, binder, or chemical additives were used. **Table 8** shows the different formulations tested in this work to synthesize the alumina/CFA-based tubular membrane.

Table 8 – Materials proportion used in the membrane tubes preparation and the membranes abbreviation used in this work.

Abbreviation	**Dry basis (wt./wt.%)**		**Wet basis (wt./wt.%)**		
	Al_2O_3	CFA	Al_2O_3	CFA	Water
CFA0	100.0	0.0	45.0	0.0	55.0
CFA10	90.0	10.0	40.5	4.5	55.0
CFA20	80.0	20.0	36.0	9.0	55.0
CFA30	70.0	30.0	31.5	13.5	55.0
CFA40	60.0	40.0	27.0	18.0	55.0

The CFA was sifted through a 100-mesh sieve, and a fraction of 90 % or more of the particles passed through the sieve. Thus, it can be considered that most of the particles have sizes smaller than 0.149 mm. The portion that passed through the sieve was used for the production of ceramic membranes.

Alumina, CFA, and distilled water were weighted and mixed, forming an aqueous suspension, and placed on the magnetic stirrer for 10 minutes. To ensure a better

homogenization, the suspension was left in the ultrasonic bath for another 10 minutes; this causes the grain deagglomeration and dispersion. Again, the solution was left under stirring for 10 minutes and then it was introduced into the metallic mold (15.1 cm long and 1.0 cm diameter) until filling it up completely. The metallic mold was attached horizontally to the centrifugal casting home-built equipment (Figure 30).

Figure 30 – Sequence steps for obtaining the centrifugal casted green tube.

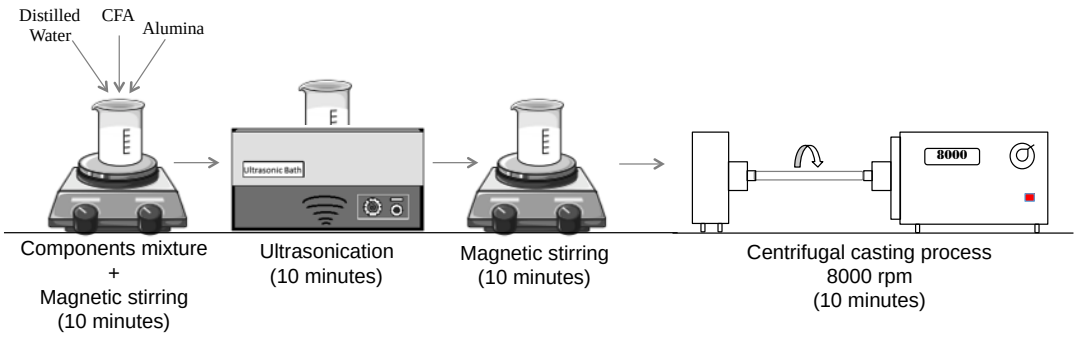

The centrifugal casting equipment comprises a high-speed motor, a metallic mold, and two holders, one for each mold extremity. In this technique, the mold speed rotation creates the centrifugal force and allows tube production. Based on previous studies carried out by Bertotto *et al*. (2019), the velocity applied was 8000 rpm and the specified processing time was 10 minutes.

The tubes were dried, inside the mold, in a climatic chamber at 25 °C and 60 % of humidity, for moisture removal and reducing the thermal stress, for four to seven days, depending on the composition, until they can be released from the metallic mold. If the tubes were free of defects or fissures, they were sintered in a muffle furnace until 1200 °C, following the heating temperature profile shown in Figure 31 and cooling back to room temperature naturally.

Figure 31 – Temperature profile used for the sintering process of the ceramic tubes.

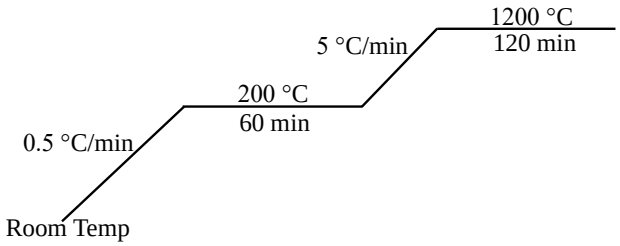

The temperature rise was 0.5 °C min^{-1} until 200 °C in order to avoid the rapid water release from the ceramic membrane supports during the initial sintering stage.

Figure 32 shows images of the tubular ceramic membranes prepared with alumina and different alumina/CFA proportions by centrifugal casting. It is possible to notice a grey gradient, which becomes more evident for tubes with a higher CFA concentration. The speed, at which the mold rotates when using assorted particle sizes can create asymmetry due to the difference in grain settling according to the grain size. Prasad, Murali, and Mukunda (2010) found that applying low mold speed can lead to poor cylinders formation with a symmetric structure. Meanwhile, too high mold speeds may cause asymmetry, i.e., non-uniform distribution of the grains. Grain size classification leads to a clearing of the internal surface due to the predominance of smaller alumina grains. Observing the surface of these tubes, it is also possible to notice that the roughness of the tubes increases with the increase in the CFA concentration, probably due to the larger size of the CFA grains.

Figure 32 – Images of the ceramic tubes illustrating the typical differences in the visual aspects and grains settling. (a) Longitudinal view of ceramic tubes (b) radial view. From left to right: CFA0, CFA10, CFA20, CFA30 and CFA40.

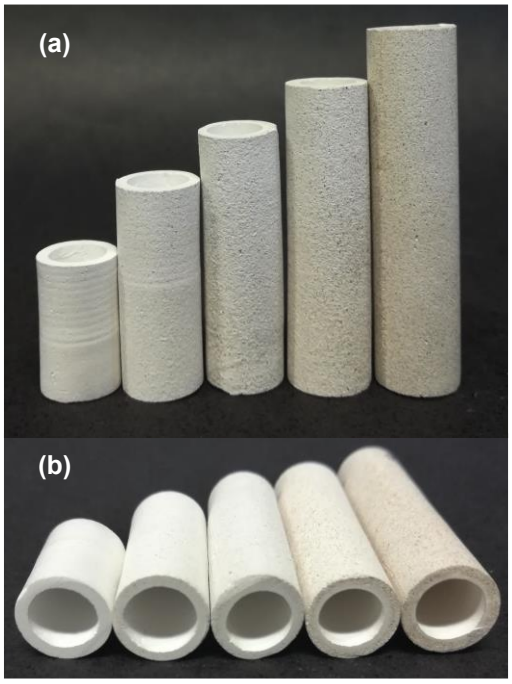

The differential particle settlement shown in the ceramic tubes is in accordance with the expected for ceramic particles in a viscous liquid under high velocities of centrifugal force. Once the terminal velocity for particles in a fluid, V_p, is governed by the Stokes' Law (Equation 17), the velocities acquired by the particles are dependent on the particle diameter, d, and particle density, ρ_p (WATANABE; KAWAMOTO; MATSUDA, 2002; KANG; ROHATGI, 1996).

$$V_p = \frac{d^2 \left(\rho_p - \rho_l\right) b}{18\,\mu} \qquad \textbf{(Equation 17)}$$

The liquid density, ρ_l, dynamic viscosity, μ, and centrifugal acceleration, $b = r\omega^2$ (where ω is the angular velocity and r the radius of the cast tube), are the same for both CFA and alumina particles.

Despite CFA particles presented, according to the data depicted in Table 7, lower density than alumina particles, the larger particle size (diameter around 45 µm), when compared to alumina (0.45 µm), seems to be more relevant to confer a higher terminal velocity to the CFA particles. Approximate calculations indicate that the velocity of the CFA particles is 7000 times greater than the velocity of the alumina particles. Thus, the CFA particles were arranged first close to the metallic mold wall, followed by the alumina particles.

4.3.Ceramic membrane characterizations

The accomplished characterizations, shown below, aimed the comparison between the synthesized samples, to elucidate the question of how the addition of CFA impacts the alumina ceramic membranes. The results were discussed and corroborated with data available in the literature.

4.3.1 Linear shrinkage

After the drying in the climate chamber, a small shrinkage is already perceived. The tube length and diameter decrease due to the release of the excess of water remaining and the conjunction of the material constituents. A non-significant shrinkage of the tubes is expected, as it is necessary to allow the green body to detach from the metal mold. However, after the sintering process, the total shrinkage values presented differences according to the composition. Figure 33 shows the average retractions for the tested tubes.

Tubes containing CFA in their structure showed less shrinkage compared to those prepared with alumina only. The increase in the CFA content decreases shrinkage, possibly due to differences in the size of the alumina and ash particles that promote irregular compaction of the body with the asymmetric morphology obtained by the centrifugal casting method.

Figure 33 – Average linear shrinkage in percentage for the alumina-based tubular membrane incorporated with different CFA concentrations.

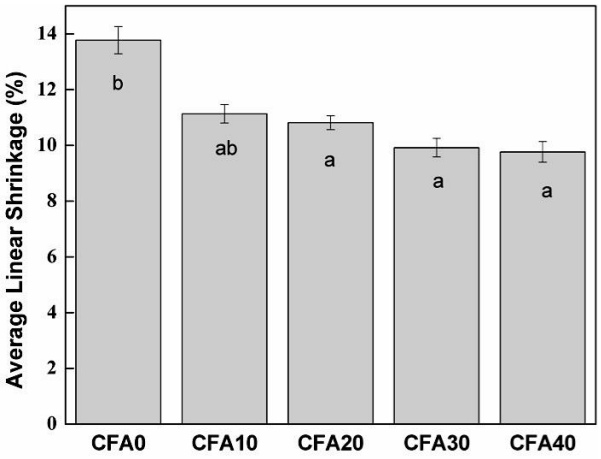

***Numbers followed by different letters are statistically different $p \leq 0.05$ (Tukey's Test).**

These results agree with those by Bissett, Zah, and Krieg (2008), who have tested three different alumina particle sizes and cited that small particle structures presented higher retraction due to more contact points between the grains, which stimulates the shrinkage.

As already mentioned, the centrifugal force action promotes that large CFA particles accommodate preferentially on the mold wall and the smaller particles in the central portion of the tube. Therefore, the empty spaces between the larger particles, which were not occupied by the smaller grains, resulted in a smaller number of contact points per volume unit and a lower driving force in the coalescence and shrinkage of the grains. Thus, the use of a broad particle

size distribution associated with the centrifugal casting technique implies smaller length retractions, which reduces the amount of raw material and, consequently, production costs.

4.3.2 Apparent porosity

The apparent porosity of the ceramic tubes was measured using the Archimedes Method. For statistical analysis, fifteen (15) samples of each alumina/CFA composition were analyzed. The apparent porosity increases with CFA addition, as observed in Figure 34. The average apparent porosity obtained for tubes without CFA was in the range of 25.3 %, while the ceramic with the highest amount of CFA, CFA40, presented 39.7 %.

Figure 34 – Average apparent porosity percentage for the alumina-based tubular membrane incorporated with different CFA concentrations.

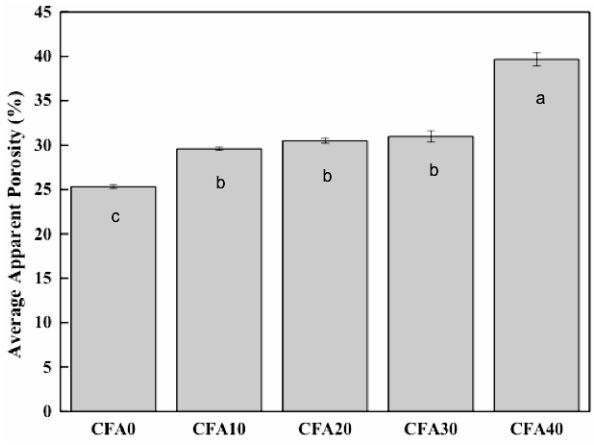

***Numbers followed by different letters are statistically different p ≤ 0.05 (Tukey's Test).**

Two conditions could have contributed to the increase in apparent porosity. In a first moment, approximately 6.0 % of CFA is removed from the sample during the thermal treatment, quantified by the loss on ignition values (Table 6). Such losses can lead to the void formation in the membrane structure, increasing the porosity. However, the greater apparent

porosity when using CFA can also be explained by the difference between the sizes of the alumina and ash particles and consequent wide particle size distribution. In this way, fine particles are less likely to be located within the interstices formed by larger particles due to segregation. The interstices become voids, increasing the porosity of the body. Steenkamp *et al.* (2001) used two different sizes of alumina particles and a mixture of these two powders to produce centrifugal casting tubes. The results achieved by the author corroborate with the data obtained in the present work, showing an increase in porosity with the increase in particle size.

These results are in line with the linear shrinkage results, showing an inverse correlation. As the CFA content increases, there is an increase in porosity and a decrease in linear shrinkage of the ceramic tubes.

4.3.3 Morphology

Figure 35 shows SEM photomicrographs for all prepared ceramic tubular membranes: CFA0, CFA10, CFA20, CFA30, and CFA40, outer and inner surfaces, and cross-sections in the magnifications of 100, 500, and 50x. The analysis of the images reveals that the external surfaces present more irregularities. Either coarser particles can be perceived compared to the internal surface images, which exhibit fine particles and smoother surfaces. The arrangement of larger particles on the outer surface and smaller particles on the inner face of the tube is due to the size classification caused by the centrifugal force acting in the centrifugal force.

It can be clearly seen that the alumina/ash composite membranes present asymmetric morphologies at the cross-section while alumina membrane (CFA0, Figure 35(c)) show slight segregation of the particles between the inner and outer sides of the tube because of the narrow particle size distribution of the commercial alumina (Table 5). For membranes based on mixtures of alumina and CFA, a clear size gradient is observed along the cross-section since

the CFA presents larger particles than commercial alumina (ten times, approximately) and wide distribution of particle sizes. The size gradient becomes even more pronounced as the CFA content increases.

Still, by observing the cross-section of tubes CFA10 and CFA20, Figure 35(f) and Figure 35(i), it is possible to notice a mixture between alumina and CFA particles, i.e., the stratification is not yet fully defined. For CFA30 and CFA40 tubes, the increase in CFA content leads to better particle separation and classification, forming two well-defined phases, one more porous and the other denser, Figure 35(l) and Figure 35(o).

Figure 35 – SEM micrographs of alumina-based tubular membranes incorporated with different CFA concentrations: outer (a, d, g, j, m), inner (b, e, h, k, n) and cross-section (c, f, i, l, o).

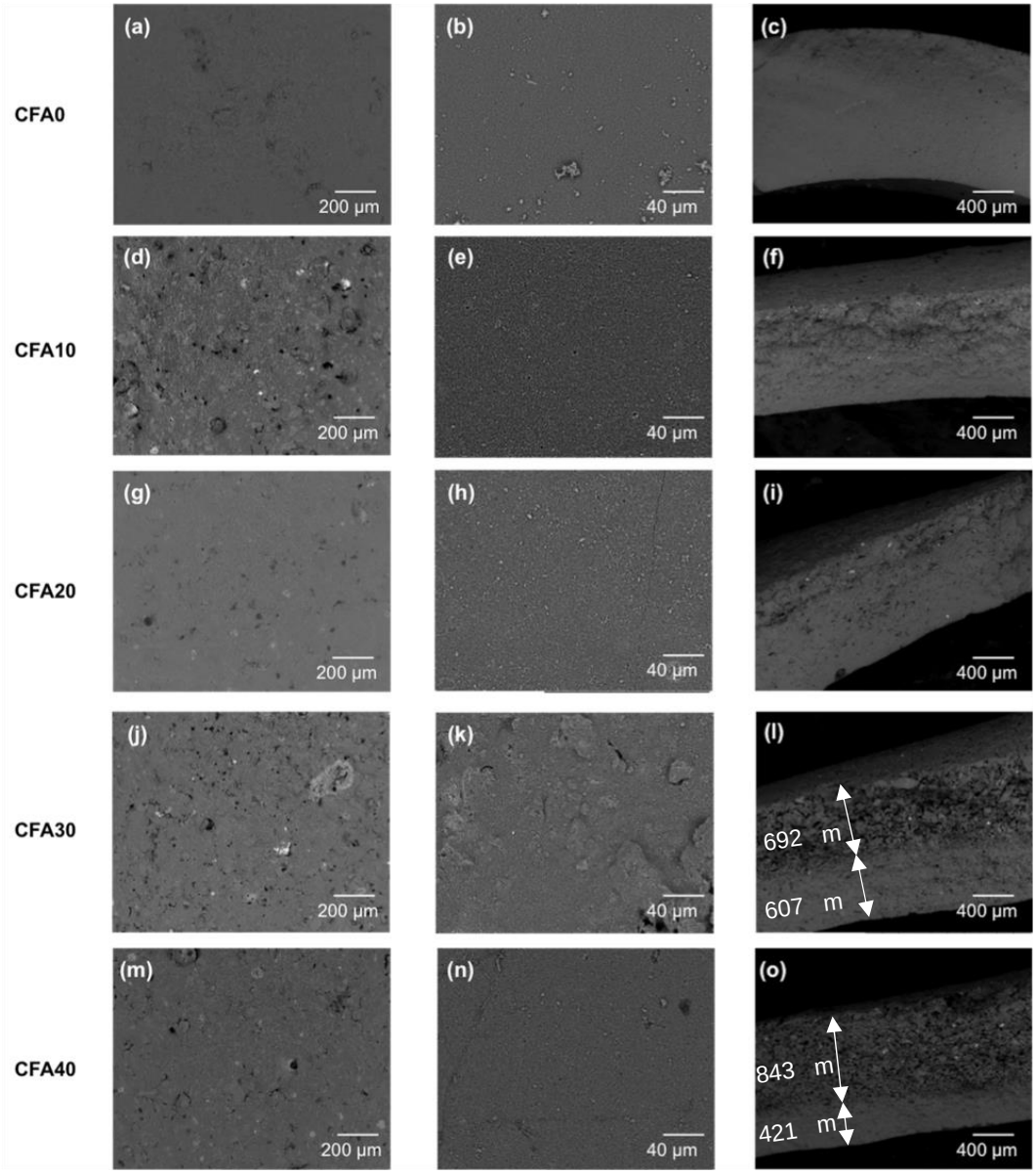

4.3.4 Mechanical strength

The results of mechanical resistance for the alumina-based tubular membranes incorporated with different amounts of CFA are shown in Table 9.

Table 9 – Average strength results of the alumina-based tubular membranes incorporated with different CFA concentrations.

Membrane	Average Strength (MPa)
CFA0	12.0 ± 0.3^{c}
CFA10	9.0 ± 0.5^{ab}
CFA20	8.0 ± 0.4^{a}
CFA30	10.9 ± 0.8^{bc}
CFA40	7.4 ± 0.7^{a}

***Numbers followed by different letters are statistically different $p \leq 0.05$ (Tukey's Test).**

The ceramic tubes obtained in this work are formed by alumina, resulting in a less porous layer due to the smaller size of the particles, and ash, which confers a more porous layer to the membrane. The CFA0 membranes, containing only commercial alumina, therefore less porous, showed the highest mechanical strength. With the addition of CFA, the tubes have become more porous, with less mechanical resistance. The greater porosity in tubes containing CFA is probably due to the larger size of the CFA particles and the burning residual carbon from the CFA that generates structural voids. Porous materials are more fragile and, consequently, with lower mechanical strength. Bisset (2005) and Chen *et al.* (2004) reported a decrease in mechanical strength with an increase in the porosity of the tested ceramic membranes.

As shown in the SEM analysis (Figure 35), the structure of the cross-section for the tubes CFA10 and CFA20 was not well stratified. In contrast, for the tube CFA30, the regions of CFA and alumina particles had almost the same thickness, and greater stratification was observed; this may have caused an increase in mechanical strength, although the porosity was statistically equal to the CFA10 and CFA20 membranes. For the CFA40 membrane, the alumina layer was really thin, and the highest concentration of CFA produced a thicker porous layer, which caused a reduction in mechanical strength. These results might be related to the

differences in strength between alumina and CFA, the increase in porosity, and the synergy between them.

4.3.5 Hydraulic permeance and observed retention

The membrane water permeance (L_P) was evaluated through water flux measurements in four transmembrane pressures 3.0, 2.5, 2.0, and 1.5 bar, feed flow rate of 150 L.h^{-1}, and temperature of 24 °C, for all the membranes, as described in Section 3.3.5. The same behavior was observed, the water permeate flux was directly proportional to the pressure applied, as expected for pure water in porous media. The hydraulic permeance was obtained by the slope of these curves (Equation 5). For a better comparison, the hydraulic permeance (sample triplicates) of the membranes is presented in Figure 36.

Figure 36 – Average hydraulic permeance obtained for the alumina-based tubular membranes incorporated with different CFA concentrations (24 °C, 150 L h^{-1} at 3.0, 2.5, 2.0, and 1.5 bar).

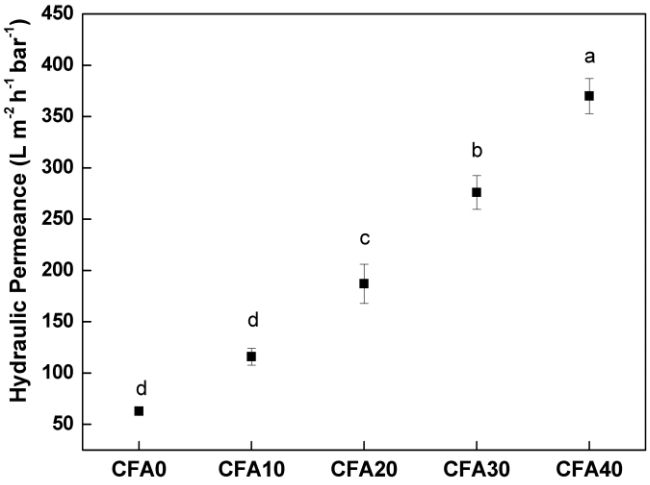

***Numbers followed by different letters are statistically different p ≤ 0.05 (Tukey's Test).**

Based on the data presented for the average hydraulic permeation, a linear increase in hydraulic permeance is observed as the CFA content increases in the formulation of the

membranes. These results demonstrate a reduction in the resistance to water flux (CFA0> CF10> CF20> CF30> CFA40) as the porosity increases. As mentioned by Steenkamp *et al.* (2001), who tested two sizes of alumina particles in the preparation of ceramic tubes by centrifugal casting, with the increase in the particle size of the raw materials, an increase in water permeability occurs. It is worth mentioning that as the CFA content increases, resistance to flux decreases due to the increase of the layer with larger particles, i.e., the asymmetry increases (Figure 35.c, f, i, l, o).

The observed retention is the relative resistance of the membrane on the transfer of a specific solute (in this case, cornstarch), determined by Equation 15. The retention tests revealed that all tested membranes prevented more than 99 % of the passage of cornstarch particles (Table 10).

Table 10 – Observed retention of cornstarch for the ceramic membranes.

Membrane	**R_{obs} (%)**
CFA0	99.89 ± 0.02
CFA10	99.82 ± 0.07
CFA20	99.61 ± 0.23
CFA30	99.73 ± 0.08
CFA40	99.06 ± 0.22

Since the size of the cornstarch particles is about 12 μm and the average retention was greater than 99 %, the membrane pore sizes are smaller than this value. The CFA40 membrane showed the lowest retention and the highest hydraulic permeance, suggesting that, in addition to greater porosity, as shown in Figure 34, it also has a larger pore size. The hydraulic permeance and retention ranges found in this study suggest that the ceramic tubes could be considered as membranes, since the pore sizes are less than 12 μm and the water permeance is

higher than 100 $L.m^{-2}.h^{-1}.bar^{-1}$. Other tests are necessary to establish the range of filtration and correct specify these ceramic membranes as microfiltration or nanofiltration technology.

The iodine test was carried out to detect the presence of cornstarch in the permeate stream. The starch is a polysaccharide of formula $(C_6H_{10}O_5)_n$ composed, on average, by 20 % amylose and up to 80 % amylopectin in weight. The amylose molecule is linear and has a helical shape, while amylopectin has a branched structure. Amylose can form helical inclusion complexes with iodine, exhibiting a blue color (HERRERO-MARTÍNEZ; SCHOENMAKERS; KOK, 2004). The complex of amylopectin molecules with iodine has a red-violet color. However, because of the non-helical structure, due to the ramifications, the complex will have less intense color. The pure iodine present in an aqueous solution has an intense yellow-brown color, visible even at great dilution (ANDRADE, 2021). As expected, the solutions collected in the retentate stream turned blue in contact with the iodine droplets. The permeate stream showed a yellow color for all experiments, confirming the absence of cornstarch as shown in Figure 37.

Figure 37 – Photographs of feed and permeate solutions after the Iodine test. The dark blue color is positive, and the yellow color is a negative test for cornstarch presence.

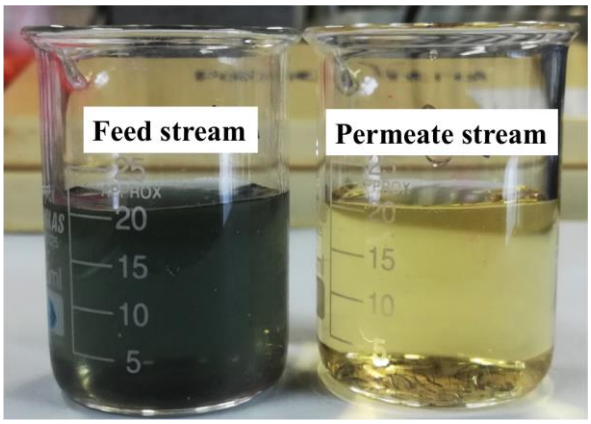

4.4. Conclusion

In Chapter 4, alumina-based asymmetric, tubular membranes incorporated with coal fly ash (CFA) were developed, characterized, and tested successfully. The membranes were prepared using the centrifugal casting technique without dispersants, binder or chemical additives, and contained up to 40 wt.% CFA (dry basis).

The addition of CFA to the slurry composed of alumina and water significantly modifies the structure and characteristics of the tubes. The observed phenomena are attributed to the differences in the characteristics of each material, such as the wide distribution of CFA particle sizes, the remaining carbon on the CFA sample and the processing conditions used in the centrifugal casting method. The presence of CFA in the ceramic membranes resulted in a higher porosity, which increased from 25 to 40 % in comparison with samples prepared with alumina only. There was also an increase in hydraulic permeance for membranes containing CFA, which was almost 6 times higher for CFA40. Membranes with CFA show up to 27 % less shrinkage than membranes without CFA after sintering.

All membranes showed an observed retention of cornstarch above 99 %. The retention did not change significantly with the increase in the CFA concentration, showing an excellent separation for the size of the cornstarch molecule. This result associated with the permeation results shows the possibility of applying the prepared tubes as membranes. However, further characterization studies must be carried out in order to determine the correct pore size of the membrane and their pores distribution and, thus, classify the membrane.

CFA is an industrial waste that requires proper disposal and represents a problem for the environment. The search for alternative uses can bring together both economic and environmental benefits. The methodology developed in this work proposes the efficient use of

CFA for the development of inorganic membranes without additives or binders. The addition of CFA reduces the manufacturing costs of these membranes, pointing out alternatives for several applications, such as the treatment of effluents, or even as supports for carbon and zeolite membranes.

CHAPTER 5

DESIGN AND PROPERTIES OF ALUMINA-CFA COMPOSITE MEMBRANES COATED WITH ZSM-5 ZEOLITE

ABSTRACT

The membrane separation can be enhanced by deposition of microporous materials over ceramic membranes. Moreover, in the zeolite-containing membranes, containing catalytically functional groups, separation and catalytic reaction can occur simultaneously, turning the reaction selectivity to the specific products and with lower capital and processing costs.

The objective of this chapter is the preparation, characterization and application zeolitic membranes supported on the CFA-based ceramic membranes elaborated in Chapter 4. The ZSM-5 zeolite membranes were successfully synthesized on the tubes via *in-situ* crystallization using the seeding method followed by the direct hydrothermal synthesis without organic structure-directing agent. The zeolites and resulting membranes were characterized by X-ray diffraction (XRD), Fourier transform infrared spectroscopy (FTIR) and scanning electron microscopy (SEM). The Alumina-CFA composite ceramic membranes coated with the ZSM-5 zeolite were tested in a membrane reactor for separation and reaction of aromatic compounds. We observed promising separation properties for molecules with kinetic diameter larger than 0.9 nm such as tri-isopropyl benzene and enhanced selectivity in the isomerization of *ortho*-xylene to *para*-xylene.

Zeolites are crystalline aluminosilicates, which are built from the SiO_4 and AlO_4 tetrahedra and with small micropores comparable to the sizes of molecules. Separation of chemical compounds by adsorption or using the membrane technology is an import area of zeolite application. The zeolites may contain cations or acid hydroxyl groups, which exhibit catalytic activities in numerous chemical reactions.

Deposing a thin layer of microporous materials over ceramic membranes can enhance the separation. This chapter describes the synthesis and separation properties of alumina-CFA composite ceramic membranes coated with zeolite layers. A variety of methods have been reported for the synthesis of zeolite and their deposition over the membrane surface. In this work the membranes were prepared via secondary growth crystallization method of ZSM-5 zeolites over the alumina-CFA composite membranes described in Chapter 4. After extensive characterization, the zeolite membranes were tested for separation of aromatic compounds and for conducting of selective xylene isomerization reactions.

5.1 Zeolite Coating

To perform a preliminary deposition test, the zeolite coating was prepared over the inner or outer surfaces of the alumina/CFA-based tubes. The Secondary Growth method of zeolite synthesis was applied to achieve a homogenous and defect-free layer over the tubular supports. As previously mentioned, the seeding step assists in the crystallization of the target zeolite framework and in obtaining a homogeneous deposition. In the cited method, the seeding stage is followed by the hydrothermal synthesis, without organic structure-directing agent (OSDA).

The hydrothermal synthesis of the ZSM-5 zeolites with a Si/Al theoretical ratio of 50 and molar ratio of SiO_2:0.01Al_2O_3:0.3 Na_2O:114H_2O was performed following the process

adapted from the works of Kim and Kim (2004), Schneider (2019), and Schneider *et al.* (2021). The reagents colloidal silica (LUDOX® 30 wt. %, Merk), sodium aluminate ($NaAlO_2$ anhydrous, Sigma-Aldrich), and sodium hydroxide (NaOH ≥ 97%, pellets, Sigma-Aldrich) were used, respectively, as a source of silica and sources of aluminum and sodium.

To implement the preliminary test, a total of eight tubes, two of each CFA concentration (10, 20, 30, and 40 wt.%), were used. As shown in Figure 38, one tube of each concentration was used to test the internal zeolite coating, covering the external tube face with a Teflon® tape. The other tubes were used for testing the zeolite deposition externally, and their extremities were covered with a Teflon® billet and Teflon® tape. Before the seeding stage, the tubes were immersed in a solution of 2 % acetone in distilled water for 1 h as a cleaning step.

Figure 38 – General scheme of the zeolitic deposition process, involving cleaning, seeding and hydrothermal synthesis.

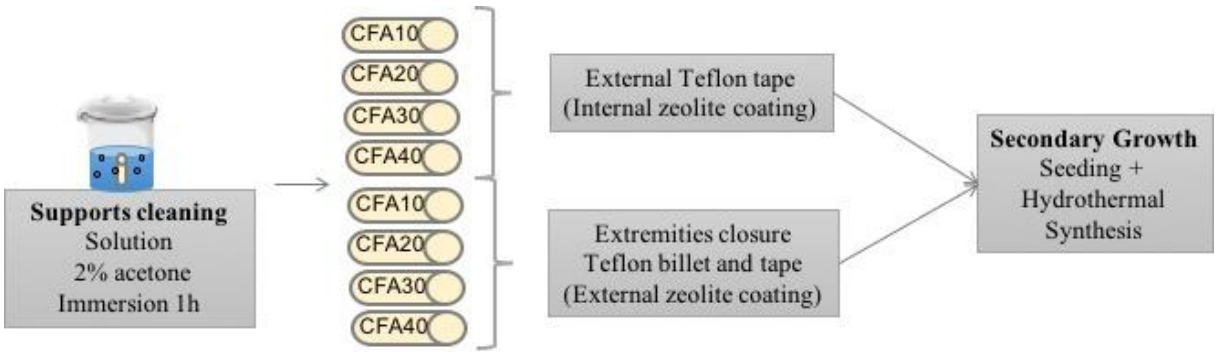

This preliminary test aimed to analyze the behavior of the zeolitic layer over the inner and outer surfaces of the alumina/CFA-based ceramic membrane since the surface morphology strongly affects surface phenomena as adhesion. Beyond that, the differences in local dissolution of the support material can influence the zeolite Si/Al ratio enabling the formation of other types of zeolites.

5.1.1 Seeding

The commercial ZSM-5 zeolite from *Zeolyst* (CBV 2314) was applied for seeding the ceramic tubes. The methodology used was adapted from Wei *et al*. (2017) and Schneider (2019).

According to the supplier, the ZSM-5 from *Zeolyst* (CBV 2314) presents a SiO_2/Al_2O_3 ratio of 23 and NH_4^+ as the compensation cation. A calcination step was necessary to transform the ammonium form into hydrogen form. The heat-treating was carried out at 550 °C in air for 5 h. The obtained H-ZSM-5 zeolite was mixed to Ethanol (analytical grade) to prepare a suspension 0.005 g ml^{-1} for the seeding method. The suspension was first submitted to the ultrasonic bath for 1 h for dispersing the crystals. After, the suspension was placed in the magnetic stirrer for 30 minutes.

Dip-coating was used for the seeding stage. Briefly, the ceramic tube was immersed in the seed suspension for 15 seconds after being washed with distilled water in abundance to remove the seeds not strongly attached to the surface of the supports. The tube was dried at 110 °C, in the vertical position for 1 h. The dip-coating and drying procedures were repeated two more times. After the third immersion in the suspension, the supports were dried overnight at 110 °C. The sequence applied for the seeding stage can be seen in Figure 39.

Figure 39 – Steps of the seeding procedure performed with the supports already clean.

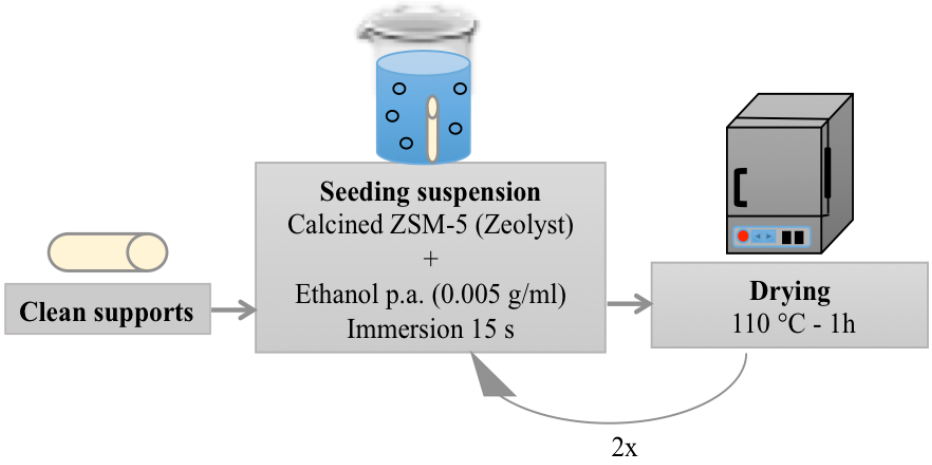

5.1.2 Hydrothermal Synthesis

For the hydrothermal synthesis, 5.61 g of sodium hydroxide (purity ≥ 98 % Sigma Aldrich in pellets) was dissolved in 70.16 g of deionized water forming **Solution 1**, divided into two different parts for the preparation of **Solution 2** (silica source) and **Solution 3** (alumina source). Briefly, 92 wt.% of **Solution 1** was mixed with 48.85 g of colloidal silica (LUDOX® HS40, Sigma Aldrich) and 102.87 g of deionized water, forming **Solution 2**; 8 wt.% of **Solution 1** was mixed with 0.47 g sodium aluminate (anhydrous Sigma Aldrich) and 193.82 g of deionized water, forming Solution 3. **Solutions 2 and 3** were mixed to obtain **Solution 4**, the synthesis solution. The methodology proposed here was based on the works of Kim and Kim (2004) and Schneider (2019) and followed the sequence presented in Figure 40.

The technique implemented is template-free to decrease costs of consumed chemicals and to facilitate the calcination step. Regarding the supported zeolite structure, the suppression of the calcination step to the organic template removal avoids cracks and defects on the deposited zeolite film. Also, the calcination of these compounds generates gases from these compounds directly to the atmosphere.

Figure 40 – Steps for the synthesis solution of ZSM-5 SDA-free.

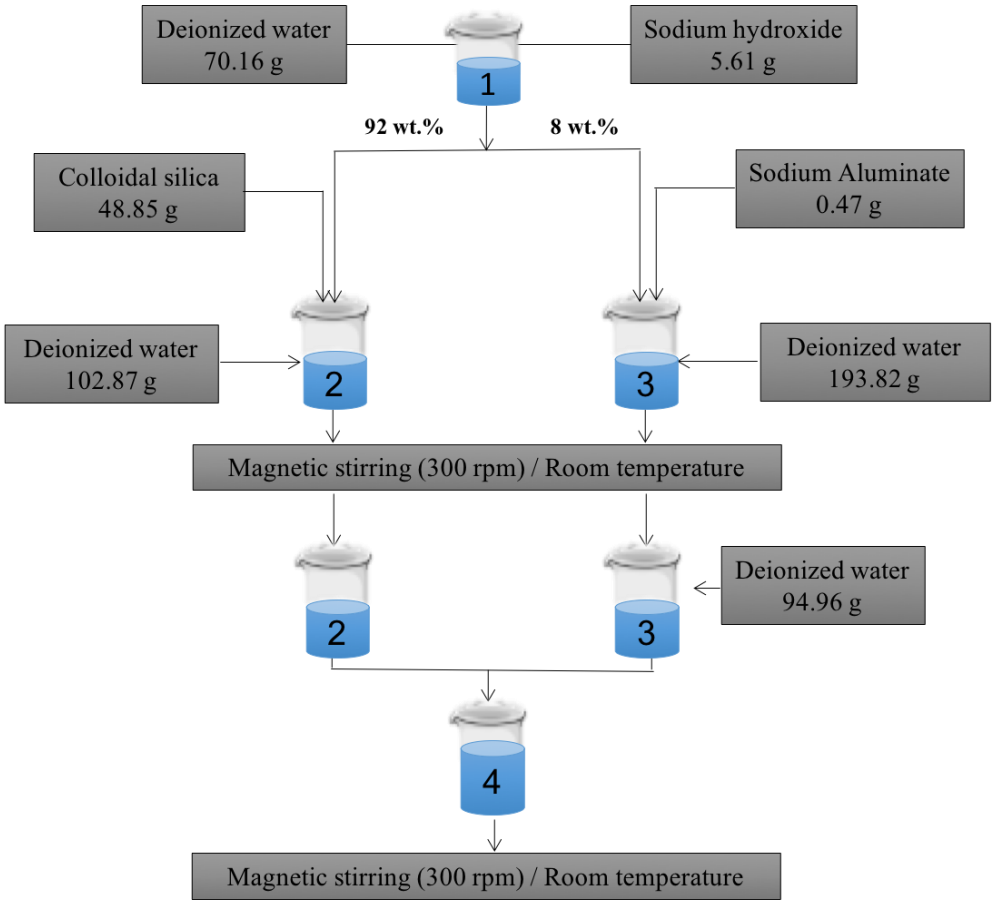

Adapted from Schneider (2019).

Solution 4 obtained was deposited in a 500 mL capacity Teflon®/autoclave (Figure 41). Five seeded supports, one of each CFA concentration (CFA0, CFA10, CFA20, CFA30, and CFA40), were also deposited in the Teflon®/autoclave vertically. The apparatus was settled in the oven at 180 °C for 24 hours.

Figure 41 – Image of the Teflon® and autoclave used for the hydrothermal synthesis (www.metalquimica.com).

After the elapsed time inside the oven and the completion of crystallization under autogenous pressure without stirring, the autoclave was cooled down. The supports were removed from the autoclave and washed with distilled water. For the release of not strongly adhered materials, the tubes were immersed in a beaker with distilled water, placed at the ultrasonic bath for 2 minutes, and dried at 80 °C.

After performing the preliminary tests (results available in the **Appendix**), the subsequently zeolite depositions were done on the inside surfaces, following the same steps already described above. However, the hydrothermal synthesis time was increased by 2.5 hours in order to optimize the process and obtain a better crystallization of the zeolite layer. Tubes CFA10, CFA20, CFA30, CFA40, and commercial pure alumina tubes (TCB99 from Tecnicer Cerâmica/Brazil) were used. The zeolite powder remaining inside the autoclave, after the hydrothermal synthesis, was subjected to a wash with 1 liter of distilled water and filtration through a vacuum pump. The powder was dried in an oven at 80 °C overnight.

Some membranes were used for testing the two successive synthesis and deposition of ZSM-5 layers. This means that after the steps of seeding, hydrothermal synthesis, and drying, the membrane was subjected to the second hydrothermal synthesis, following the same methodology already described previously for the first hydrothermal synthesis.

5.2 Ion Exchange

To perform catalytic tests over the zeolitic membranes, the ion exchange step is required to generate the desired acidity for the reactive processes. The catalysts supported in the tubes were converted to the H-ZSM-5 form by ion exchange with NH_4NO_3 (≥ 99 % Sigma Aldrich).

The zeolite membranes were immersed in a solution of NH_4NO_3 1 mol L^{-1} in distilled water for 1.5 h at a temperature of 80 °C. This procedure was performed twice to obtain a complete exchange of sodium ions for ammonium ions. After the first exchange, the materials were washed with deionized water and dried for 1 h at 80 °C. Thereafter, the materials were dried overnight at the same temperature. The H-ZSM-5 zeolites in the membrane layer were obtained after a calcination step (Figure 42).

Figure 42 – ZSM-5 ion exchange with NH_4NO_3 comprising the washing and drying steps and temperature profile for the calcination.

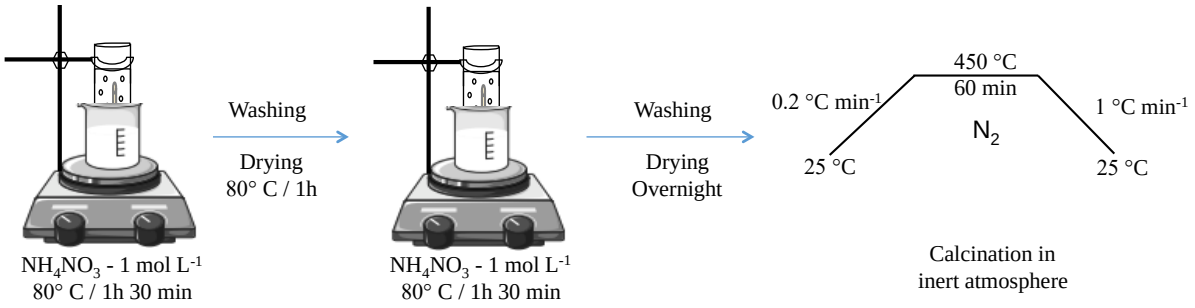

The calcination step was carried out in a tubular glass reactor within a tubular furnace, in a controlled atmosphere of N_2 flowing at 1 mL min^{-1}. The slow heating ramp, made according to Hedlund *et al.* (2002), started at 25 °C, finishing at 450 °C, and remaining at the maximum temperature for 1 hour. A ramp with a higher heating rate (5 °C min^{-1}) with a step at 450 °C, cooling back to room temperature naturally, was also used to compare the zeolite layer behavior.

5.3 Zeolite membrane characterization

The alumina/CFA membranes presented satisfactory properties, as good mechanical strength, high porosity, and adequate hydraulic permeance allowing their application as supports for zeolite coating.

The performed characterizations on the zeolitic layer was aimed to verify the deposition homogeneity and the structure of the formed zeolites. The preliminary test, depicted in the **Appendix**, aimed to investigate and compare the behavior of the proposed method of synthesis over the internal and external faces of the ceramic membranes CFA-based. From these results, it was decided to cover the inner part of the tubes with zeolite since the better-packed layer, composed of alumina, is located on the inner surface. For XRD and FTIR analysis, the samples were the precipitate contained in the Teflon® container after hydrothermal synthesis. The samples were named as indicated in Table 11.

Table 11 – Abbreviation given to hydrothermal syntheses performed and composition of the supports placed inside the reaction vessels.

Hydrothermal Synthesis	Zeolite Deposition	Supports
HS1	1st	1x CFA50, 4x commercial
HS2	1st	1x CFA0, 1x CFA10, 1x CFA20, 1x CFA30, 1x CFA40
HS3	1st	1x CFA0, 1x CFA10, 1x CFA20, 1x CFA30, 1x CFA40
HS4	1st	1x CFA20, 1x CFA30, 1x CFA40
HS5	2nd	1x CFA20, 1x CFA30, 1x CFA40 (from HS4)
HS6	1st	1x CFA30, 1x CFA40, 2x CFA 50, 1x commercial

5.3.1. X-Ray Diffraction (XRD)

The crystallographic phases obtained through X-ray diffractions for the precipitates extracted from the autoclave after different hydrothermal syntheses are shown in Figure 43. The obtained peaks could be successfully compared with the peaks found in the literature for the ZSM-5, MFI type zeolite, as can be seen in the work of Rasouli *et al.* (2012), and with the diffractogram obtained for the commercial zeolite CBV 2314 from *Zeolyst*.

Figure 43 – XRD diffractogram for (a) the zeolite powders formed after hydrothermal synthesis 1 to 6 (b) the commercial zeolite CBV2314 Zeolyst. HS = Hydrothermal Synthesis; Z – ZSM-5, M – Mordenite, A – Analcime and K - Kenyaite crystals.

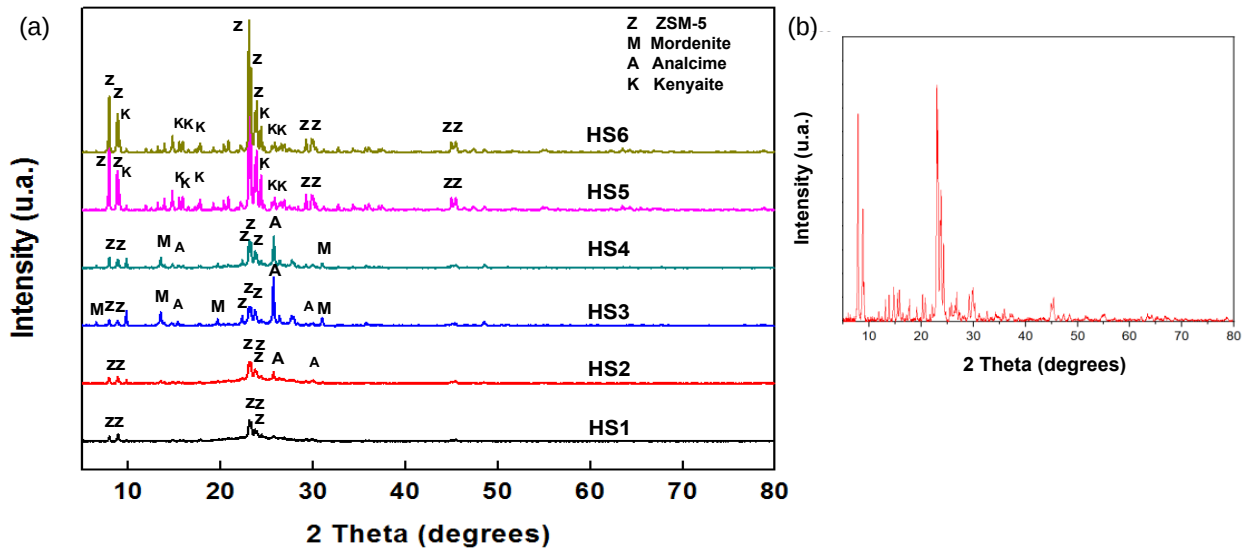

The peaks obtained were analyzed using the Collection of Simulated XRD Powder Patterns for Zeolites from IZA (TREACY; HIGGINS, 2001). A predominant occurrence of ZSM-5 crystals could be observed even in the diffractograms showing weak signals. However, although the synthesis conditions were the same, the peaks of mordenite and analcime crystals could be found in diffractograms for samples HS3 and HS4. This result is consistent with the literature. Similarly, in the work of Mascarenhas (2004), the formation of mordenite in the

preparation of zeolites MCM-22 was reported with a SiO_2/Al_2O_3 ratio of 50, when $NaAlO_2$ was used as a source of alumina, same conditions applied in the present work to obtain ZSM-5 zeolites. The appearance of different types of zeolite, or polymorphism, can be based on Ostwald rule of stages. Zeolites are metastable structures that follow an evolution of structure with time, beginning with the formation of a metastable phase that transforms through a series of stages to a more thermodynamically stable structure (OLEKSIAK; RIMER, 2014).

Since zeolites are extremely sensitive structures, the differences in the formations found may have been influenced by the dissolution of the different supports placed in contact with hydrothermal synthesis. Nishiyama, Ueyama, and Matsukata (1996) and Katsuki *et al.* (2005), among others, reported the support dissolution during zeolite synthesis. In the work of Cichocki (1985) the effect of the silica leached from the glass vessel during the hydrothermal synthesis in the produced zeolite was verified, leading to difficulties in the reproducibility of the product. The differences in the concentrations of coal fly ash (mainly composed of silica) and alumina in the ceramic tubes hinder a direct relationship between the products of one hydrothermal synthesis and another since the support may have dissolved during the process.

The experiments of hydrothermal synthesis were carried out in the sequence HS1 to HS6. The significant increase in the signal in the peak regions referring to the ZSM-5 overtime may be due to the deliberate choice of not performing rigorous cleaning (with acid) of the Teflon® used for the syntheses. According to Lowe and Nee (1994), it is believed that the crystallization of high-silica zeolites from inorganic systems is very sensitive to the presence of organic impurities and traces of material that might seed the crystallization. Therefore, the non-removal of these impurities adhered to the surface of the Teflon® reactor favors the formation of the type of zeolite synthesized previously, functioning as a structure driver.

The HS5 sample is related to the second hydrothermal synthesis of the tubes that participated in hydrothermal synthesis 4 (HS4). Formation of kenyaite can be seen in the diffractograms of hydrothermal syntheses 5 and 6 (HS5 and HS6). The kenyaite can be synthesized from aqueous suspensions containing SiO_2 and NaOH with ratios SiO_2/NaOH between 5 and 20 and H_2O/NaOH ratios from 50 to 500 (BENEKE; LAGALY, 1983). Since the HS5 sample was composed of supports with the zeolite already deposited, with a high Si/Al ratio, the increase in the concentration of Si may have favored the formation of kenyaite. As already mentioned, no chemical cleaning was performed in the reaction vessels so that the remained zeolites may have led to the subsequent formation of kenyaite, but more mildly, in the hydrothermal synthesis HS6.

5.3.2. Fourier Transform Infrared Spectroscopy (FTIR)

Infrared spectroscopy was used to identify the composition of the synthesized NaZSM-5 samples (Figure 44). The analysis was performed for the zeolite powders remaining after hydrothermal syntheses.

It was possible to observe that the synthesis favored the ZSM-5 zeolite formation, as expected. The band around 535 cm^{-1} is correspondent to the double ring from the pentasil framework composing the MFI type zeolite. The band at 790 cm^{-1} represents the symmetric stretching of the Si-O groups and the bands at 1200 and 1080 cm^{-1} represent the external and internal asymmetric stretching of Si-O (GONÇALVES *et al.* 2008; ROHAYATI, KRISNANDI, SIHOMBING, 2017).

Figure 44 – FTIR-ATR spectra performed for the remaining powder after the hydrothermal syntheses 1 to 6, indicating the presence of the NaZSM-5 zeolite characteristic bands.

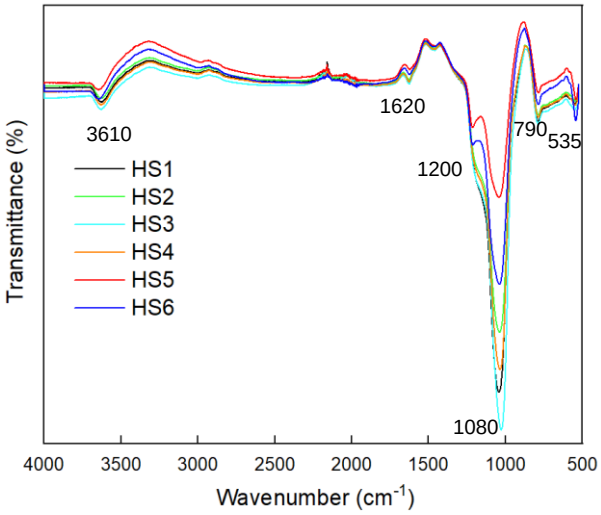

According to Jentys *et al.* (1989), the bands shown around 1620 and 3610 are relative to the O-H stretching vibration and to the bending vibration of adsorbed water, respectively, that decrease in intensity with the heat treatment. The spectra for HS1 to HS4 samples show typical curve shapes for mordenite around 1200 cm^{-1}, where a shoulder appears and analcime zeolites, where an intense broadband appears (ALY; MOUSTAFA; ABDELRAHMAN, 2012). These results suggest the presence of other zeolite types besides the ZSM-5 zeolites and are in accordance with XRD analyzes.

5.3.3. FTIR measurements of the zeolite acidity with adsorbed pyridine (Py)

The IR spectra of Py adsorption on the HS1 and HS6 zeolites are shown in Figure 45 and Figure 46**.** The band at 1616 cm^{-1} is attributed to physisorbed Py, linked by the hydrogen bonding to the surface hydroxyl groups. The band at 1546 cm^{-1} corresponds to the C-C stretching vibrational frequency typical of pyridinium ions (PyH^{+}), formed as a result of Py

protonation by the Brønsted acid sites (BUZZONI *et al*., 1995). The bands at 1634, 1616 and 1450-1455 cm^{-1} correspond to υ_{8a} and υ_{19a} modes of molecularly coordinated Py (PyL), indicative of the presence of Lewis acid sites. The bands at 1490-1492 cm^{-1} indicates the mixture of both types of acid sites (AL-DUGHAITHER; DE LASA, 2014). The Brønsted acid sites are relevant to the presence of zeolite, while the Lewis acid sites can be due to both zeolite and alumina of the composite membrane (LIU; TRUITT, 1997), which also exhibits noticeable Lewis acidity. Evacuation of zeolite at 250, 350, and 450 °C results in the progressive decrease in the intensity of FTIR bands assigned to both Brønsted acid sites. The intensity of the Py-L peak also decreases for the two samples following desorption above 150 ºC, however, after desorption above 350 ºC, there is a small increase in the relative intensity of this peak. This increase is due to the appearance of a shoulder at ~1462 cm^{-1} (Figure 45(b) and Figure 46(b)), which can be assigned to iminium ions, as previously suggested for zeolites H-BEA (VIMONT; THIBAULT-STARZYK; LAVALLEY, 2000; SANDOVAL-DÍAZ; GONZÁLEZ-AMAYA; TRUJILLO, 2015) and MAZ (GUISNET *et al*., 1997) as Py molecules coordinated to LAS interact with the neighboring BAS (MARQUES *et al*., 2003). Alternatively, it could be due to the aromatic products of Py transformation above 350 °C.

By using the extinction coefficients (εB = 1.67 and εL= 2.22 cm μmol^{-1}) (QIN *et al*., 1985) for the 1546 and 1451 cm^{-1} bands, the concentrations of both types of Brønsted and Lewis acid sites were calculated. The concentrations of Brønsted acid sites as functions of temperature are shown in Figure 47 for both HS1 and HS6 samples. The concentration of both sites decreases after evaluation at higher temperature. The similar shape of temperature dependence curves (Figure 47) for both Lewis and Brønsted acid sites suggest their similar strength in the HS1 and HS6 samples.

Figure 45 – FTIR spectra of (a) Py adsorbed on HS1 at 100°C followed by evacuation at 150, 250, 350, and 450 °C; (b) spectral decomposition of the Lewis band for each desorption temperature.

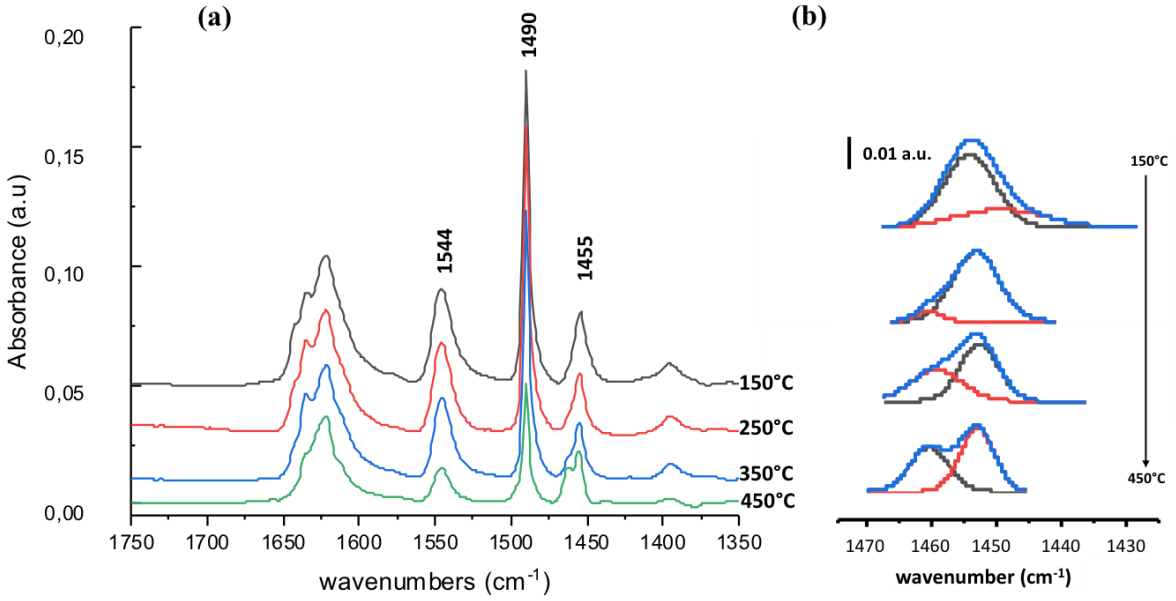

Figure 46 – FTIR spectra of (a) Py adsorbed on HS6 at 100°C followed by evacuation at 150, 250, 350, and 450 °C; (b) spectral decomposition of the Lewis band for each desorption temperature.

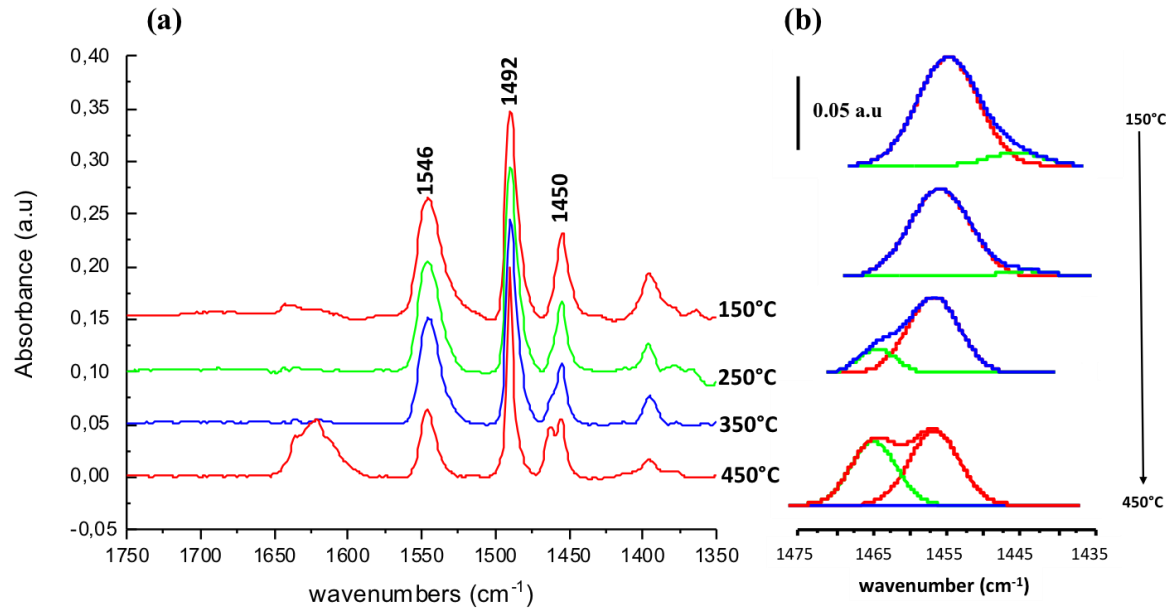

Figure 47 – Evolution of both Lewis and Bronsted concentrations (µmol g^{-1}) as functions of the temperature for HS1 and HS6 zeolites.

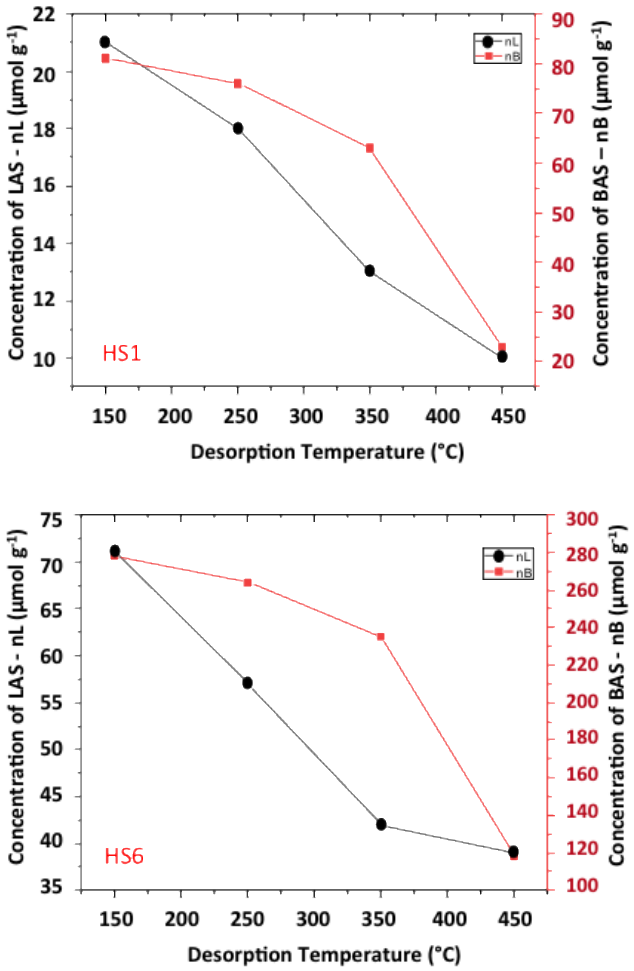

Higher concentration of the Brønsted acid site in the HS6 sample is also consistent with higher crystallinity of HS6 sample also observed by XRD and FTIR. The characterization of the powdered precipitates taken from autoclaves after the zeolite synthesis clearly indicates the presence of H-ZSM-5 zeolite, possibly with some impurities of other zeolites. Note that the Si/Al ratio in the prepared samples can be affected to some extent by the membrane support and can be also rather sensitive to the synthesis conditions.

5.3.4. Scanning Electron Microscopy (SEM), Dispersive Energy Spectroscopy (EDS)

According to Szostak (1989), the seeding stage ensures the ZSM-5 zeolite crystallization over a varied type of supports. The SEM images of Figure 48 show in (a) a support CFA40 before seeding and the same support concentration after the seeding with the commercial ZSM-5 zeolite. In Figure 48(b), only a few crystals are scattered on the support's inner surface.

Figure 48 – (a) Support CFA40 before seeding step and (500x and 15.0 kV); (b) after seeding step (500x and 4.0 kV).

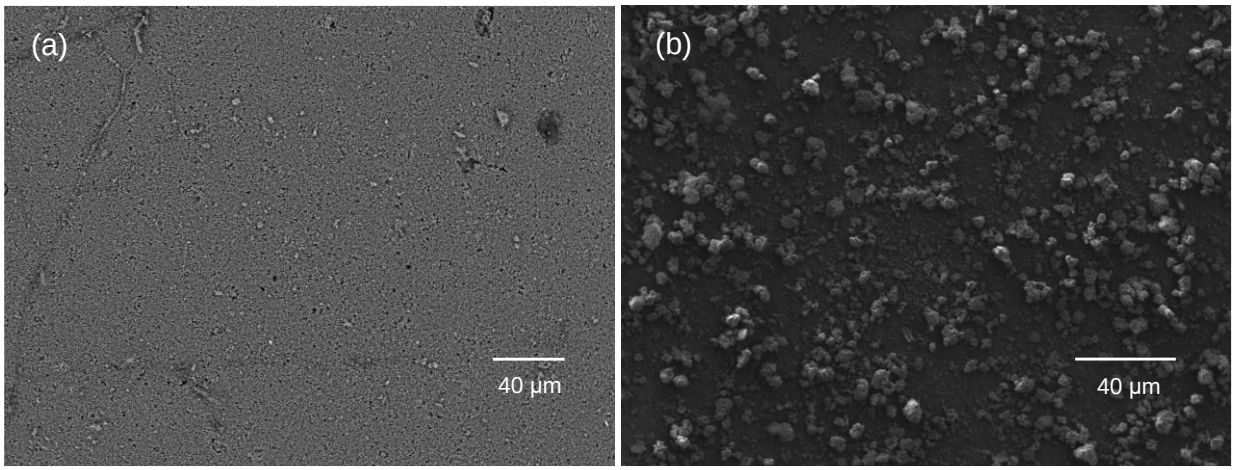

The seeding technique has been vastly used to eliminate the need for heterogeneous nucleation and expand the window of conditions for development of a continuous ZSM-5 zeolite film (LAI; GAVALAS, 1998) over membranes. In the work of Öhrman, Hedlund and Sterte (2004), the difference between a seeded and a non-seeded support after hydrothermal treatment is shown. According to the results, the seed crystals grew to form a homogeneous and continuous zeolite film covering the surface of the monolith. In contrast, using “direct synthesis” method (where no seeds are used), a very low zeolite coating was obtained in the same synthesis solution. Consequently, it was possible to observe that the seeds facilitated the

homogeneous growth of the zeolite film on the support. According to Szostak (1989), in the absence of organic cations, Na^+, obtained from NaOH in this work, acts as the structure directing species in zeolitization. As stated by Lai, Yan and Gavalas (2000), small colloidal particles are attracted to the solid surface by dispersion forces and agglomerate there creating aggregates that provide the preferential sites of nucleation and crystallization.

SEM micrographs allow verifying the successful ZSM-5 deposition on the ceramic support after seeding followed by hydrothermal synthesis, template-free, for 26.5 hours. Innumerous authors as Zang *et al.* (2015), Said *et al.* (2015), Lai, Yan and Gavalas (2000), among others, show through scanning micrographs a homogeneous coverage with ZSM-5 zeolite morphologies as seen in the present work. The surface and cross-section morphologies of the zeolitic membranes are shown in Figure 49.

During preparation of the samples for SEM analysis, the membranes were subjected to an ultrasonic bath for the detachment of crystals not firmly deposited on the support. After drying, they were broken with a tool to obtain small pieces to perform the SEM analyses. The images show that it was possible to obtain a continuous and firmly adhered covering to the support, even after cleaning and breaking the samples. No cracks or uncovered parts of the support were perceived. The layers shown in Figure 49(a) and Figure 49(b) present one and two depositions, respectively, being apparently dense and continuous with no defects or pinholes.

The cross-section image of the support with one deposition (Figure 49(c)) shows that the first zeolitic layer has an average thickness between 6 and 10 μm. When covering the substrate with two layers of zeolitic film (Figure 49(d)), the thickness of the zeolitic layer practically doubled, with values around 15.7 μm. As can be seen, the zeolitic layer was well adhered to the support, an important condition for using the ceramic tube as support.

Figure 49 – SEM images of the zeolite deposition over the supports: (a) and (c) are the surface and the cross-section of support with one deposition layer; (b) and (d) surface and cross-section of the support with two deposition layers (surface: 2500x, 4.0 kV; cross-section: 1500x, 5.0 kV).

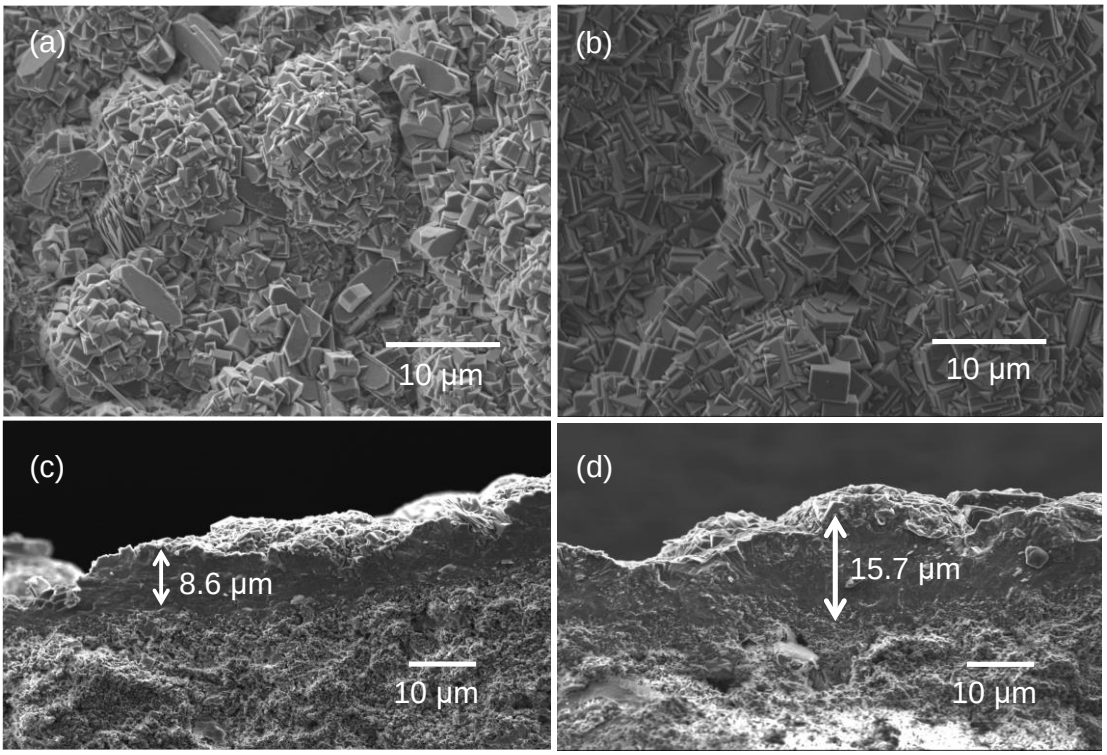

The EDS analysis was used to assist in visualizing the interface between the surface of the ceramic tube and the deposited zeolite layer. Figure 50 show the micrograph of the CFA40 support with two depositions of zeolite on its top. The yellow map, which corresponds to Silica, is shown mostly in the part related to zeolite and, to a lesser extent, in the support region since the concentration of silica in the CFA is predominant, as shown in Table 6. Meanwhile, the pink map (Figure 50(c)), corresponding to the aluminum element, focuses more on the part of the support where it is predominant. It is also possible to notice an intermediate region at the interface of the two materials, possibly due to the growth of crystals in the inner layers of the support caused by the penetration of the synthesis solution through the pores of the CFA/alumina support.

Figure 50 – EDS for the cross-section image of a CFA40 as support with two zeolite depositions.

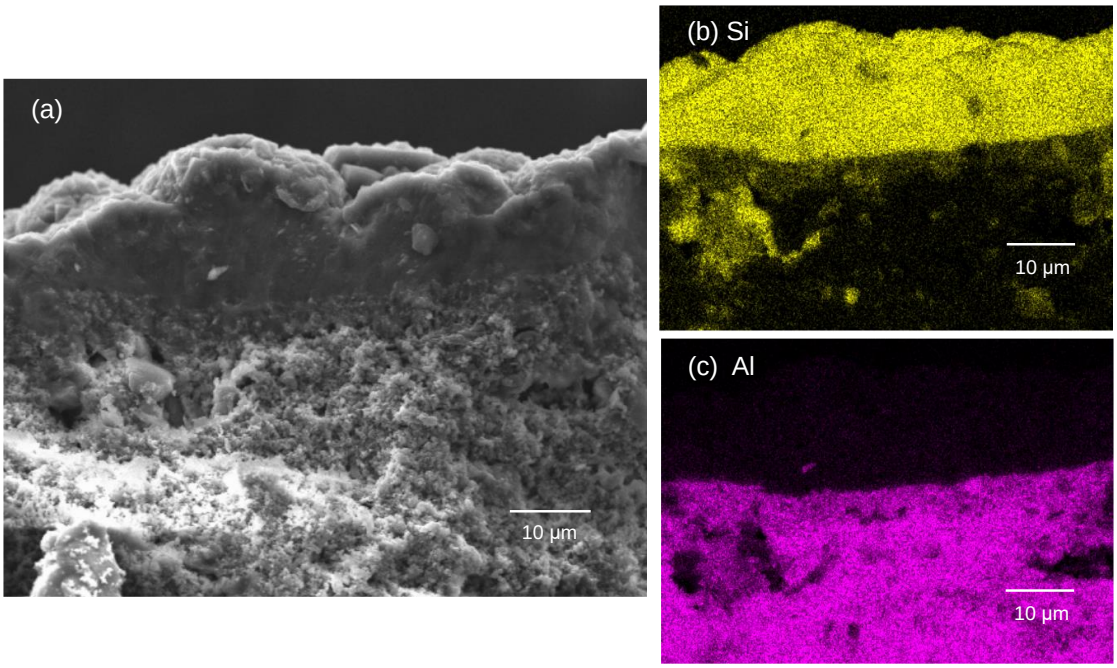

The EDS was used to obtain the Si/Al ratio estimation for the support and zeolite layer. The regions used to measure the concentrations of Si and Al are marked in Figure 51 and the results are reported in Table 12. The support, richer in alumina compared to the zeolitic layer, also had the Si/Al ratio calculated by EDS (spectra 2 and 4). As expected, the support containing a higher CFA concentration showed a higher concentration of silica since its main component is silica (Table 6).

Figure 51 – Spectra selected (CFA 30 (a) and CFA 40 (b) supports) to the calculation of Si/Al ratio at the zeolite and the ceramic support.

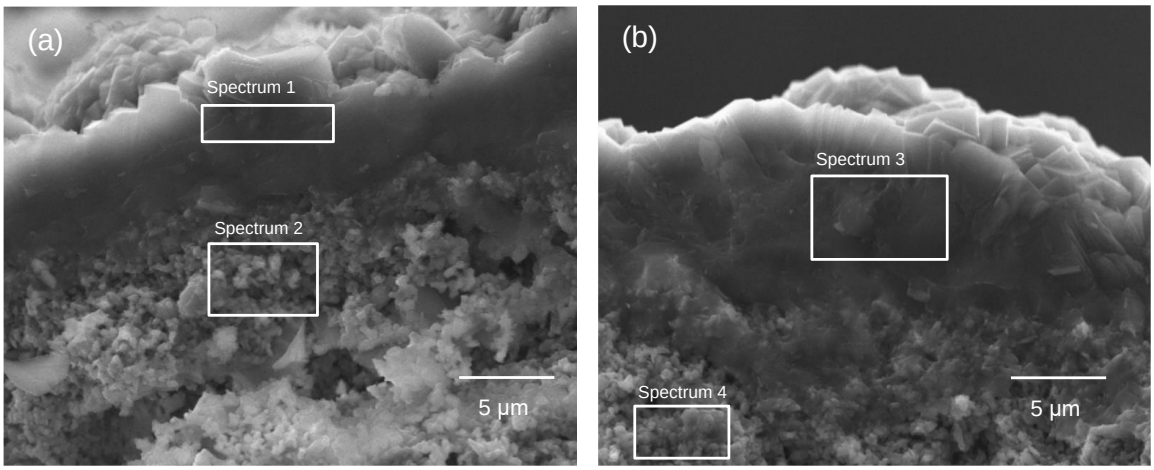

According to Lai, Yan, and Gavalas (2000), in supported synthesis using aluminum, the Si/Al ratio decreases due to the substrate dissolution. The effect of leaching could be seen by the Si/Al ratio of the zeolitic layer synthesized, which decreased from 50 to values around 10.5 (Table 12).

Table 12 – Si/Al ratio obtained by EDS analysis on the ceramic supports and zeolite layers with one and two depositions.

Spectrum	Si	Al	Si/Al
1 - Zeolite (1 deposition)	28.3	2.6	10.9
2 - Support CFA30	4.2	34.3	0.1
3 - Zeolite (2 depositions)	28.4	2.7	10.5
4 - Support CFA40	7.2	27.5	0.3

In the heat treatment, the slow heating rate is an essential parameter for synthesizing zeolites and their structural integrity. The micrographs of Figure 52 exhibit two cracks observed at different points in the same synthesized zeolitic layer, even though a slow heating rate

(0.2 °C min^{-1}) has been used. This same effect was observed in the micrographs of other samples.

Figure 52 – SEM micrographs of zeolite membrane with two depositions over CFA40 supports. Defects observed along the same zeolitic membrane after the heating treatment (10000x and 4.0 kV; 5000x and 10.0 kv).

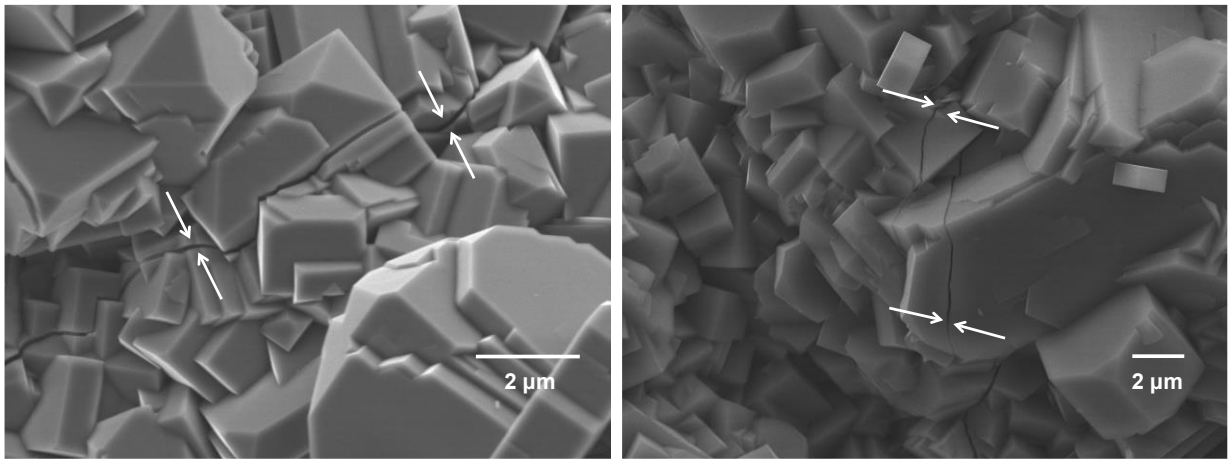

These images corroborate the diverse information in the literature, as manifested in Sano *et al.* (1994), stating that cracks are easily formed inside the membrane during the treatment process. Such defects occur due to differences in expansion and contraction between support and zeolites and cause a decrease in the membrane separation efficiency.

As shown in the X-ray diffraction patterns of the zeolite powders remaining after hydrothermal synthesis (Figure 43), the micrographs of the powders showed the formation of mordenite, analcime and kenyaite morphologies (Figure 53).

Figure 53 – Micrographs of other types of zeolites present in the power remaining after hydrothermal syntheses (5000x and 5.0 kV) (a) Kenyaite; (b) Mordenite and (c) Analcime.

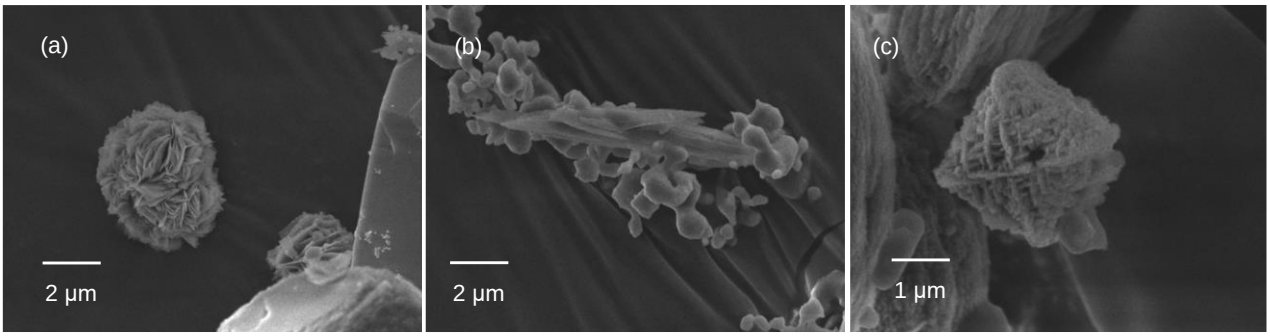

Synthetic kenyaites are often obtained in more or less spherical nodules of plate-like crystal aggregates (Figure 53(a)). Sometimes the nodules are embedded in a matrix of amorphous silica (BENEKE and LAGALY, 1983). The needle-shaped zeolite seen in Figure 53(b) according to Kalipçilar and Çulfaz (2007) and Schineider (2019), are the mordenites, MOR framework. Analcime, shown in Figure 53(c) has icosahedron morphology (SCHINEIDER, 2019).

The crystals shown are not perfectly formed and the coexistence of both amorphous and crystalline phases can be seen in Figure 53 for the remaining zeolite powders. Crystallization, therefore, was noticeably faster on ceramic tubes. This occurs because the gel layer formation on the supports takes place first by attraction and aggregation of small particles moving by the Brownian motion, and zeolitization is initiated in colloidal particles. The larger, less active particles settle down on the vessel bottom under gravity (LAI; YAN; GALAVAS, 2000).

5.4 Separation of aromatic molecules over zeolite coated alumina-CFA membranes

The separation tests with Alumina-CFA composite membranes coated with one and two layers of zeolite were performed for the following two mixtures:

- *ortho*-, *meta*-, and *para*-xylenes;

- *ortho*-, *meta*-, *para*-xylene, mesitylene and tri-isopropyl benzene.

The chemical formulas of aromatic compounds used in this work and their critical diameters are shown in Figure 54. The tests were carried out at atmospheric pressure and at the 175-320 °C temperature range. The experimental conditions allowed keeping the aromatic compounds in the gaseous phase.

Figure 54 – Organic compounds with their critical diameters used in separation and reaction tests over the ZSM-5 membranes.

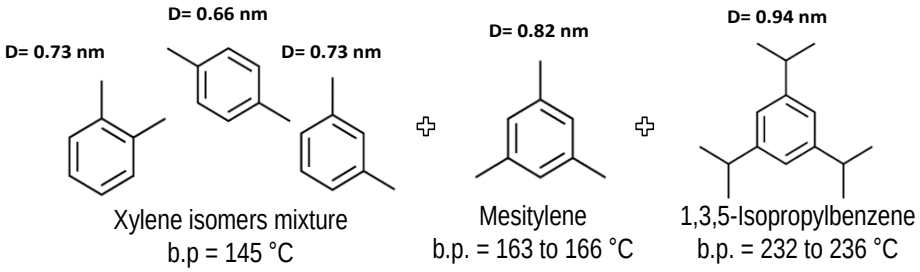

The zeolites deposed over membranes were used without ion exchange. In this way, such tests were intended to test only the selectivity of the membrane to separation of the xylene compounds.

5.4.1. Separation of xylenes

Improving the separation efficiency between xylene isomers is a major challenge in the industry. Because to the similarity of the boiling points of *p*-xylene (138 °C), *m*-xylene (139 °C) and *o*-xylene (144 °C), their separation in industry is currently performed (LI *et al*. 2020) via either fractional crystallization operating at ~220 K or adsorption over cation-exchanged FAU-type zeolites X and Y. In the fractional crystallization, the recovery of *p*-xylene is limited to 60–70%. In adsorption-based processes, such as the commercial Parex process (BAO *et al*. 2016), high temperature (~ 180 °C) and pressure (~ 9 bar) are required to promote the separation.

The commercial xylene mixture used in this work was composed of 25.0 % *meta*-xylene, 71.2 % *para*-xylene and 3.8 % *ortho*-xylene. For the separation tests were used the membranes with the synthesized Na-ZSM-5 zeolite layer. At temperatures around 170 °C and using a mixture of xylene isomers with two values of flow rate, 450 and 100 μL min^{-1}, no relevant separation selectivity to any specific xylene was achieved on the ZSM-5 zeolite layer. It is important to consider that at the molecular level, the critical diameter of the molecules and the pore sizes are not considered absolute values once the molecular and porous structures are not completely rigid.

A possible reason of the low separation selectivity results might be molecule permeation through defects has dominated the overall transport rate of the xylenes in the case of an irregular layer of zeolites has been formed. Another possibility would be the permeation of the compounds in pores larger than the critical diameters of the molecules. As shown in Table 2, the mordenite pores, which according to XRD results may have been formed in the zeolitic layer, are slightly larger than the molecular sizes of the xylene isomers, with 0.7 nm. This

contamination by other types of zeolites, mainly mordenite and analcime, may have facilitated permeation, reducing the separation performance of the zeolitic membrane.

5.4.2. Separation of other aromatics over the zeolite layers over membranes

Separation tests were then performed for xylene isomers, mesitylene and 1,3,5-triisopropylbenzene. Because of higher boiling points of mesitylene and 1,3,5-triisopropylbenzene (236 °C), in order to keep the aromatic compounds in gaseous phase, the separation was performed at higher temperatures (around 300 °C). The feed flow was 450 μL min^{-1}.

The molecules of xylene isomers and mesitylene were able to permeate through the zeolitic membrane. Similar to 170 °C, we did not observe any noticeable separation of the xylene isomers at 300 °C. The 1,3,5-triisopropylbenzene molecules, which present as minimum critical diameter the value of 0.94 nm, exceeding the theoretical ZSM-5 pore opening of 0.55 nm, were not observed in the chromatograms of the permeate stream (Table 13). These results indicate that the separation performance is strongly dependent upon the differences in the molecular size and suggest the existence of crystals pores smaller than 0.93 nm diameter This suggest that the prepared zeolite coated alumina-CFA composite membranes can used for separation of molecules with a critical diameter larger than 0.9 nm.

Table 13 – Membrane selectivity obtained for the separation tests with the mixture of organic compounds.

Conditions	
Feed composition	Xylene mixture, mesitylene, triisopropylbenzene
Ceramic supports	CFA40 (HS3)
Feed flow rate (μl min^{-1})	450
Selectivity to *para*-xylene	0
Selectivity to mesitylene	0
Selectivity to triisopropylbenzene	Total
Temperature (°C)	300

5.5 Separation and isomerization tests using *ortho*-xylene

Separation and isomerization tests using *ortho*-xylene as feed stream were conducted at 1 bar and temperatures around 300 °C, using the H-ZSM-5 zeolite membrane. The reaction involves Brønsted acid sites. The presence of these sites in the synthetized zeolites was confirmed in this work by FTIR with adsorbed Py. The goal was to evaluate the isomerization reaction of *ortho*-xylene and the membrane selectivity to *para*-xylene.

The feed was composed of 99.7 % *ortho*-xylene and 0.3 % *para*-xylene. For the N_2, used as carrier gas, the flow rate was 7 ml min^{-1}. The feed flow rate was decreased to test the reaction at lower space velocities (WHSV). The catalyst mass was estimated to be 180 mg, in agreement with the weight gain per support area obtained in Schneider et al. (2021). The applied values were 100 and 30 μL min^{-1} (WHSV = 29.2 and 8.8 h^{-1}, respectively), according to values found in the literature for the same reaction and catalyst (YOUNG; BUTTER; KAEDING, 1982; ALBAHAR; LI; ZHOLOBENKO; GARFORTH, 2020). The decrease in the space velocity leads to a higher contact time between the catalyst and reactants/products.

The isomerization experiments were carried out starting with pure *o*-xylene at 320 °C. For values of *ortho*-xylene flow rate of 30 μL min^{-1}, the conversion to *para*-xylene reached 11 %, with an average of 6.8 %. The equilibrium composition of different xylenes at 300 °C is given in Table 14. It seems that *meta*-xylene should be the most abundant product according to the thermodynamic considerations. The results depicted in the present work (**Table 15**) suggest that the conversion of *ortho*-xylene over the zeolite coated Alumina-CFA membrane is not governed by the thermodynamics but mostly by kinetics, with the highest selectivity to *para*-xylene, which has the smallest molecular size among the xylene isomers (0.66 nm).

Table 14 – Xylene isomers in the equilibrium composition at 300 °C.

	Equilibrium composition (%)		
	meta-xylene	*para*-xylene	*ortho*-xylene
300 °C	54.4	21.5	24.4

MINCEVA *et al.* 2008

Much higher concentration of produced *para*-xylene was detected in the permeated compared to the retained stream of the membrane. The presented separation selectivity of *para*-xylene to *ortho*-xylene was 1.5. This introduces the effect of shape selectivity for isomerization of aromatics over zeolite coated alumina-CFA membranes. Since was not observed any noticeable effect of xylene separation in the absence of isomerization, higher selectivity *ortho*-xylene conversion to *para*-xylene combined with the separation can be due to the shape-selectivity effect attributed to the reaction transition state, which slows down production of very thermodynamically stable *meta*-xylene. High *ortho*-xylene conversion to *para*-xylene observed in this work suggests sufficient quality of the zeolite layer over the ceramic membranes, which may unveil perspectives for *in-situ* separation of *ortho*- and *para*-xylene in the isomerization reaction.

Table 15 – Conversions of *ortho*-xylene to *para*-xylene in the isomerization test with *o*-xylene as feed (H-ZSM-5 zeolite**).**

Conditions	
Feed composition	*o*-xylene
Ceramic supports	CFA20 and CFA30 (HS4)
Feed flow rate (μl min^{-1})	30
Average conversion to para-xylene (%)	6.78
Selectivity to *para*-xylene	1.53
Temperature (°C)	320

For similar conditions, such as pure *ortho*-xylene as feed at 300 °C, Haag *et al.* (2006) found conversion values of 2.6 % for isomerization of xylenes on H-ZSM-5 membranes. The conversion increased to 7.3 % with an increase in temperature to 400 °C. In the works of Sakai, Tomita and Takahashi (2001), Wegner, Dong and Lin, (1999), and Collins and Medina (1983), low selectivity values for *para*-xylene over ZSM-5 membranes were also found. According to the authors, mainly permeation through defects on the zeolitic membranes may have resulted in these results.

5.6 Conclusion

The synthesis, characterization and application of zeolite membranes were demonstrated. The seeding technique was used to ensure the homogeneity of the zeolitic deposition. Meanwhile, the hydrothermal synthesis time has been increased in order to optimize the zeolitic deposition and obtain a better formation of the ZSM-5 crystals. The experimental results allowed drawing several conclusions about the development of the zeolitic membrane supported in CFA/alumina tubes.

X-ray diffraction provided information about the effectiveness of the synthesis method employed in obtaining the ZSM-5 zeolite. The XRD patterns showed peaks characteristic of ZSM-5, sometimes contemplating the formation of mordenite, analcite and kenyaite.

Silica and alumina substrates can dissolve and change the silica/alumina ratio during the hydrothermal synthesis. The FTIR spectra identified the presence of the ZSM-5 zeolite bands and typical curves of mordenite and analcite, suggesting the presence of other frameworks besides ZSM-5 in agreement with XRD.

The ion exchange step was carried out with the purpose of applying the zeolitic membranes to the catalytic tests. The procedure, followed by activation by calcination, generates the necessary acidity for the reactive processes. FTIR with Py adsorption showed that the concentration of Brønsted acid sites depends on the crystallinity of the zeolite samples. The optimized ion-exchange and calcination procedures with an extremely slow heating and cooling ramp, of 0.2 °C/min and 1 °C/min, respectively, were applied trying to avoid the formation of cracks in the zeolite coating.

The analysis of the micrographs confirmed the formation of microstructures with the coffin shape, characteristic of the ZSM-5 zeolite, in the layers deposited on the support. The cross-sectional image of the support with one deposition showed an average thickness between 6 and 10 μm, while the supports with two zeolitic depositions had their thickness practically doubled. EDS was used to obtain the estimate of the Si/Al ratio for the support and the zeolite layer. The membrane alumina-CFA supports showed a low Si/Al ratio, between 0.1 and 0.3. Meanwhile, for the zeolitic layer the Si/Al ratio was around 10.5 and 10.9 for one and two depositions, respectively. Despite the slow temperature ramp applied to activate the acidic sites after the ionic exchange, some cracks could still be found through SEM analysis.

Potential application of zeolite membranes obtained with the proposed methodology and supported on CFA-based ceramic membranes was shown for the separation and isomerization of aromatics. It is also worth noting that a contamination-free ZSM-5 synthesis is important for the successful separation. The membranes showed complete separation of xylene from the 1,3,5-triisopropylbenzene molecules, suggesting the existence of crystals pores smaller than 0.94 nm diameters. On the other hand, the conversion tests using pure *ortho*-xylene as feed with low flow rate values led to higher *para*-xylene selectivity. Further studies would be of great importance for improving the synthesis of the zeolite layer, which may result in greater selectivity in these membranes for the combined separation-reaction processes.

CHAPTER 6

CONCLUSIONS AND FUTURE PERSPECTIVES

6.1. Conclusions

In this study, asymmetric tubular membranes based on alumina incorporated with coal fly ash (CFA) were developed. The membranes were prepared using the centrifugal casting technique without dispersants, binder or chemical additives, and contained up to 40 wt.% CFA (dry basis). This study consisted of raw material characterization, centrifugal casting processing of the tubes, physical and morphological analysis, and performance tests. Besides, these membranes were studied as a support for the deposition of the ZSM-5 zeolite, without the use of organic structure-directing agents. Preliminary catalytic tests were carried out using the zeolite membranes for isomerization of xylenes and simultaneous p-xylene separation. The membranes composed of Alumina-CFA, the zeolite ZSM-5 layers and the zeolites dispersed inside the reactor vessel were properly characterized due to their crystalline structure, chemical properties, morphologies and performance tests.

Regarding the development of tubular membranes, the addition of CFA to the slurry composed of alumina and water significantly modifies the structure and characteristics of the tubes. The observed phenomena are attributed to the differences in the characteristics of each material, such as the wide distribution of CFA particle sizes, the remaining carbon on the CFA sample, and the processing conditions used in the centrifugal casting method. The presence of CFA in the ceramic membranes resulted in a higher porosity, which increased from 25 to 40 % compared to samples prepared with only alumina. There was also an increase in hydraulic permeance for membranes containing CFA; the increase was almost 6 times higher for the

membrane containing 40 % by CFA weight. Membranes with CFA show 27 % less shrinkage after sintering.

The observed retention of cornstarch was greater than 99 % for all the tested membranes, showing an excellent separation for the size of the cornstarch molecule. For the CFA40 membrane, retention was slightly less, possibly due to the increase in pore size caused by the higher concentration of larger particles in the membrane. This result associated with the permeation shows that the prepared tubes can be considered membranes.

The alumina-CFA-based membranes were used as a support for ZSM-5 zeolites. Zeolite coatings were performed over these ceramic membranes using the secondary growth method without an organic template. The seeding was carried out with the calcined commercial ZSM-5 zeolite containing small crystallites followed by hydrothermal synthesis. The membranes composed of alumina-CFA and zeolite ZSM-5 were successfully prepared. Our results also demonstrate that the zeolites can be deposited on the ceramic tube by in-situ crystallization without the use of organic templates in the hydrothermal synthesis. This demonstrates once again the search for economy and care with the environment in the present work.

The XRD analyzes of the remained synthesis material showed the predominant presence of the ZSM-5 zeolite and some characteristic peaks of kenyaite, analcime, and mordenite zeolites. The bands presented in the FTIR-ATR analysis confirm the predominance of the ZSM-5 zeolite in the hydrothermal synthesis since the format and frequencies of the bands coincide with the expected for this type of zeolite. A small overlap in the 1200 cm^{-1} region suggests the presence of other types of zeolites, corroborating XRD results. Py adsorption showed that the number of Brønsted acid sites in the H-form of synthesized zeolite is a function of the zeolite crystallinity. SEM analysis showed a continuous layer deposited on the ceramic support with prismatic or coffin-shaped zeolites, configuring the structure of the ZSM-5. The presence of

kenyaite, analcime and, mordenite, in small proportions, in some samples, could be seen by SEM images and corroborates information from the XRD peaks and also from the literature about the formation of these types of zeolites in the synthesis of ZSM-5 without the use of organic templates. Through the SEM cross-section images, it was possible to observe that two zeolitic deposits increased approximately twice the thickness of the zeolite layer. The EDS technique allowed better visualization of the transition between ceramic support and zeolitic layer, evidencing the differences between the silica/alumina concentrations of the two interfaces.

The membranes composed of Alumina-CFA and zeolite ZSM-5 were tested in the separation and isomerization of aromatics catalyzed by the Bronsted acid sites. Meanwhile, the zeolite coated alumina-CFA membranes presented total separation for 1,3,5-triisopropylbenzene from xylenes. Preliminary tests showed that in the ortho-xylene isomerization, the formed zeolitic membrane presents high selectivity for *para*-xylene.

6.2. Perspectives

The method used to obtain ceramic tubes with coal fly ash can be considered innovative, since it uses no chemical additives in the formulation and find several applications. The main impediment to greater applicability of ceramic membranes, compared to the polymeric ones, is due to the high fabrication costs. The elaborated ceramic membranes have lower production costs and, when used in great quantities, can help to solve the waste problematic of this product. The search for an alternative to the use of CFA brings economic and environmental benefits. The increase of CFA in the structure of ceramic membranes can and should be studied in order to further reduce the costs related to synthesis while providing a proper destination for this residue.

The manufacturing of such membranes does not release hazardous chemicals to the environment, in particular during the thermal steps. The alumina-CFA membranes containing up to 40 wt.% coal fly ash may be used in numerous industrial processes to purification of particles greater than 12 micrometers in suspension, in the treatment of effluents. Further characterization of the membrane must be carried out to determine the pores size and its distribution and, thus, correctly classify the membrane.

Our results show that the elaborated ceramic alumina/CFA membranes can be used as well as supports for metallic, carbon, or zeolitic deposition, in order to increase the selectivity of the membrane to a component. The resulting membranes can also provide coupling of molecule separation and catalytic reactions involving zeolite acid sites. Other applications that can be cited are the catalytic cracking of molecules as 1,3,5-triisopropylbenzene and the biomass fast pyrolysis.

Further studies, other analysis and a greater number of tests would be of paramount importance for the zeolitic layer deposited on the tubes to be optimized. Optimizations in order to decrease the polymorphism would be also important to guarantee the successful application of these membranes for separation and reaction of organic compounds.

REFERENCES

ABEGUNDE, O.O.; AKINLABI, E.T.; OLADIJO, O.P.; AKINLABI, S.; UDE A.U. "Overview of thin film deposition techniques." *AIMS Materials Science*, 6(2), 174–199, 2019.

AL-DUGHAITHER, A.S.; LASA, H. "HZSM-5 Zeolites with Different SiO_2/Al_2O_3 Ratios. Characterization and NH_3 Desorption Kinetics." *Industrial & Engineering Chemistry Research* 53(40), 15303–16, 2014.

AL-KHATTAF, S.; TUKUR, N. M.; AL-AMER, A. "Modeling Xylene Reactions over ZSM-5 Zeolite in a Riser Simulator: 1,3- versus 1,2-Methyl Shift." *Ind. Eng. Chem.* Res. 44, 7957–7968, 2005.

ALBAHAR, M.; LI, C.; ZHOLOBENKO, V.L.; GARFORTH, A.A. "The effect of ZSM-5 zeolite crystal size on p-xylene selectivity in toluene disproportionation." *Microporous and Mesoporous Materials* 302, 110221, 2020.

ALY, H.M.; MOUSTAFA, M.E.; ABDELRAHMAN, E.A. "Synthesis of mordenite zeolite in absence of organic template." *Advanced Powder Technology* 23, 757–760, 2012.

ANDERSON, C. "Factors affecting MFI membrane quality." Doctoral Thesis. Luleå University of Technology, Sweden, 2007.

ANDRADE, J.C. "Determinações Iodométricas." *Rev. ChemKeys*, Campinas, SP – Brazil. 2001.

ARGAUER, R.J.; LANDOLT, G.R. "Crystalline zeolite ZSM-5 and method of preparing the same." *US Patent* 3702886, 1972.

ASTM C1684-18. "Standard Test Method for Flexural Strength of Advanced Ceramics at Ambient Temperature—Cylindrical Rod Strength." ASTM International, West Conshohocken, PA, 2018.

ASTM C373-88. "Standard Test Method for Water Absorption, Bulk Density, Apparent Porosity, and Apparent Specific Gravity of Fired Whiteware Products." ASTM International, West Conshohocken, PA, 2006.

ASTM D3174-82. "Standard Test Method for Ash in the Analysis Sample of Coal and Coke from Coal." Philadelphia, 1982.

AUERBACH, S.M.; CARRADO, K.A.; DUTTA, P.K. “Handbook of zeolite science and technology.” New York: CRC Press Book, 1170, 2003.

BAKER, R. W. “Membrane technology and Applications.” Second Edition. England: Wiley Online Library. 2004.

BAO, Z.; CHANG, G.; XING, H.; KRISHNA, R.; REN, Q.; CHEN, B. "Potential of microporous metal-organic frameworks for separation of hydrocarbon mixtures." *Energy Environ. Sci*. 9, 3612–3641, 2016.

BASILE, A. “Handbook of Membrane Reactors.” V. 2. Woodhead Publishing Limited. 2013.

BAUMANN, S.; SERRA, J.M.; LOBERA, M.P.; ESCOLASTICO, S.; KUPPERSA, F.S.; MEULENBERGA, W.A. “Ultrahigh oxygen permeation flux through supported $Ba_{0.5}Sr_{0.5}Co_{0.8}Fe_{0.2}O_{3-\delta}$ membranes.” *Journal of Membrane Science* 377. 198–205, 2011.

BENEKE, K.; LAGALY, G. “Kenyaite – Synthesis and Properties.” *American Mineralogist*. V.68, 818–826, 1983.

BENES, N.; NIJMEIJER, A.; VERWEIJ, H. “Microporous silica membranes.” *Membrane Science and Technology* V. 6. Elsevier Masson SAS, 2000.

BERNAL, M.P.; CORONAS, J.; MENÉNDEZ, M.; SANTAMARÍA, J. “Coupling of reaction and separation at the microscopic level: esterification processes in a H-ZSM-5 membrane reactor.” *Chemical Engineering Science* 57, 1557–1562, 2002.

BERTOTTO, R.C.T. “Membranas tubulares à base de alumina preparadas por Centrifugal Casting.” Doctoral Thesis. Federal University of Rio Grande do Sul - UFRGS. Porto Alegre. 159 pages. 2019.

BERTOTTO, R.C.T.; VIRGINIE, M.; KHODAKOV, A.; AMBROSI, A.; POLLO, L.D.; MARCILIO, N.R.; TESSARO, I.C. “Influence of sintering temperature on the development of alumina membrane shaped by centrifugal casting for gas separation.” *Cerâmica V*. 65, supl. 1, 2019.

BIESHEUVEL, P. M.; BREEDVELD, V.; HIGLER, A.P.; VERWEIJ, H. “Graded Membrane Supports Produced by Centrifugal Casting of a Slightly Polydisperse Suspension.” *Chemical Engineering Science* 56(11), 3517–25, 2001.

BISSETT, H. “Manufacture and Optimization of Tubular Ceramic Membrane Supports.” Master dissertation. North-west University. 111 pages, 2005.

BISSETT, H.; ZAH, J.; KRIEG H.M. “Manufacture and optimization of tubular ceramic membrane supports.” *Powder Technology* 181, 57–66, 2008.

BHAVE, I.; RAMESH, R. “Inorganic membranes: synthesis, characteristics and applications.” New York: Chapman & Hall, 129, 83–84, 1991.

BOFFA, V.; MAGNACCA, G.; JØRGENSEN, L.B.; WEHNER, A.; DÖRNHÖFER, A.; YUE, Y. “Toward the effective design of steam-stable silica-based membranes.” *Microporous and Mesoporous Materials* 179, 242–249, 2013.

BOSE, S.; DAS, C. “Preparation and characterization of low cost tubular ceramic support membranes using saw dust as a pore-former.” *Materials Letters* 110, 152–155, 2013.

BRECK, DW. 1974. “Zeolite Molecular Sieves.” New York: Wiley, 2013.

BROACH, R.W. “Zeolites in Industrial Separations and Catalysis: Zeolite Types and Structure.” Wiley. Des Plaines, 2010.

BUZZONI, R.; BORDIGA, S.; RICCHIARDI, G.; SPOTO, G.; ZECCHINA, A. “Interaction of H_2O, CH_3OH, $(CH_3)_2O$, CH_3CN, and Pyridine with the Superacid Perfluorosulfonic Membrane Nation: An IR and Raman Study.” *Journal of Physical Chemistry* 99(31), 11937–51, 1995.

CALLISTER, W.; RETHWISCH, D. “Materials science and engineering: an introduction.” 7th Ed. USA: John Wiley & Sons Inc, 2007.

CAPELLAZZO, O.; CAO, G.; MESSINA, G.; MORBIDELLI, M. “Kinetics of Shape-selective Xylene Isomerization over a ZSM-5 Catalyst.” *Ind. Eng. Chem. Res.* 30, 2280–2287, 1991.

CHE, Q.; YANG, M.; WANG, X.; YANG, Q.; WILLIAMS, L.R.; YANG, H.; ZOU J.; ZENG, K.; ZHU, Y.; CHEN, Y.; CHEN, H. “Influence of physicochemical properties of metal modified ZSM-5 catalyst on benzene, toluene and xylene production from biomass catalytic pyrolysis.” *Bioresource Technology* 278, 248–254, 2019.

CHEN, C. H.; TAKITA, K.; HONDA, S.; AWAJI, H. “Fracture behavior of cylindrical porous alumina with pore gradient.” *Journal of the European Ceramic Society* 25, 385–391, 2004.

CHEN, C.; ISIGURO, S.; HONDA, S.; AWAJI, H. “Homogenous alumina tube with controlled pore morphology.” *Materials Science and Engineering A* 407, 167–173, 2005.

CHERAITIA, A.; AYRAL, A.; JULBE, A.; ROUESSAC, V.; SATHA, H. “Synthesis and characterization of microporous silica-alumina membranes.” *Journal of Porous Materials, 17*(3), 259–263, 2010.

CICHOCKI, A. “Effect of glass corrosion on the synthesis of zeolite T.” *Zeolites vol. 5*, 1985.

COLLINS, D.J.; MEDINA, R.J. “Xylene isomerization by ZSM-5 zeolite catalyst.” *The Canadian Journal of Chemical Engineering*, V. 61, 1983.

CONTRERAS, C.A.; SUGITA, S.; RAMOS, E.; TORRES L.M.; SERRATO J. “A New Production Method of Submicron Alumina Powders.” *AZo Journal of Materials Online*, V. 2, 1–7, 2006.

CUNDY, C. S.; COX, P. A. “The hydrothermal synthesis of zeolites: Precursors, intermediates and reaction mechanism.” *Microporous and Mesoporous Materials* 82, n. 1–2, 1–78, 2005.

DARAMOLA, M.O.; ARANSIOLA, E.F.; OJUMU, T.V. “Potential Applications of Zeolite Membranes in Reaction Coupling Separation Processes.” *Materials 5*, 2101–2136, 2012.

DA SILVA BIRON, D.; DOS SANTOS, V.; ZENI, M. “Ceramic Membranes Applied in Separation Processes.” 1st edition. Caxias do Sul. Springer, 2017.

DAS, N.; MAITI, N.H. “Effect of Size Distribution of the Starting Powder on the Pore Size and its Distribution of Tape Cast Alumina Microporous Membranes.” *Journal of the European Ceramic Society* 19, 341–345, 1999.

DAVID, E.; KOPAC, J. “Development of palladium/ceramic membranes for hydrogen separation.” *International Journal of Hydrogen Energy* 36, 4498–4506, 2011.

DE VOS, R.; VERWEIJ, H. “Improved performance of silica membranes for gas separation.” *Journal of Membrane Science* 145, 37–51, 1998.

DONG, J.; LIN, Y.S.; HU, M.Z-C.; PEASCOE, R.A.; PAYZANT E.A. “Template-removal-associated microstructural development of porous-ceramic-supported MFI zeolite membranes.” *Microporous and Mesoporous Materials* 34, 241–253, 2000.

DONG, Y.; LIN, B.; ZHOU, J.; ZHANG, X.; LING, Y.; LIU, X.; MENG, G.; HAMPSHIRE, S. “Corrosion resistance characterization of porous alumina membrane supports.” *Materials Characterization* 62, 409–418, 2011.

DUTOURNIÉ, P.; LIMOUSY, L.; ANQUETIL, J.; DÉON S. “Modification of the Selectivity Properties of Tubular Ceramic Membranes after Alkaline Treatment.” *Membranes 7*, 65, 2017.

FAN, M.; BROWN, R. C. “Comparison of the Loss-on-Ignition and Thermogravimetric Analysis Techniques in Measuring Unburned Carbon in Coal Fly Ash”. *Energy & Fuels 15*, 2001.

FANG, J.; QIN, G.; WEI, W.; ZHAO, X. “Preparation and characterization of tubular supported ceramic microfiltration membranes from fly ash.” *Separation and Purification Technology* 80, 585–591, 2011.

FISHER, M.L.; COLIC, M.; RAO, M.P.; LANGE, F.F. "Effect of Silica Nanoparticle Size on the Stability of Alumina/Silica Suspensions." *J. Am. Ceram. Soc.*, 84[4], 713–18, 2001.

FLANIGEN, E.M.; BROACH, R.W.; WILSON, S.T. “Zeolites in Industrial Separations and Catalysis: Introduction.” Wiley. Des Plaines, 2010.

FOTOU, G.P.; LIN, Y.S.; PRATSINIS, S.E. “Hydrothermal stability of pure and modified microporous silica membranes.” *Journal of Material Science* 30, 2803–2808, 1995.

FRANCK, H.G.; STADELHOFER, J.W. “Industrial Aromatic Chemistry.” Springer-Verlag, Berlin-Heidelberg, 1988.

GALLUCCI, F.; BASILE, A. “Membranes for membrane reactors: preparation, optimization and selection.” United Kingdom: John Wiley & sons, 1–61, 2011.

GAVALAS, G. R. “Zeolite membranes for gas and liquid separations.” In: YAMPOLSKII, Y.; PINNAU, I.; FREEMAN, B. *Materials Science of Membranes for Gas and Vapor Separation*. West Sussex: John Wiley and Sons Ltd., 307– 336, 2006.

GERMAN, R. M. “Coarsening in Sintering: Grain Shape Distribution, Grain Size Distribution, and Grain Growth Kinetics in Solid-Pore Systems.” *Critical Reviews in Solid State and Materials Sciences* 35(4), 263–305, 2010.

GERMAN, R. M.; SURI, P.; PARK, S.J. “Review: Liquid Phase Sintering.” *Journal of Materials Science* 44(1), 1–39, 2009.

GHANBARIAN, B.; HUNT, A.G.; EWING, R.P.; SAHIMI, M. “Tortuosity in Porous Media: a Critical Review.” *Soil Science Society of America Journal*. V.77, Issue 5, 1461–1477, 2013.

GITIS, V.; ROTHENBERG, G. “Ceramic Membranes. New Opportunities and Practical Applications.” Wiley-VCH Verlag GmbH & Co. KGaA, 2016.

GOLABEK, K.; TARACH, K.A.; GÓRA-MAREK, K. “Xylenes Transformation over Zeolites ZSM-5 Ruled by Acidic Properties.” *Spectrochimica Acta - Part A: Molecular and Biomolecular Spectroscopy* 192, 361–67, 2018.

GÓMEZ-HORTIGUELA, L.; CAMBLOR, M. “Introduction to the Zeolite Structure- Directing Phenomenon by Organic Species: General Aspects.” *Structure and Bonding* 175, 1–42, 2018.

GONÇALVES, M.L.; DIMITROV, L.D.; JORDÃO, M.H.; WALLAU, M.; URQUIETA-GONZALEZ, E.A. “Synthesis of mesoporous ZSM-5 by crystallisation of aged gels in the presence of cetyltrimethylammonium cations.” *Catalysis Today* 133–135, 69–79, 2008.

GORGOJO, P.; IGLESIA, O.; CORONAS, J. “Preparation and Characterization of Zeolite Membranes. In Membrane Science and Technology Series 13. Inorganic Membranes – Synthesis, Characterizations and Applications.” Elsevier. Oxford, 2008.

GU, Z.Y.; YAN, X.P. “Metal-Organic Framework MIL-101 for High-Resolution Gas-chromatographic Separation of Xylene Isomers and Ethlbenzene.” *Angewandte Chemie - International Edition* 49(8), 1477–80, 2010.

GUECHI, A.; HARABI, A.; CONDOUM, S.; ZENIKHERI, F.; BOUDAIRA, B.; BOUZERARA, F.; FOUGHALI, L. “Elaboration and characterization of tubular supports for membranes filtration.” *Desalination and water treatment* 57 (12), 5246–5252, 2015.

GUISNET, M.; AYRAULT, P.; COUTANCEAU, C.; ALVAREZ, M.F.; DATKA, J. "Acid properties of dealuminated beta zeolites studied by IR spectroscopy." *J. Chem Soc., Faraday Trans*. 93, 1661–1665, 1997.

GUISNET, M.; GNEP, N. S.; MORIN, S. “Mechanisms of xylene isomerization over acidic solid catalysts.” *Microporous and Mesoporous Materials* 35–36, 47–59, 2000.

HAAG, S.; HANEBUTH, M.; MABANDE, G. T. P.; AVHALE, A.; SCHWIEGER, W.; DITTMEYER R. “On the use of a catalytic H-ZSM-5 membrane for xylene isomerization.” *Microporous and Mesoporous Materials* 96, 168–176, 2006.

HABERT, C.A.; BORGES, C.P.; NOBREGA, R. “Processos de Separação por Membranas.” 1st Ed. Rio de Janeiro: e-papers. 180 pages, 2006.

HAMM, J.B.S.; AMBROSI, A.; GRIEBELER, J.G.; MARCILIO, N.R.; TESSARO, I. C.; POLLO, L. D. “Recent advances in the development of supported carbon membranes for gas separation.” *International Journal of Hydrogen Energy* 42. 24830–24845, 2017.

HAMM, J.B.S. “Supported carbon membranes for gas separation.” PhD Thesis. Federal University of Rio Grande do Sul, UFRGS. Porto Alegre, 2018.

HAN, B.; SHEN, Z.; WICKRAMASINGHE, S.R. “Cyanide removal from industrial wastewaters using gas membranes.” *Journal of Membrane Science* 257, 1–2, 171–181, 2005.

HARABI, A.; BOUZERARA, F. “Fabrication of Tubular Membrane Supports from Low Price Raw Materials Using Both Centrifugal Casting and/or Extrusion Methods.” *Expanding Issues in Desalination*. InTech. Prof. Robert Y. Ning (Ed.), ISBN: 978-953-307-624-9, 2011.

HE, J.; LIU, H.; SHAN, P.; ZHANG, K.; QIN, Y.; LIU, L. “Supported-gas-membrane process for removal and recovery of aliphatic amines from aqueous streams**.”** *Chemical Engineering Science* 141, 330–341, 2016.

HEDLUND, J.; KORELSKIY, D.; SANDSTRÖM, L.; LINDMARK, J. “Permporometry analysis of zeolite membranes.” *Journal of Membrane Science* 345, 276–287, 2009.

HEIDRICH, C.; FEUERBORN, H-J.; WEIR, A. “Coal Combustion products: a global Perspective.” *World of Coal Ash (WOCA) Conference*, Lexington, Kentucky, 2013.

HERRERO-MARTÍNEZ, J.M.; SCHOENMAKERS, P.J.; KOK W.T. “Determination of the amylose–amylopectin ratio of starches by iodine-affinity capillary electrophoresis.” *Journal of Chromatography A* 1053, 227–234, 2004.

HUBADILLAH, S.K.; OTHMAN, M.H.D.; MATSUURA, T.; ISMAIL, A.F.; RAHMAN, M.A.; HARUN, Z.; JAAFAR, J.; NOMURA, M. **“**Fabrications and applications of low

cost ceramic membrane from kaolin: A comprehensive review." *Ceramics International* 44, 4538–4560, 2018.

HUISMAN, W.; GRAULE, T.; GAUCKLER, L.J. "Alumina of High Reliability by Centrifugal Casting." *Journal of the European Ceramic Society* 15, 81l–821, 1995.

IUPAC, 1996. Koros, W.J.; Ma Y.H.; Shimidzu, T. "Terminology for Membrane and Membrane Processes." *Pure and Applied Chemistry* 68, 1479–1489, 1996.

IUPAC, 1997. McNaught, A. D.; Wilkinson, A. "Compendium of Chemical Terminology." 2nd Ed. Blackwell Scientific Publications, Oxford, 1997.

JEDIDI, I.; SAÏDI, S.; KHMAKEM, S.; LARBOT, A.; ELLOUMI-AMMAR, N.; FOURATI, A.; CHARFI, A.; AMAR, R.J. "New Ceramic Microfiltration Membranes from Mineral Coal Fly Ash." *Arabian Journal of Chemistry* 2(1), 31–39, 2009.

JENTYS, A.; WARECKA, G.; DEREWINSKI, M.; LERCHER, J. A. "Adsorption of water on ZSM-5 zeolites." *The Journal of Physical Chemistry* 93, 4837–4843, 1989.

JIMENEZ, E.M.; DING, D.; SU, L.; JOSHI, A.R.; SINGH, A.; REEJA-JAYAN, B.; BEUTH, J. "Parametric analysis to quantify process input influence on the printed densities of binder jetted alumina ceramics." *Additive Manufacturing* 30, 2019.

JIN, F.; LI, Y. "A FTIR and TPD examination of the distributive properties of acid sites on ZSM-5 zeolite with pyridine as a probe molecule." *Catalysis Today* 145, 101–107, 2009.

JULBE, A. "Introduction to Zeolite science and practice, Chapter 6 - Zeolite membranes: synthesis, characterization and application." 3rd Ed. Institut Européen des Membranes de Montpellier, France. Elsevier, 2007.

JULBE, A.; DROBEK, M.; IN: DRIOLI E., GIORNO L. (Eds). "Seeding for Zeolite Membranes. Encyclopedia of Membranes." Springer, Berlin, Heidelberg, 2016.

KALIPÇILAR, H.; ÇULFAZ, A. "Template-Free Synthesis of ZSM-5 Type Zeolite Layers on Porous Alumina Disks." *Turkish Journal of Chemistry* 31, 233–242, 2007.

KANG, C.G.; ROHATGI, PK. "Transient thermal analysis of solidification in a centrifugal casting for composite materials containing particle segregation." *Metallurgical and Materials Transactions B* 27B, 277–85, 1996.

KATSUKI, H.; FURUTA, S.; WATARI, T.; KOMARNENI, S. “ZSM-5 zeolite/porous carbon composite: Conventional- and microwave-hydrothermal synthesis from carbonized rice husk.” *Microporous and Mesoporous Materials* 86, 145–151, 2005.

KIM, Y. S.; KUSAKABE, K.; MOROOKA, S.; YANG, S. M. “Preparation of Microporous Silica Membranes for Gas Separation.” *Korean Journal of Chemical Engineering*, *18*(1), 106–112, 2001.

KIM, K.; CHO, S.; YOON, K.; KIM, J.; HA, J.; CHUN, D. “Centrifugal casting of alumina tube for membrane application.” *Journal of Membrane Science* 199, 69–74, 2002.

KIM, W.J.; KIM, S.D. “Method of preparing ZSM-5 using variable temperature without organic template.” WO 2004/058643. *International Patent Application.* 2004.

KOSINOV, N.; GASCON, J.; KAPTEIJN, F.; HENSEN, E.J.M. “Recent developments in zeolite membranes for gas separation.” *Journal of Membrane Science* 499, 65–79, 2016.

KUMAR, R.V.; GHOSHAL, A.K.; PUGAZHENTHI, G. “Elaboration of Novel Tubular Ceramic Membrane from Inexpensive Raw Materials by Extrusion Method and Its Performance in Microfiltration of Synthetic Oily Wastewater Treatment.” *Journal of Membrane Science* 490, 92–102, 2015.

LAI, R.; GAVALAS, G. “Surface Seeding in ZSM-5 Membrane Preparation.” *Ind. Eng. Chem. Res*. 37, 4275–4283, 1998.

LAI, R.; YAN, Y.; GAVALAS, G. “Growth of ZSM-5 films on alumina and other surfaces.” *Microporous and Mesoporous Materials* 37, 9–19, 2000.

LI, K. “*Ceramic Membranes for Separation and Reaction*.” Wiley. West Sussex, 2007.

LI, G.; KIKUCHI, E.; MATSUKATA, M. “A study on the pervaporation of water–acetic acid mixtures through ZSM-5 zeolite membranes.” *Journal of Membrane Science* 218, 185–194, 2003.

LI, X.; WANG, J.; BAI, N.; ZHANG, X.; HAN, X.; DA SILVA, I.; MORRIS, C.G.; XU, S.; WILARY, D.M.; SUN, Y.; CHENG, Y.; MURRAY, C.A.; TANG, C.C.; FROGLEY, M.D.; CINQUE, G.; LOWE, T.; ZHANG, H.; RAMIREZ-CUESTA, A.J.; THOMAS, K.M.; BOLTON, L.W.; YANG S.; SCHRÖDER, M. "Refinement of pore size at sub-angstrom precision in robust metal–organic frameworks for separation of xylenes." *Nature Communications* 11, Article number: 4280, 2020.

LIANG, D.; HUANG, J.; ZHANG, H.; FU, H.; ZHANG, Y.; CHEN, H. “Influencing factors on the performance of tubular ceramic membrane supports prepared by extrusion.” *Ceramics International* 47, Issue 8, 10464–10477, 2021.

LIU, J.; DONG, Y.; DONG, X.; HAMPSHIRE, S.; ZHU, L.; ZHU, Z.; LI, L. “Feasible recycling of industrial waste coal fly ash for preparation of anorthite-cordierite based porous ceramic membrane supports with addition of dolomite.” *Journal of the European Ceramic Society* 36, 1059–1071, 2016.

LIU, X.; TRUITT, R.E. “DRFT-IR Studies of the Surface of γ-Alumina.” *Journal of the American Chemical Society* 119(41), 9856–60, 1997.

LORENTE-AYZA, M. M.; MESTRE, S.; MENÉNDEZ, M.; SÁNCHEZ, E. “Comparison of extruded and pressed low cost ceramic supports for microfiltration membranes.” *Journal of the European Ceramic Society* 35, 3681–3691, 2015.

LOWE, B. M.; NEE, J. R. D. “Crystallization of “inorganic” ZSM-5 in the system K_2O-Al_2O_3-SiO_2-H_2O.” *Zeolites 14*, 1994.

LOWELL, S.; SHIELDS, J.E.; THOMAS, M.A.; THOMMES, M. “Characterization of porous solids and powders: surface area, pore size, and density.” Boynton Beach: Kluwer Academic Publishers, 2004.

LUITEN-OLIEMAN, M.W.J.; WINNUBST, L.; NIJMEIJER, A.; WESSLING, M.; BENES, N.E. “Porous stainless steel hollow fiber membranes via dry–wet spinning.” *Journal of Membrane Science* 370, 124–130, 2011.

MALLMANN, J.E.C. “Metodologia de dosagem racional do concreto compactado com rolo (CCR) usando *coal fly ash* e cal hidratada em substituição ao cimento Portland.” Doctoral thesis, Federal University of Rio Grande do Sul - UFRGS. Porto Alegre. 223 pages, 2018.

MARQUES, J.P.; GENER, I.; AYRAULT, P.; BORDADO, J.C.; LOPES, J.M.; RAMÔA, F.R.; GUISNET, M. "Infrared spectroscopic study of the acid properties of dealuminated BEA zeolites." *Microporous Mesoporous Mater*. 60, 251–262, 2003.

MARTÍN-RUIZ, M.M.; PÉREZ-MAQUEDA, L.A.; CORDERO, T.; BALEK, V.; SUBRT, J.; MURAFA, N.; PASCUAL-COSP, J. “High surface area α-alumina preparation by using urban waste.” *Ceramics International* 35, n. 6, 2111–2117, 2009.

MASCARENHAS J.S. “Utilização dos catalisadores zeolíticos Fe-, Co- e Cu-MCM-22 na decomposição dos óxidos de nitrogênio.” Doctoral Thesis, UNICAMP, São Paulo. 236 pages, 2004.

MASIÁ, A. A. T.; BUHRE, B. J. P.; GUPTA, R. P.; WALL, T. F. “Characterising ash of biomass and waste.” *Fuel Processing Technology* 88, 1071–1081, 2007.

MERTINS, F.H.B.; KRUIDHOF, H.; BOUWMEESTER, H.J.M. “Centrifugal casting of tubular perovskite membranes.” *Journal of the American Ceramic Society* 88, n. 11, 3003–3007, 2005.

MINCEVA, M.; GOMES, P.S.; MESHKO, V.; RODRIGUES, A.E. "Simulated moving bed reactor for isomerization and separation of p-xylene." *Chemical Engineering Journal* 140, 305–323, 2008.

MINTOVA, S.; HEDLUND, J.; VALTCHEV, V.; SCHOEMAN, B.J.; STERTE, J. “ZSM-5 films prepared from template free precursors.” *Journal of Materials Chemistry*, 8(10), 2217–2221, 1998.

MIRTH, G.; ČEJKA, J., LERCHER, J. “Transport and isomerization of xylenes over hzsm-5 zeolites.” Journal of Catalysis 139, 24–33, 1993.

MONASH, P.; PUGAZHENTHI, G.; SARAVANAN, P. “Various fabrication methods of porous ceramic supports for membrane applications.” *Reviews in Chemical Engineering* 29, n. 5, 357–383, 2013.

MULDER, M. “Basic Principles of Membrane Technology.” 2nd Ed. Kluwer Academic Publisher, 564 pages, 1996.

NARENDRANATH S.; KUMAR, G.C.M. “Properties of Centrifugal Casting at Different Rotational Speeds of the Die.” *International Journal of Emerging Technology and Advanced Engineering 3*, Issue 1, 2013.

NIEN, K.C.; CHANG, F.T.; CHANG, M.B. “Adsorption of mesitylene via mesoporous adsorbents.” *Journal of the Air & Waste Management Association*, 67:12, 1319–1327, 2017.

NISHIYAMA, N.; UEYAMA, K.; MATSUKATA, M. “Synthesis of defect-free zeolite-alumina composite membranes by a vapor-phase transport method.” *Microporous Materials* 7, 299–308, 1996.

ODUNAYO, A.R.; OMONIYI, P.; PETRIK, L.; OLORUNFEMI, O. “Comparative Chemical and Trace Element Composition of Coal Samples From Nigeria and South Africa.” *American Journal of Innovative Research and Applied Sciences,* 2016.

OHLIN, L. “An In-Situ ATR-FTIR Spectroscopy study of adsorption in MFI zeolites.” Doctoral Thesis. Lulea University of Technology. 198 pages, 2015.

ÖHRMAN, O.; HEDLUND, J.; STERTE, J. “Synthesis and evaluation of ZSM-5 films on cordierite monoliths.” *Applied Catalysis A: General* 270, 193–199, 2004.

OLEKSIAK, M.D.; RIMER, J.D. “Synthesis of zeolites in the absence of organic structure-directing agents: factors governing crystal selection and polymorphism.” *Reviews in Chemical Engineering* 30(1), 1–49, 2014.

OLIVEIRA, I.; STUDART, A.; PILEGGI, R.; PANDOLFELLI, V. “Dispersão e Empacotamento de Partículas - Princípios e Aplicações Em Processamento Cerâmico.” São Paulo, 224 pages, 2000.

OTAKE, M. “MFI zeolite crystallization under controlled dosage of TPA template.” *Zeolites* 14, n. 1, 42–52, 1994.

PABBY, A. K.; RIZVI, S. S. H.; SASTRE, A. M. “Handbook of Membrane Separations: Chemical, Pharmaceutical, Food, and Biotechnological Applications.” 2nd Ed. CRC Press, 2015.

PAILLAUD, J.-L.; PATARIN, J. “Initial materials for synthesis of zeolites.” In: MINTOVA, S.; BARRIER, N. *Verified Syntheses of Zeolitic Materials*. [s.l.] *Synthesis Commission of the International Zeolite Association*, 24–28, 2016.

PAN, M.; LIN, Y.S. “Template-free secondary growth synthesis of MFI type zeolite membranes.” *Microporous and Mesoporous Materials* 43, 319–327, 2001.

PASCUAL, M.J.; DURÁN, A.; PASCUAL, L. “Sintering process of glasses in the system NA_2O–B_2O_3–SiO_2.” *Journal of Non-Crystalline Solids* 306, 58–69, 2002.

PEREGO, C.; POLLESEL, P. “Advances in Aromatics Processing Using Zeolite Catalysts.” *Advances in Nanoporous Materials* 1, 2010.

PRASAD, K.S.K.; MURALI, M.S.; MUKUNDA, P.G. “Analysis of fluid flow in centrifugal casting.” *Front. Mater. Sci. China* 4**,** 103–110, 2010.

QIN, G; ZHENG, L; XIE, Y; WU, C. “On the Framework Hydroxyl Groups of H-ZSM-5 Zeolites.” *Journal of Catalysis* 95(2), 609–12, 1985.

RAJESH, S. “Studies on polyamide-imide incorporated ultra and nanofiltration membranes.” Doctoral Thesis. Faculty of Science and Humanities - Anna University, India, 2011.

RAHAMAN, M.N. “Ceramic Processing and Sintering.” 2nd Ed. CRC Press, 2003.

RASOULI, M.; YAGHOB, N.; CHITSAZAN, S.; SAYYAR, M. H. “Influence of monovalent cations ion-exchange on zeolite ZSM-5 in separation of para-xylene from xylene mixture.” *Microporous and Mesoporous Materials* 150, 47–54, 2012.

REED, J. S. “Principles of Ceramics Processing.” New York : Wiley, ISBN: 978-0-471-59721–6, 2nd Ed., 1995.

ROHAYATI, KRISNANDI, Y. K.; SIHOMBING, R. “Synthesis of ZSM-5 zeolite using Bayat natural zeolite as silica and alumina source.” *AIP Conference Proceedings*, 2017.

SACKS, M. D.; LEE, H.; ROJAS, O.E. “Suspension Processing of SiC Whisker-Reinforced Composites.” *MRS Proceedings* 120, 1988.

SAID, A.; LIMOUSY, L.; NOUALI, H.; MICHELIN, L.; HALAWANI, J.; TOUFAILY, J.; HAMIEH, T.; DUTOURNIÉ, P.; DAOU, T.J. “Synthesis of mono- and bi-layer MFI zeolite films on macroporous alumina tubular supports: Application to nanofiltration.” *Journal of Crystal Growth* 428, 71–79, 2015.

SAKAI, H.; TOMITA, T.; TAKAHASHI, T. “P-Xylene Separation with MFI-Type Zeolite Membrane.” *Separation and Purification Technology* 25(1-3), 297–306, 2001.

SALEM, R. E. P.; CHINELATTO, A. S. A.; CHINELATTO, A. L. “Síntese de pós de alumina por meio de um método Pechini modificado com adição de sementes em diferentes atmosferas de calcinação.” *Cerâmica* 60, n. 353, 108–116, 2014.

SANDOVAL-DÍAZ, L-E.; GONZÁLEZ-AMAYA, J-A.; TRUJILLO, C-A. "General aspects of zeolite acidity characterisation." *Microporous Mesoporous Materials* 215, 229–243, 2015.

SANO, T.; HASEGAWAA, M.; KAWAKAMIA, Y.; KIYOZUMIB, Y.; YANAGISHITAB, H.; KITAMOTOB, D.; MIZUKAMIB, F. “Potentials of silicalite membranes for the separation of alcohol/water mixtures.” *Zeolites and Related Microporous Materials: State of the art* 1994, *Studies in Surface Science and Catalysis* 84, 1994.

SANTANA E.; SAMPAIO C.; TEIXEIRA E.; ANDRÉANI P.; BENEZET J.; ADAMIEC P.; BENHASSAINE, A.; SCHÜTZ, R. "Caracterização de cinzas sulfatadas de carvão visando utilização na indústria de cimento - reconstrução mineralógica do carvão de Candiota (Brasil)." *Revista Brasileira de Geociências* 41(2), 220–227, 2011.

SCHNEIDER, H. “Preparação de membranas de zeólita ZSM-5 suportadas em -alumina por tratamento hidrotérmico secundário.” Master Dissertation. Federal University of Rio Grande do Sul, UFRGS. Porto Alegre, 2019

SCHNEIDER, H.; SCHINDEL, L.K.; GOMES, L.B.; TESSARO, I.C.; MARCILIO, N.R. “Template-free ZSM-5 membrane preparation on alumina support by secondary hydrothermal synthesis.” *Current Research in Green and Sustainable Chemistry* 4, 2021.

SILVA, N.I.W.; CALARGE, L. M.; CHIES, F.; MALLMANN, J. E.; ZWONOK, O. “Caracterização de cinzas volantes para aproveitamento cerâmico.” *Cerâmica* 45, n. 296, 184–187, 1999.

SINGH, G.; BULASARA, V.K. “Preparation of low-cost microfiltration membranes from fly ash.” *Desalination and Water Treatment*, 53:5, 1204–1212, 2015.

SINGH, A.K; MASTO, R.E.; HAZRA, B.; ESTERLE, J.; SINGH, P.K. “Ash from coal and Biomass combustion.” Springer Nature Switzerland, 118 pages, 2020.

SONG, A.; MA, J.; XU, D.; LI, R. “Adsorption and Diffusion of Xylene Isomers on Mesoporous Beta Zeolite.” *Catalysts* 5, 2098–2114, 2015.

STEENKAMP, G.C.; NEOMAGUS, H.W.J.P.; KRIEG, H.M.; KEIZER, K. "Centrifugal casting of ceramic membrane tubes and the coating with chitosan." *Separation and Purification Technology* 25, 407–413, 2001.

STÖCKER, M. “Gas phase catalysis by zeolites.” *Microporous and Mesoporous Materials* 82, 257–292, 2005.

SZOSTAK, R. “Molecular Sieves: Principles of Synthesis and Identifications.” Van Nostrand Reinhold, New York, 1989.

TAVOLARO, A.; DRIOLI, E. “Zeolite Membranes.” *Advanced Materials* 11, N° 12, 1999.

TREACY, M.M.J.; HIGGINS, J.B. “Collection of Simulated XRD Powder Patterns for Zeolites.” Structure Commission of the International Zeolite Association. 4th Ed. Elsevier. 586 pages, 2001.

VAN DER GAAG, F.J. “ZSM-5 type zeolites: Synthesis and use in gasphase reactions with ammonia.” Doctoral Thesis, Delft University of Technology. Delft, Netherlands, 1987.

VAN DYK, L.; LORENZEN, L.; MIACHON, S.; DALMON, J. “Xylene isomerization in an extractor type Catalytic Membrane Reactor.” *Catalysis Today* 104, 274, 2005.

VIEIRA, L. H.; RODRIGUES, M. V; MARTINS, L. “Cristalização convencional de zeólitas e induzida por sementes.” *Química Nova* 37, n. 9, 1515–1524, 2014.

VIMONT, A.; THIBAULT-STARZYK, F.; LAVALLEY, J.C. “Infrared Spectroscopic Study of the Acidobasic Properties of Beta Zeolite." *J. Phys. Chem. B* 104, 2, 286–291, 2000.

VISWANATHNATHAN, B.; SIVASANKER, S.; RAMASWAMY, A.V. “Catalysis: Principles and Applications.” Narosa, 1st Ed. 412 pages, 2002.

WANG, Y.; ZHANG, Y.; LIU, X.; MENG, G. “Microstructure control of ceramic membrane support from corundum-rutile powder mixture.” *Powder Technology,* 125–133, 2006.

WATANABE, Y.; KAWAMOTO, A.; MATSUDA, K. “Particle size distributions in functionally graded materials fabricated by the centrifugal solid-particle method.” *Composites Science and Technology* 62, 881–888, 2002.

WEE, S.; TYE, C.; BHATIA, S. “Membrane separation process-Pervaporation through zeolite membrane.” *Separation and Purification Technology* 63, 500–516, 2008.

WEGNER, K.; DONG, J.; LIN, Y.S. “Polycrystalline MFI zeolite membranes: xylene pervaporation and its implication on membrane microstructure.” *Journal of Membrane Science* 158, 17–27, 1999.

WEI, X.; LIANG, S.; XU, Y.; SUN, YA.; AN, J.; CHAO, Z. “Patching NaA zeolite membrane by adding methylcellulose into the synthesis gel.” *Journal of Membrane Science* 530, 240–249, 2017.

XIE, Z.; DUONG, T.; HOANG, M.; NGUYEN, C.; BOLTO. B. “Ammonia removal by sweep gas membrane distillation.” *Water Research 43* (6), 1693–1699, 2009.

XU, Q.; ZHANG, W. "Next-Generation Graphene-Based Membranes for Gas Separation and Water Purifications." *Advances in Carbon Nanostructures,* 2016.

XUE, L. A.; CHEN, I. “Low-Temperature Sintering of Alumina with Liquid-Forming Additives.” *Journal of the American Ceramic Society*, 74 [8], 2011–13, 1991.

YAO, Y.; LIU, W.; ZHANG, H.F.; CAI, R.H.; WANG, Y.; GAO, S.B.; DAN WU, ZHANG, Y.S. “Research on the PVDF Hollow Fiber Gas Membrane Used for Bromine Extraction.” *Advanced Materials Research*, 217–218, 802–807, 2011.

YOUNG, L.B.; BUTTER, S.A.; KAEDING, W.W. “Shape selective reactions with zeolite catalysts.” *Journal of Catalysis* 76, 418–432, 1982.

YU, M.; NOBLE, R.; FALCONER, J. “Zeolite membranes: Microstructure characterization and permeation mechanisms.” *Accounts of Chemical Research 44*, 1196–1206, No. 11, 2011.

ZHANG, L.; SONG, Y.; LI, G.; ZHANG Q, ZHANG, S.; XU, J.; DENG, F.; GONG, Y. “F-assisted synthesis of a hierarchical ZSM-5 zeolite for methanol to propylene reaction: a b-oriented thinner dimensional morphology.” *RSC Adv.* 5, 61354–61363, 2015.

ZHOU, Y.; FUKUSHIMA, M.; MIYAZAKI, H.; YOSHIZAWA, Y.; HIRAO, K.; IWAMOTO, Y.; SATO, K. “Preparation and characterization of tubular porous silicon carbide membrane supports.” *Journal of Membrane Science* 369, 112–118, 2011.

ZAMAN, S.F.; LOUGHLIN, K.F.; AL-KHATTAF, S.S. “Kinetics of Desorption of 1,3-Diisopropylbenzene and 1,3,5-Triisopropylbenzene. 1. Diffusion in Y-Zeolite Crystals by the Zero-Length-Column Method.” *Ind. Eng. Chem. Res.* 44*,* 2027–2035, 2005.

APPENDIX

In order to investigate how zeolitic films behave with the proposed methodology, preliminary tests were performed on the internal and external faces of the CFA-based support. Figures A1 and A2 were the first SEM images obtained and allowed important understandings and improvements in the way of obtaining the zeolite layer.

Figure A1 depicts the micrographs for the samples coated on the inner support face. The typical coffin shape in these images grants the visual identification of the ZSM-5 zeolite crystals (MINTOVA *et al.*, 1998; ANDERSSON, 2007). The sample of the Figure A1(c) micrograph received excess of gold during the metallization process, making it difficult to fully visualize the images.

The needle-shaped zeolite which, according to Kalipçilar and Çulfaz (2007) and Schneider (2019), are mordenites (indicated by the arrow), can be seen in Figure A1(b) and Figure A1(d).

It was also possible to verify the predominant presence of ZSM-5 zeolite and the appearance of mordenite zeolite in Figure A2(d) due to the morphology of the crystals. The micrographs show a homogeneous and defect-free zeolitic coating on the inner and outer faces of the supports.

Figure A1 – SEM images from the zeolite films deposited in the inner surface of ceramic supports (5000x and 10 kV) (a) CFA10; (b) CFA20; (c) CFA30; (d) CFA40.

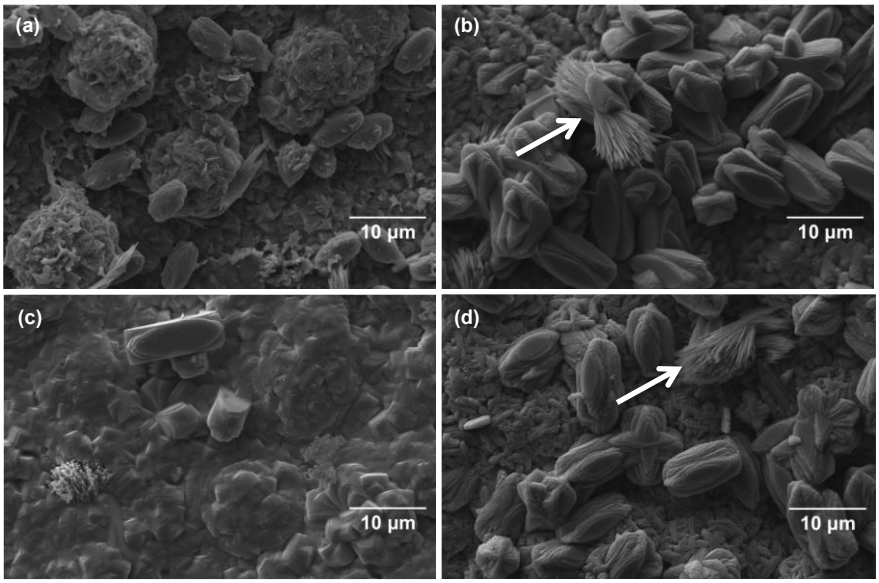

Figure A2 – SEM images from the zeolite films deposited in the outer surface of ceramic supports (5000x and 10 kV) (a) CFA10; (b) CFA20; (c) CFA30; (d) CFA40.

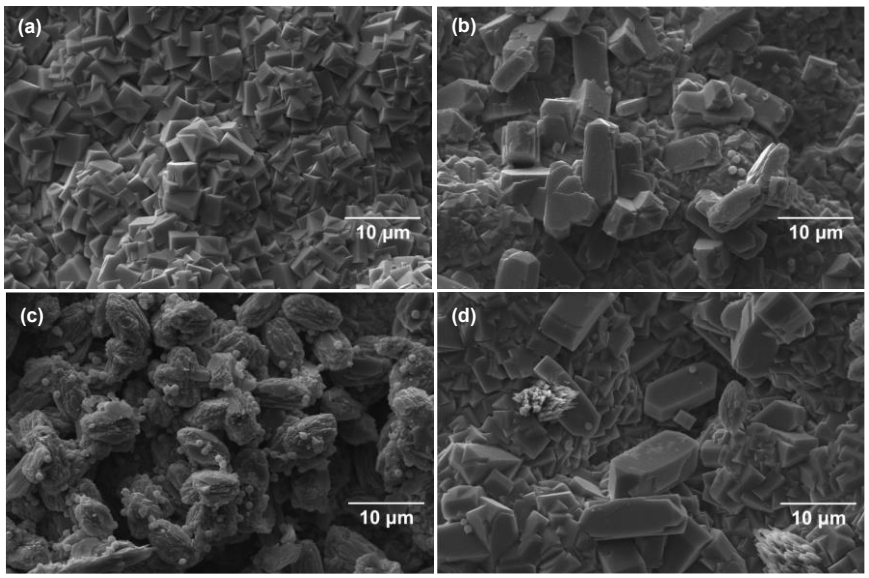

Comparison of the images for the internal and external depositions also suggests that there is incomplete crystallization of the ZSM-5 at the internal coating (Fig. A1). This result may be explained by the fact that, as studied in the work of Lai, Yan and Gavalas (2000), leaching of the support can occur during the hydrothermal synthesis of zeolites due to the highly alkalinity of the solution. According to the same authors, aluminate ions added to the synthesis mixture or leached from the substrate are found to have dual roles in the film growth: facilitate the formation of the gel layer on the support and retard zeolitization in this gel layer.

As the supports used in the present work, as already seen, present an asymmetry, with a greater predominance of alumina grains internally and CFA grains (mainly composed of Si) externally, it is assumed that the dissolution of the support may have occurred during the hydrothermal synthesis and, consequently, this material may have interfered with zeolite synthesis.

In order to perform the deposition on the internal surface of supports in the continuity of the work and allow the gradient of porosity increasing from inside to outside of the membrane, an optimization was necessary to improve the zeolite crystallization. Among the possibilities, it was decided to promote a longer crystallization time, applying another two and a half hours (in addition to the 24 hours) for the hydrothermal synthesis. This optimization could permit an effective nucleation and homogeneity in the size of crystals during the synthesis of zeolitic films.